

6 Dynamic Recrystallization: Multiple Peak and Monotonic Stress Behavior

6.1 An Introduction to Dynamic Recrystallization

Dynamic recrystallization (DRX) is the name of a recognized phenomenon, which occurs during straining of metals at high temperature, characterized by a nucleation rate of low dislocation density grains and a posterior growth rate that can produce a homogeneous grain size when equilibrium is reached. DRX, also known as discontinuous dynamic recrystallization by some authors [1], occurs after a critical amount of strain, ε_c , which is dependent on the type of strain path, the initial grain size, D_0 , temperature, T , and strain rate, $\dot{\varepsilon}$. When the critical strain is reached, on face centered cubic (fcc) metals of medium to low stacking fault energy [2], strain-hardening and dynamic recovery cease to be the principle mechanisms responsible of the stress-strain response, DRX accompanies the process. However, DRX is not a phenomenon restricted to fcc metals, it has been described on ice [3], some minerals [4], and even high purity α -Fe [5, 6, 7]. The relay of softening mechanism from strain-hardening and dynamic recovery to DRX is the reason the term discontinuous has been earned. At a microstructural level DRX begins when strain hardening plus recovery can no longer store more immobile dislocations. The grain becomes saturated of dislocation barriers in the form of cells and the grain boundaries bulge until a new grain is formed [8, 9, 10]. If the equilibrium or stable state is reached in a single cycle the hot flow curve is said to have a monotonic stress behavior. Upon the peak stress, σ_p , the stress descends following a particular kinetic rate until arriving to the steady state stress, σ_{ss} . If stress oscillations appear before reaching the steady state then several recrystallization and grain growth cycles occur and the stress behavior is said to be of the multiple peak type. The particular stress behavior before reaching the steady state depends, once again, on the initial grain size, temperature, and strain rate. The present work analyses recent theories that predict either a monotonic or multiple peak stress behaviors, and also proposes a stress-strain model, which represents both recrystallization paths.

Several criteria exist to predict a monotonic or multiple peak stress behavior, some are restricted to certain materials and test conditions, however the more recent and general theories profit earlier analyses and acknowledge the interrelationships between temperature, strain rate, the initial grain size and the stable dynamically recrystallized grain size, D_{rex} . The onset of DRX had been noticed by a stress peak on a true stress-true strain hot flow curve, however the corresponding peak strain, ε_p , does not necessarily coincide with the microstructural critical strain, ε_{cr} . In copper at higher strain rates or lower temperatures ε_{cr} occurs much earlier than ε_p , but at slower strain rates and higher temperatures $\varepsilon_p - \varepsilon_{cr}$ is smaller and almost coincide [11]. More recently analysis done on steels have shown that the ratio $\varepsilon_{cr}/\varepsilon_p$ remains constant [12], which would not make earlier observations untrue. This apparent contradiction will be explained during the subsection on the onset of DRX. A separation of both strain related concepts is needed to understand the difficulties of microstructural prediction, which is an objective of any complete model.

When the grain nucleation and growth rate have reached an equilibrium the microstructural change due to DRX is considered to have stopped and the original grains have been consumed or have been replaced by newer relatively dislocation free grains. DRX is of industrial interest when the new homogeneous dynamically recrystallized grains are smaller than the initial grains, because as a result room temperature mechanical properties improve. After the microstructural change due to DRX the stress remains relatively constant despite continued strain. One early criterion

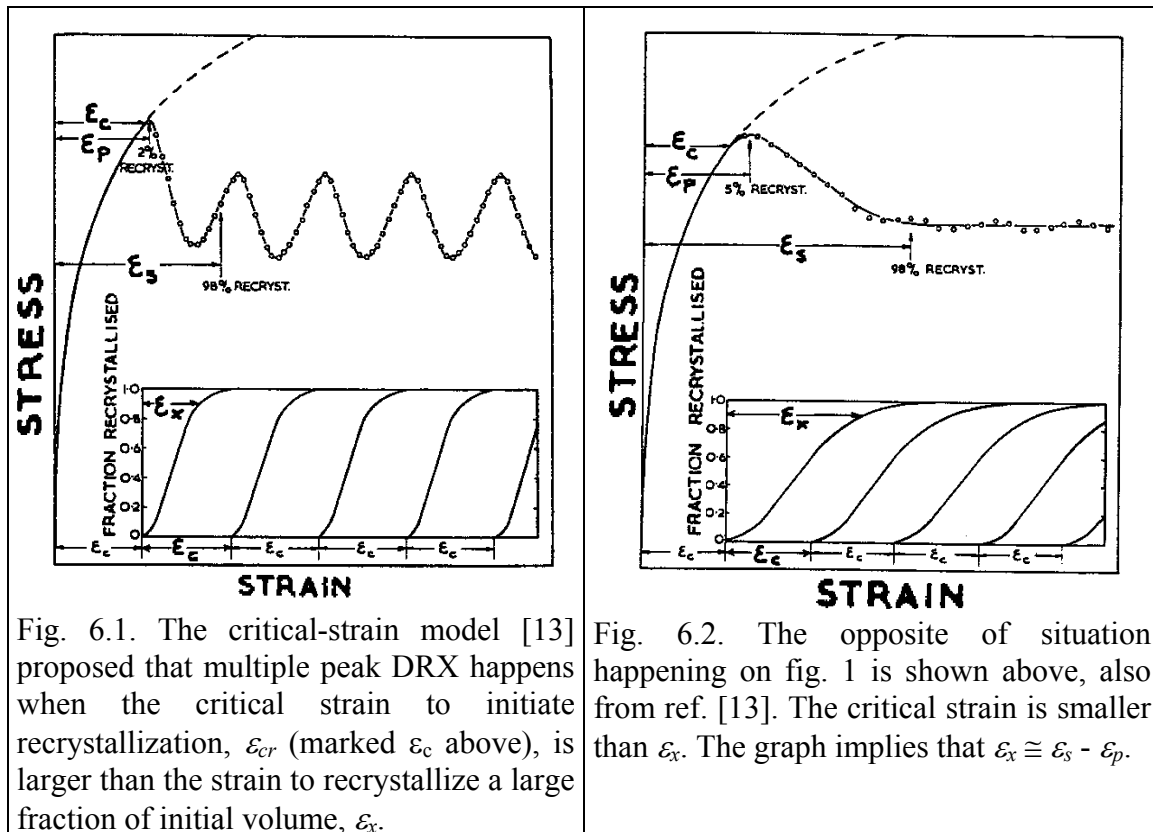
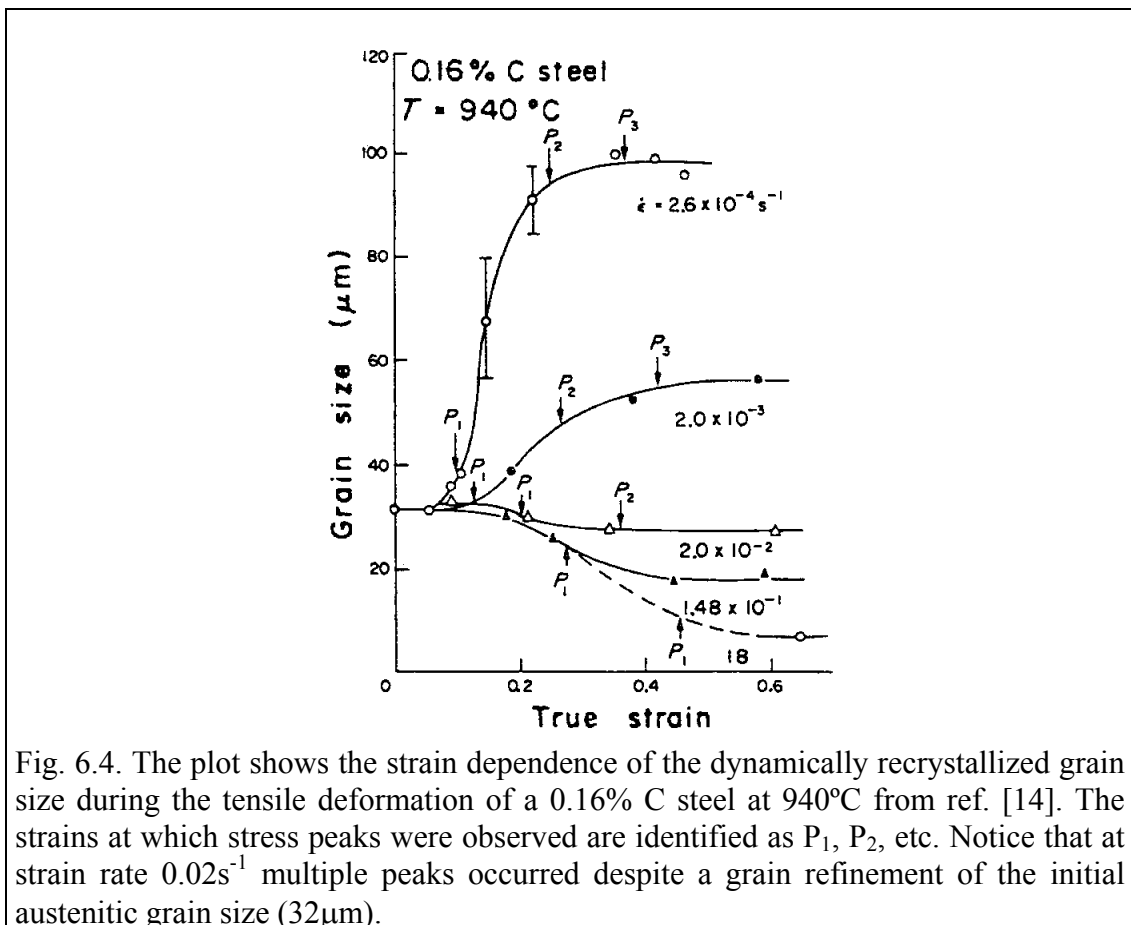
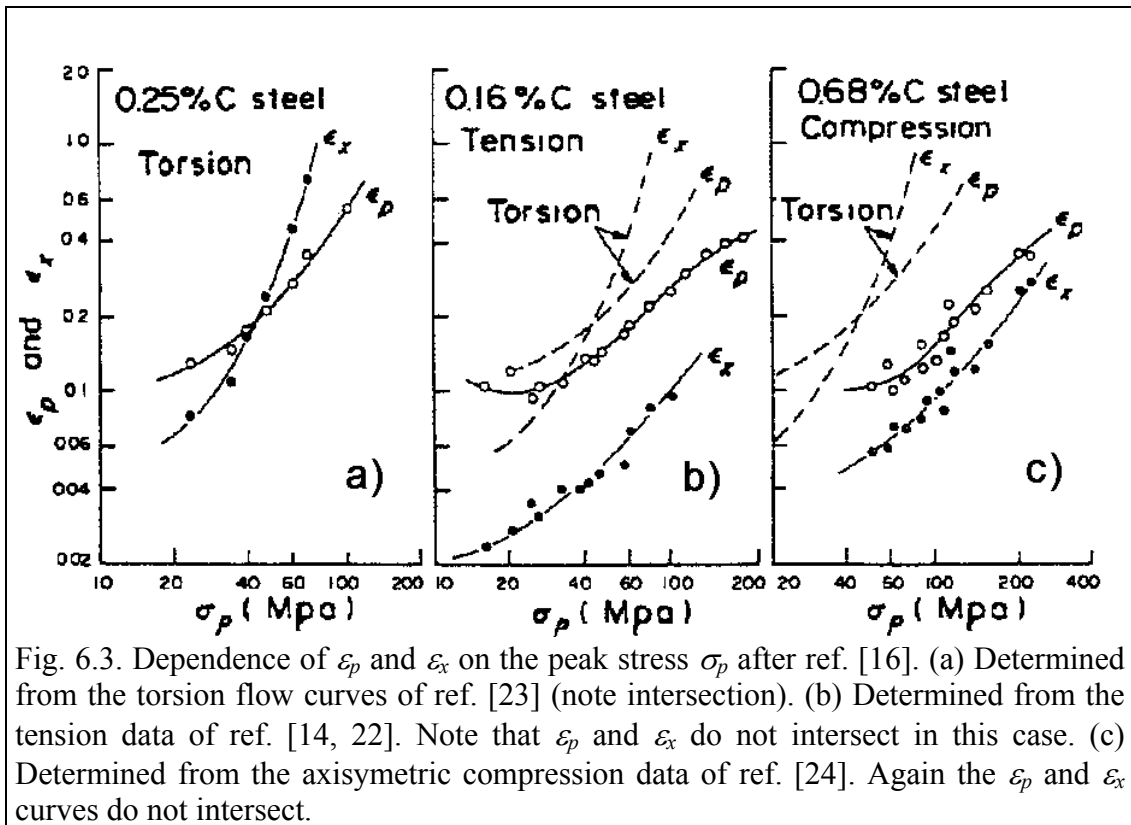


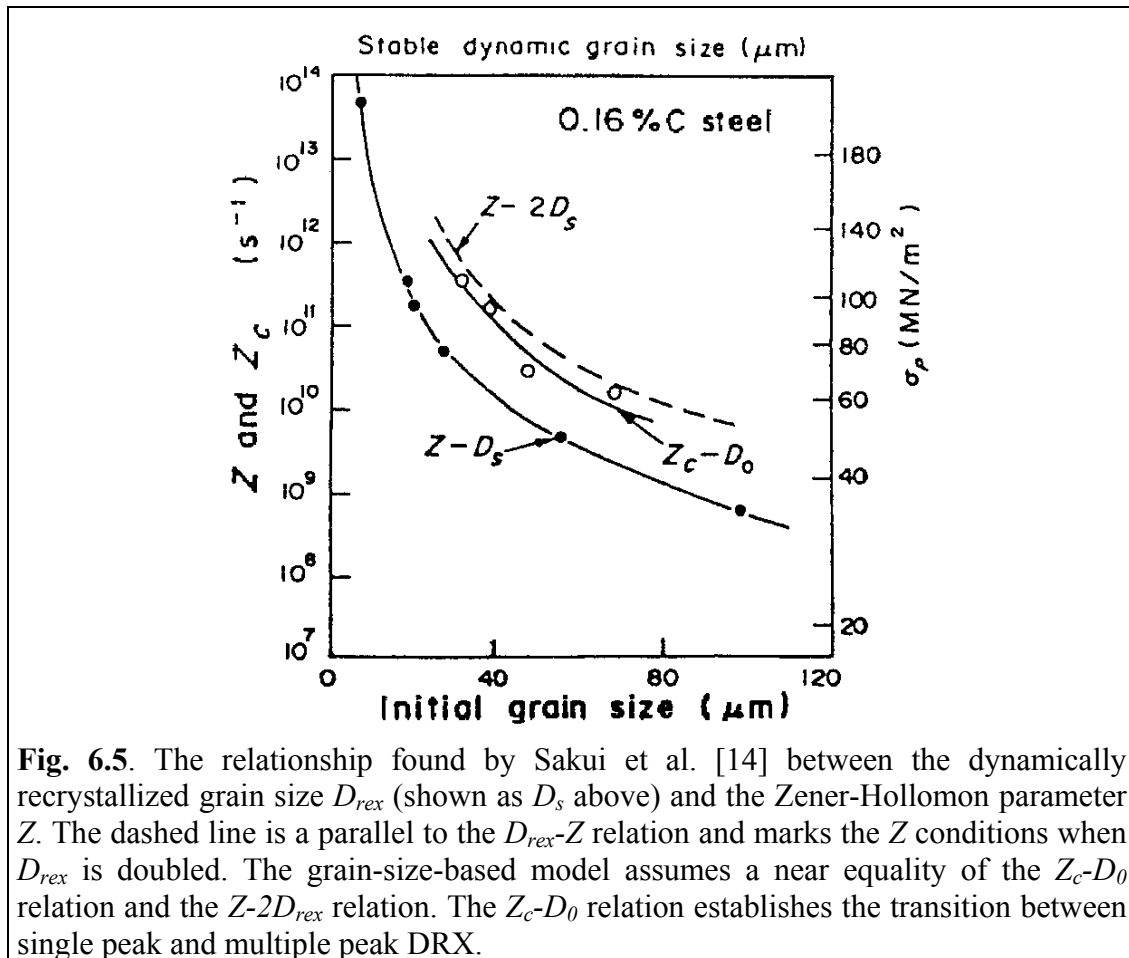
Fig. 6.1. The critical-strain model [13] proposed that multiple peak DRX happens when the critical strain to initiate recrystallization, ϵ_{cr} (marked ϵ_c above), is larger than the strain to recrystallize a large fraction of initial volume, ϵ_x .

Fig. 6.2. The opposite of situation happening on fig. 1 is shown above, also from ref. [13]. The critical strain is smaller than ϵ_x . The graph implies that $\epsilon_x \cong \epsilon_s - \epsilon_p$.

presented by Luton and Sellars [13] required comparison between the peak strain, ϵ_p , and the strain of the first DRX cycle, ϵ_x , see fig. 1 and 2. If the critical strain, ϵ_{cr} , was greater than a DRX cycle, ϵ_x , then a multiple peak stress behavior was expected.

The $\epsilon_{cr} > \epsilon_x$ criterion of the Critical-Strain model remained a useful analysis for the particular applications for which it was conceived, however methodological difficulties in the calculation of the involved strains and in the verification by other researchers [14, 15, 16] prompted further investigation. The end of the first DRX cycle according to Luton and Sellars is shown in figures 6.1 and 6.2 to be at the strain value ϵ_s after the first stress minimum when the hot flow curve reaches the steady state. An experimentally difficult matter to determine from a real hot flow curve is the steady state stress value. A horizontal stress line would ideally appear after the first or multiple DRX cycles, however during hot compression of the coppers in this study a clear horizontal stage was never present. The same observation is not unique to this study but can also be seen on hot flow curves in Pb [17, 15], Cu [18, 19], Ni and Ni-Fe [13], low carbon Steel [15] and HSLA Steel [20] just to mention few examples. Sakui *et al.* [14] and Weiss *et al.* [15] were unable to directly verify the Critical-Strain model during tension or compression tests of low carbon steel. Sandström and Lagneborg [21] also argued that ϵ_x depended on the average grain size and, because the average grain size during recrystallization varies then ϵ_x varies also. Sakai and Jonas [16] using carbon steels concluded that the critical-strain model could be applied only during torsion (see fig. 6.3). Sakui *et al.* [22, 14] using a 0.16% carbon steel in tension noticed a final stable dynamic grain size when only the strain rate was varied (see fig. 6.4). A relationship between the Zener-Hollomon parameter, $Z = \dot{\epsilon} \exp(Q/RT)$, and the stable dynamically recrystallized grain size, D_{rex} , was possible. Furthermore Sakui *et al.* without discarding the concept of a critical strain continued developing microstructural





relationships first pointing out that the initial grain size, D_0 , was related to a critical temperature and strain rate conditions, Z_c , which limited the appearance of multiple peak DRX and single peak DRX. The Z_c conditions almost matched the curve where the D_{rex} is doubled (see fig. 6.5). However this Grain-Size-Based critical condition [16] would require more experimental analysis to understand the microstructural consequences.

The $2D_{rex} < D_0$ criterion for a monotonic stress behavior seemed true, but incomplete. The assumption implied that a monotonic stress behavior would refine the initial grain size and that a multiple peak behavior ($2D_{rex} > D_0$) would coarsen the grain size. However, experimental deviations in copper [25] showed that a multiple peak behavior could refine an initial grain size of $78\mu\text{m}$ to $57\mu\text{m}$. These and other [26, 27, 28] experimental observations lead to improve the earlier criterion. An illustrative explanation of the evolved Grain-Size-Based criterion is shown on fig. 6.6. The condition shown on type I represents the original Grain-Size-Based criterion. Types II, III, IV and V illustrate what occurs mechanically and microstructurally after Montheillet and Jonas [1] re-examined experimental evidence. The second column shows real hot flow curves during compression of copper. The hot flow curve shown for the type II behavior is from ref. [25], however the curve is actually an example of type I behavior ($D_{rex} < 0.5D_0$), but was placed as an example because shows what happens when twins are considered. The hot flow behavior for type II, excluding twins, looks much like type I. The five types of hot flow behavior when twins are excluded can be seen on ref. [29].

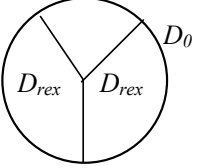
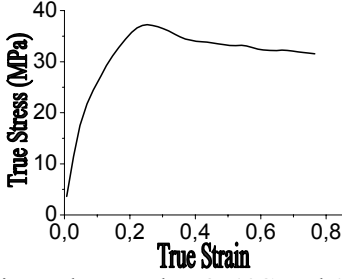
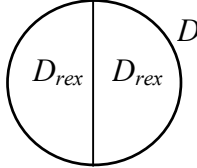
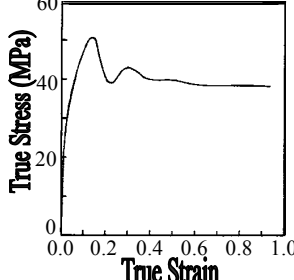
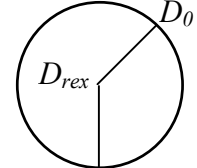
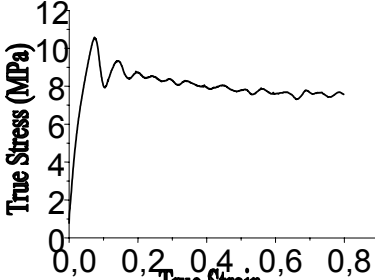
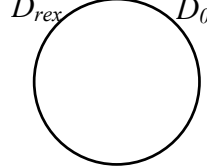
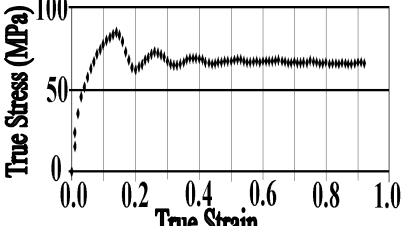
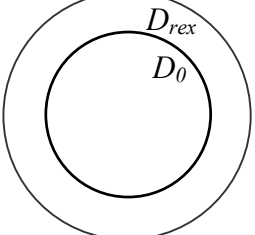
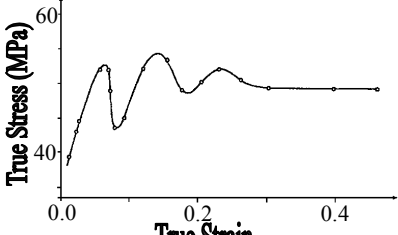
| | |
|---|---|
| <p>Type I: Single Peak DRX and Grain Refinement</p>  <p>$D_{rex} < 0.5D_0$ and $Z > Z_C$</p> |  <p>Copper A of this study tested at 850°C and 0.1s⁻¹. Grain size excluding twins: $D_0 = 637\mu\text{m}$ and $D_{rex} = 83\mu\text{m}$.</p> |
| <p>Type II: Single Peak DRX and Grain Refinement</p>  <p>$2D_{rex} = D_0$ and $Z = Z_C$</p> |  <p>Copper from ref. [25] tested at 602°C and 0.002s⁻¹. Grain size (μm) excluding/including twins: $D_0 = 164 / 78$ and $D_{rex} = 47 / 34$.</p> |
| <p>Type III: Multiple Peak DRX & Grain Refinement</p>  <p>$D_0 > D_{rex} > 0.5D_0$ and $Z < Z_C$</p> |  <p>Copper A of this study tested at 950°C and 0.001s⁻¹. Grain size excluding twins: $D_0 = 637\mu\text{m}$ and $D_{rex} = 396\mu\text{m}$.</p> |
| <p>Type IV: Multiple Peak DRX, No Grain Size Change</p>  <p>$D_{rex} = D_0$ and $Z < Z_C$</p> |  <p>Copper from ref. [29] tested at 405°C and 0.0004s⁻¹. Grain size excluding twins: $D_0 = 62\mu\text{m}$ and $D_{rex} = 62.3\mu\text{m}$.</p> |
| <p>Type V: Multiple Peak DRX & Grain Coarsening</p>  <p>$D_{rex} > D_0$ and $Z < Z_C$</p> |  <p>Copper from ref. [30] tested at 597°C and 0.0014s⁻¹. Grain size excluding twins: $D_0 = 9\mu\text{m}$ and $D_{rex} = 31\mu\text{m}$.</p> |

Fig. 6.6 Type I is the original Grain-Size-Based criterion. To see the 5 plot types see ref. [29].

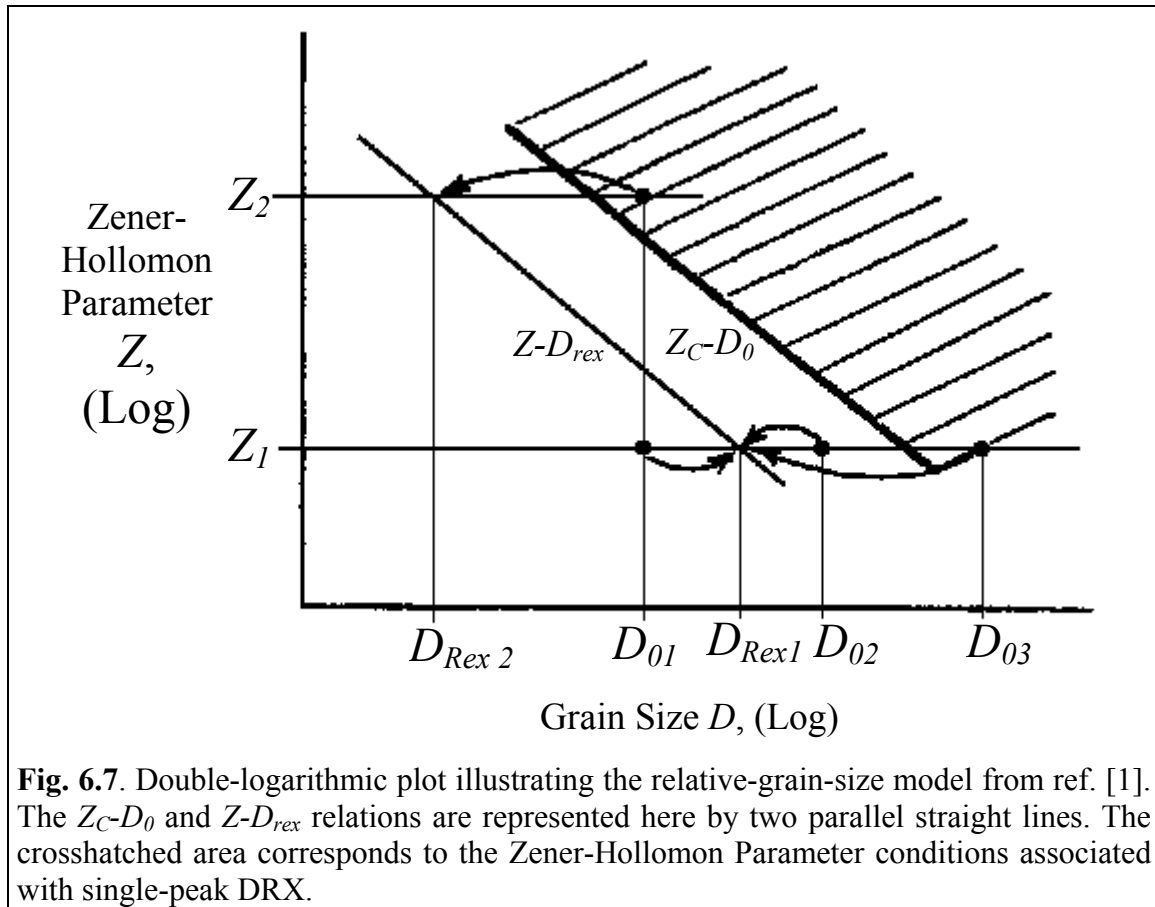


Fig. 6.7. Double-logarithmic plot illustrating the relative-grain-size model from ref. [1]. The Z_c-D_0 and $Z-D_{rex}$ relations are represented here by two parallel straight lines. The crosshatched area corresponds to the Zener-Hollomon Parameter conditions associated with single-peak DRX.

Montheillet and Jonas [1] have named this contemporary approach the Relative-Grain-Size model and is theoretically explained by fig. 6.7.

The relationship between the dynamically recrystallized grain size, D_{rex} , and the Zener-Hollomon parameter, Z , and the relationship between the initial grain size, D_0 , and the critical Zener-Hollomon value, Z_c , were schematically redrawn on a same Log-Log graph, which makes the curves presented by Sakui *et al.* straight. Both are power law relationships, which are expressed as

$$D_{rex} = K_{rex} Z^{m_{rex}} \quad (6.1)$$

and

$$D_0 = K_0 Z_c^{m_0} \quad (6.2)$$

where K and m are constants particular to the metal employed. The line on fig. 6.7 marking the Z_c-D_0 relationship divides the temperature and strain rate conditions that produce a monotonic stress behavior (hatched area) from the conditions that produce a multiple peak stress behavior. The $Z-D_{rex}$ line represents the final grain size to which any initial grain size will tend during DRX. As means of explaining the relative-grain-size model two types of experiments can be designed. Hot flow tests at identical Z values can be performed on three different initial grain sizes, D_{01} , D_{02} , and D_{03} , hopefully laying on the three different stress behavior zones; monotonic stress behavior while refining, multiple peak stress behavior while refining, and multiple peak stress behavior while grain coarsening. The other type of experiment is the most commonly

performed; hot flow tests at identical initial grain sizes, D_{0i} shown on fig. 6.7, where different Z values are tried, and hopefully the three condition types are found, this was the case of Sakui *et al.* on fig. 6.4. On both types of hot flow experiments the initial grain size will move horizontally (as shown on fig. 6.7) until reaching the D_{rex} . In the analysis of this study the abscissas and ordinates will be interchanged so that in Eq. 6.1 and 6.2 the grain size may remain as the dependent variable (as a result at a constant Z value grain sizes will change only vertically). Some unresolved matters concerning the Z_c - D_0 relationship are, for instance, the appropriate slope value, m_0 . Is the Z_c - D_0 relation just a $2D_{rex}$ offset from the D_{rex} - Z relation maintaining m_0 constant? In the original article by Sakui *et al.* [14, 22] full congruence of the Z_c - D_0 relationship was attained at $1.8D_{rex}$, and for simplicity a $2D_{rex}$ offset was used on the Grain-Size-Based critical condition [16]. The slope m_0 is believed to be the same as m_{rex} on the contemporary Relative-Grain-Size model [1]. A method to identify a value for Z_c will be shown as part of a stress-strain model to be proposed. A model that predicts not only monotonic DRX [13], but also multiple peak DRX will be presented as an objective of this study.

6.2 Relevant Experimental Procedure

A fire-refined 99.9% pure copper with low oxygen (see Cu A on table 6.1) was chosen to study the stress-strain transition from monotonic to multiple peak DRX. Copper is an fcc metal that readily demonstrates both DRX behaviors within the heating and strain rate capacity of normal laboratory hot compression machines. The fire-refined copper billet was received as the surplus material after a hot extrusion cycle, which allowed a grain size much finer than the grain after only solidification. Cylindrical samples of 10mm diameter and 15 mm height were machined. Before each test the samples were annealed at 950°C during 5 minutes until reaching an initial grain size of 637 μ m. The annealing prevented any static recrystallization due to an unknown residual stress state. The hot compression tests were performed using a software enhanced Instron 4507 electromechanical testing machine to produce a constant strain rate. The samples were protected during the tests by a flow of nitrogen gas inside the furnace chamber. The test temperature was monitored by a thermocouple adjacent to the sample. Copper A was tested at eight different temperatures from 600°C to 950°C at 50°C intervals and at six different strain rates, namely 0.3s⁻¹, 0.1s⁻¹, 0.03s⁻¹, 0.01s⁻¹, 0.003s⁻¹, and 0.001s⁻¹. The strain rate attained in each test was 0.8. After each compression test quenching in cool water retained the resulting microstructure. The apparent activation energy, Q_{app} , of Cu A is 213kJ/mole [31], which is a value close enough to the lattice self-diffusion activation energy, $Q_{sd} = 197$ kJ/mole, of purer coppers [32, 33]. The proximity of the activation energy values has allowed use of the self-diffusion activation energy as means of analyzing the stress and strain values in correlation with the Zener-Hollomon parameter [34, 35]. Self-diffusion is the ultimate rate controlling process for pure metals [36]. The low content of oxygen made choosing Cu A fit for analyzing with a single activation energy value as will be explained.

Table 6.1. Residual chemical composition in ppm of the 99.9% Cu employed and the initial grain size D_0 (μ m) before hot compression tests.

| ppm | P | Sn | Pb | Ni | Ag | S | Fe | Zn | O | D_0 |
|------|-----|------|------|------|------|------|------|------|----|-------------|
| Cu A | 297 | 86.2 | 63.5 | 31.7 | 30.8 | 22.0 | 17.2 | 15.6 | 26 | 637 μ m |

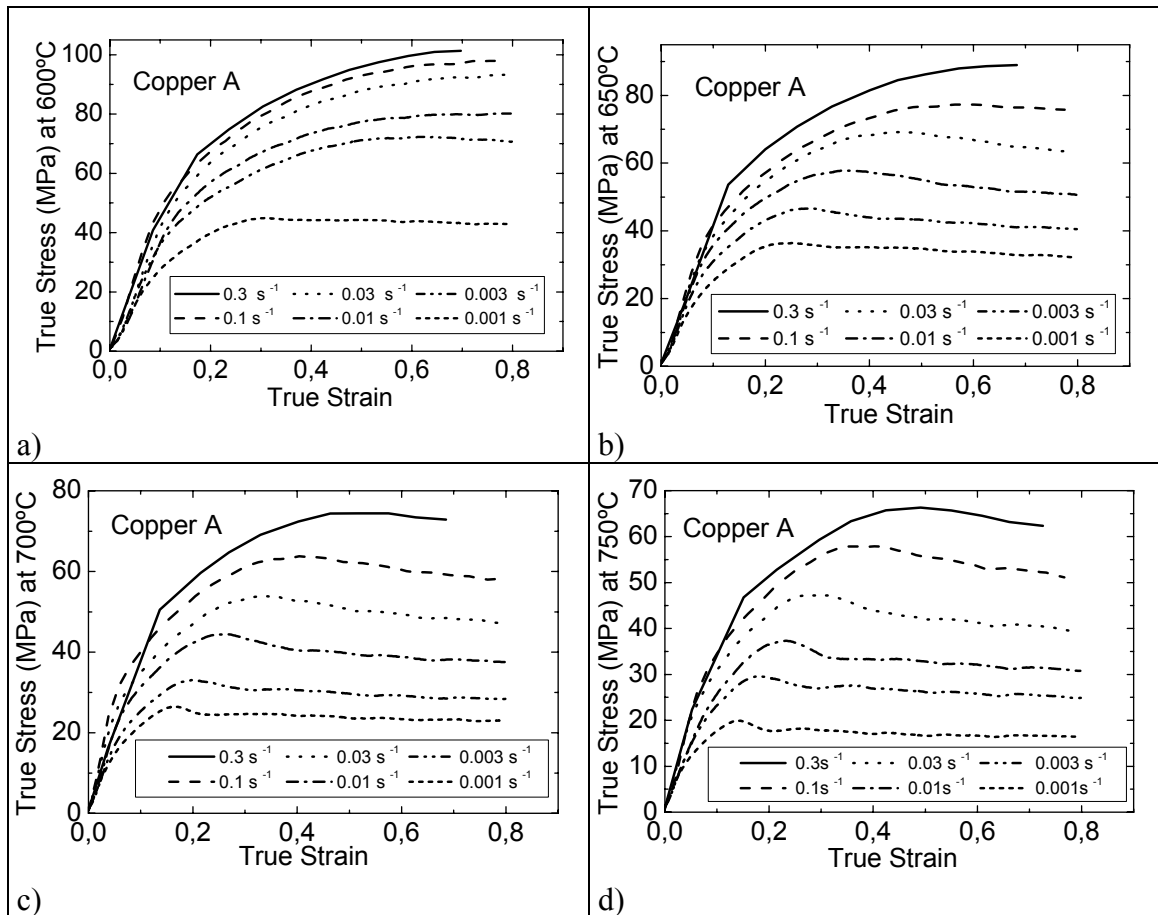


Fig. 6.8. Hot compression stress-strain curves performed at 600, 650, 700 and 750°C.

6.3 Experimental Hot Flow Curves

The selected strain rates, temperatures and initial grain size allowed hot flow curves of the types I, II, and III shown on fig. 6.6. Examples of incomplete DRX at a strain rate of 0.8 were also obtained. If the incompleteness was doubtful then the metallographical observation provided the answer [37]. Figures 6.8 and 6.9 show the true stress-true strain behavior at each of the eight temperatures and six strain rates. The common description of any hot flow curve of types III and IV is of an initial stress peak followed by damped oscillations whose amplitudes decrease to a central steady state stress value. Upon reaching certain minimum amplitude the hot flow becomes a horizontal straight line. However, a close examination of the curves pointed to redefine the common description given for the multiple peak behavior. First, the oscillations tended to a lower value instead of a central value, see fig. 6.10. Probably even further deformation was needed to reach a horizontal steady state. In compression further deformation is not realistic due to the loss of strain homogeneity. The lower value appreciated on the zoomed plots on fig. 6.10 should tend towards a saturation steady state stress value. The steady state stress value should be reached with enough strain. A model should reflect this last observation if the prediction is to match experimental data. A second objection from the general belief is that the oscillations on plots of fig. 6.10 do not disappear abruptly into a straight line instead oscillations attenuate to small amplitude. And finally, the first stress peaks and troughs appear periodic, and

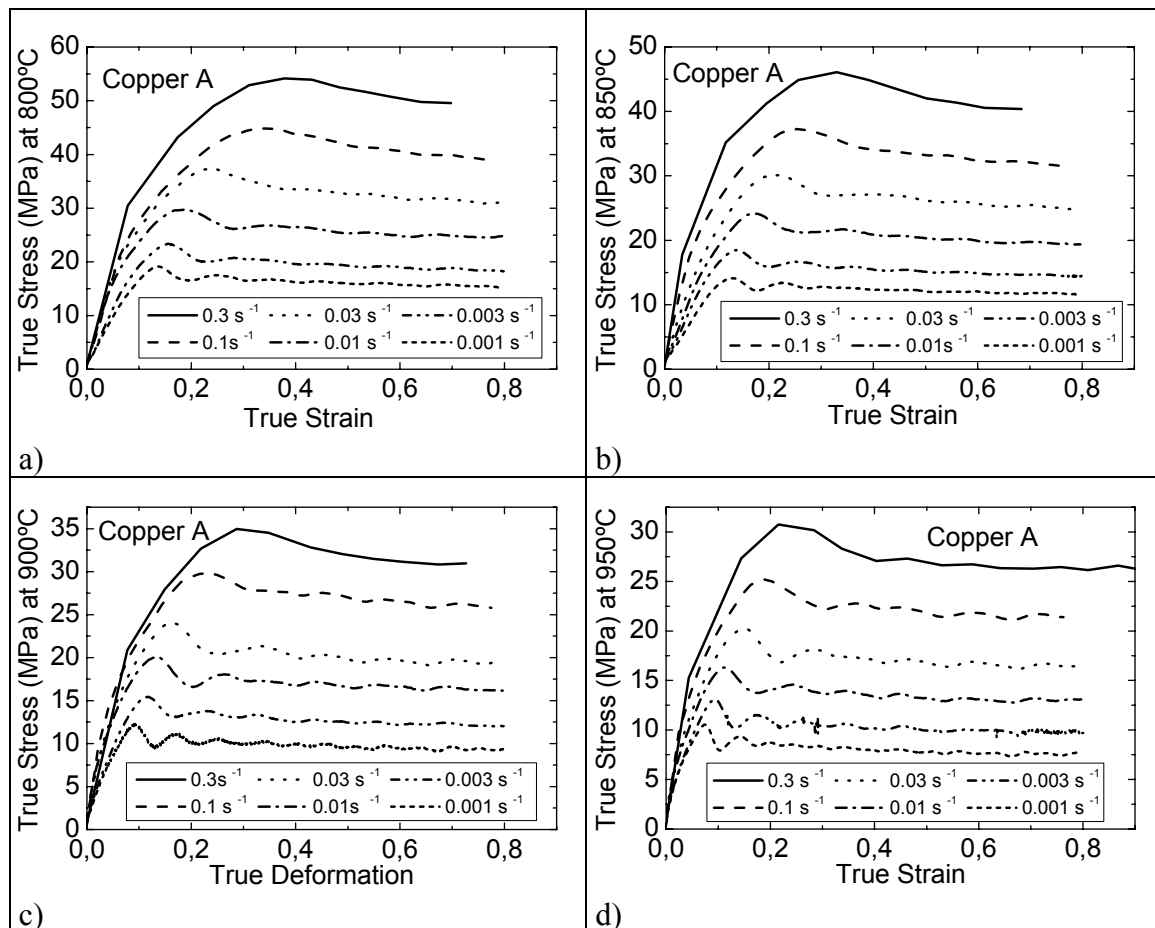


Fig. 6.9. Hot compression stress-strain curves performed at 800, 850, 900 and 950°C.

predictable. However no attempt had ever been made to describe their regularity as a function of Z . One geometric aspect of hot compression tests that should not be mistaken by a hardening mechanism is the small increment of stress registered near the end of the test. The small increase of stress responds to the approach or contact of the two cone shape volumes within the test sample, which accumulate less strain than the rest of the volume. The low strain accumulation results from the friction between the areas of the compression sample in contact with the anvils. When both cone shape volumes approach the effect is like deforming an initial grain of lower dislocation density, which will harden. No attempt will be made to model the hardening at the end of the compression test. The objections exposed through this work are not particular to this experimental study but as said earlier similar hot flow behaviors can be appreciated on other materials [13, 15, 17-20].

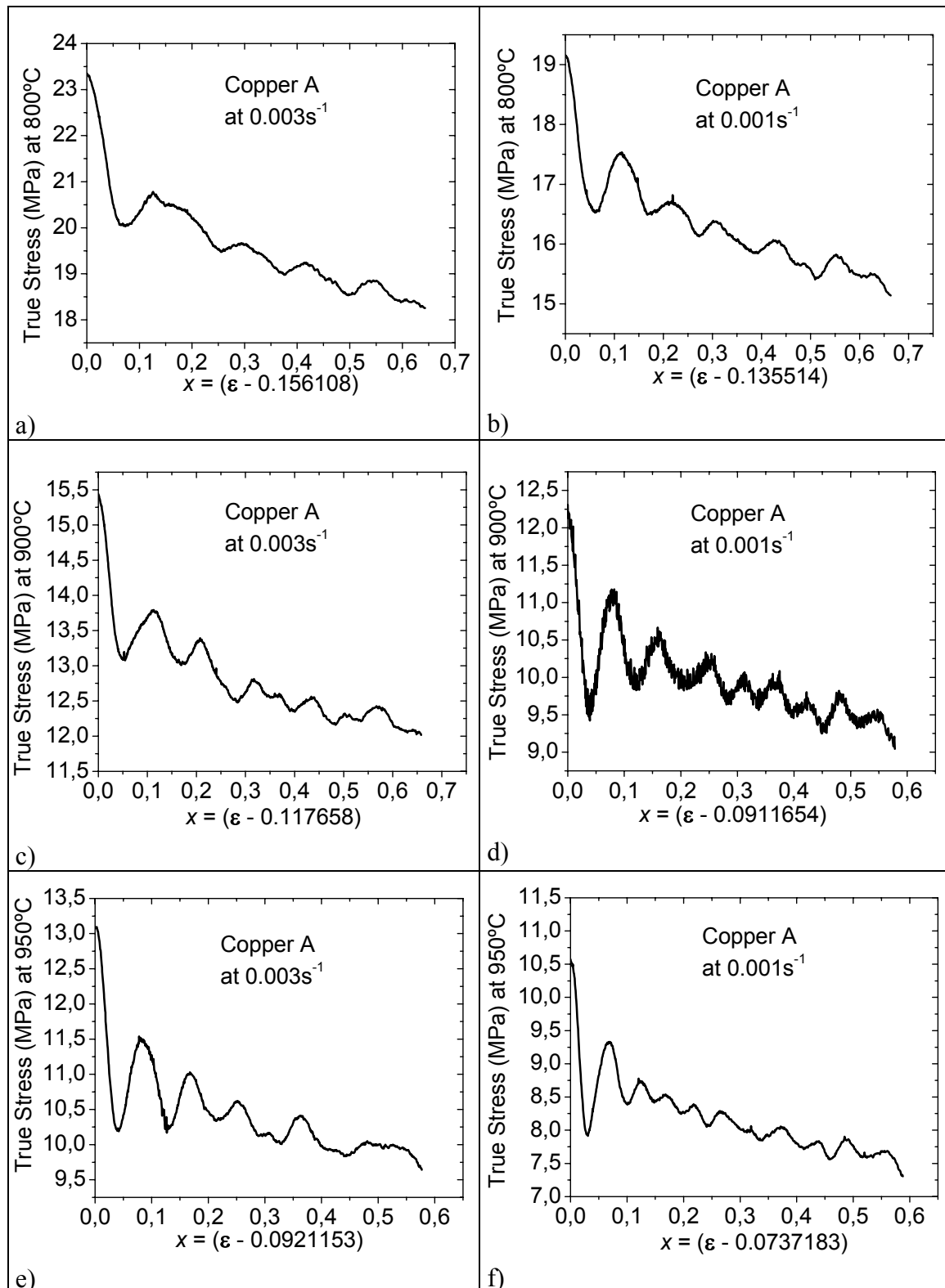


Fig. 6.10. A zoom shows the oscillating and descending behavior during DRX.

6.4 Avrami Models for DRX

Luton and Sellars [13] suggested the use an Avrami [38, 39] mathematical equation,

$$X = 1 - \exp(-K_A t^{n_A}), \quad (6.3)$$

to characterize the kinetics of the dynamically recrystallized volume fraction, X , which consumes an initial grain size. The Avrami equation had been used to quantify static recrystallization and grain growth kinetics among other transformation rates. The use of mathematical modeling to describe an ordered behavior, *i. e.* DRX, is commonly frowned upon, but the industrial necessity for kinetics prediction and the lack of acceptable correlations from physically based theories [40] urged a deductive reasoning. The deductively proposed Avrami equation has been modified to better describe the existing relationships between strain, strain rate, and temperature during DRX. In eq. 6.3 t represents the time during a single DRX cycle. If the peak strain, ε_p , the strain rate, $\dot{\varepsilon}$, and the progressing strain, ε , are known then

$$t = \frac{(\varepsilon - \varepsilon_p)}{\dot{\varepsilon}}. \quad (6.4)$$

The time for DRX to consume 50% of the initial grain volume, $t_{50\%}$, is an easier value to measure from hot flow data. The time for 100% DRX may stabilize at a low slope, which would increase the error while calculating the coefficient K_A . Since $\exp(-0.693) \cong 0.5$ the relationship between the coefficient K_A and $t_{50\%}$ can be expressed as

$$K_A = \left(\frac{-0.693}{t_{50\%}^{n_A}} \right). \quad (6.5)$$

Hence by combining equations 6.3, 6.4 and 6.5 the dynamically recrystallized volume fraction X is commonly [41, 42] expressed as

$$X = 1 - \exp \left[-0.693 \left(\frac{\varepsilon - \varepsilon_p}{\dot{\varepsilon} t_{50\%}} \right)^{n_A} \right]. \quad (6.6)$$

Equation 6.6 describes the rate at which the tested sample will soften from the peak stress, σ_p , to the steady state stress, σ_{ss} . From a mechanical point of view eq. 6.6 can be written as

$$X = \frac{\sigma_p - \sigma}{\sigma_p - \sigma_{ss}} \quad (6.7)$$

where σ is the registered stress. As a first step to characterize the kinetics of DRX the exponent n_A is calculated by measuring the slope of $\ln\{\ln[1/(1-X)]\}$ vs. $\ln[(\varepsilon - \varepsilon_p)(1/\dot{\varepsilon})]$, which is a result of substituting equations 6.4 and 6.7 into eq. 6.3 and expanding into a linear equation. The value of n_A is calculated for the first cycle of DRX whether monotonic or multiple peak. The exponent n_A can be plotted against the Zener-

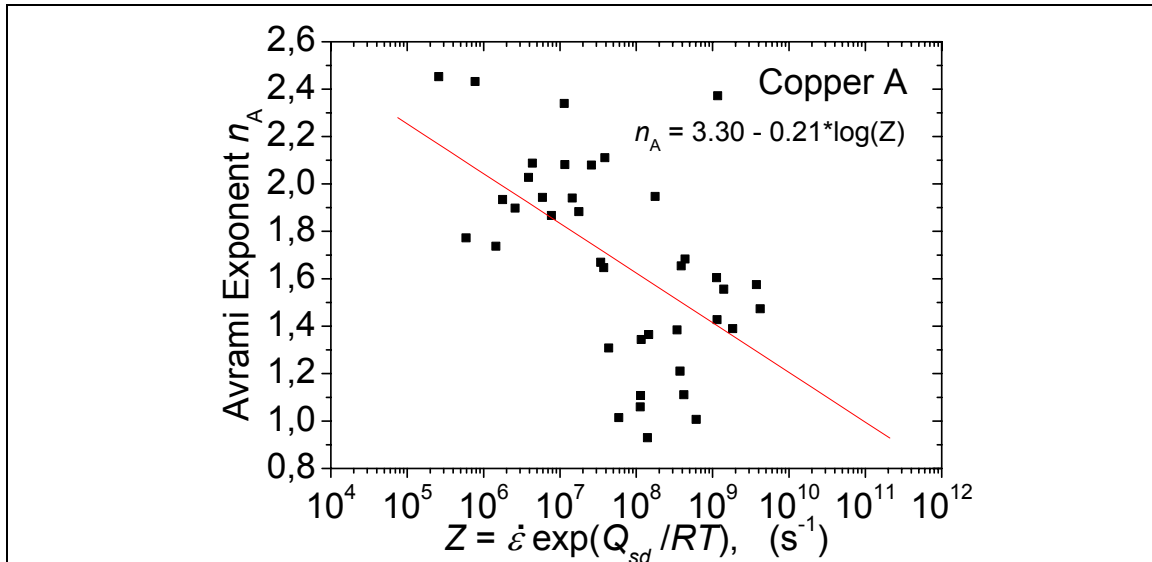


Fig. 6.11. The usual Avrami technique produced the shown dispersion of n_A values, which gather into two groups at around $n_A \sim 2$ for lower Z and around $n_A \sim 1$ for higher Z values.

Hollomon parameter as means of noting an ordered behavior, however for Cu A in the range of conditions studied, only two clouds of points could be appreciated (see fig. 6.11).

The measured exponent n_A had values near one for higher Z values, which present monotonic DRX, and presented values around two for lower Z values, which result in multiple peak DRX.

Despite the low correlation between n_A and Z the Avrami equation has been used to describe with some degree of success the hot flow curve of the copper in this study [34, 35] and of most metals. A reproduction of earlier results [34, 35] where the Avrami equation was used to model DRX kinetics in terms of strain rate and temperature is shown on fig. 6.12 and enlarged on fig. 6.13. The constitutive equation that describes stress is given by

$$\sigma = \sigma_p - (\sigma_p - \sigma_{ss}) \left\{ 1 - \exp \left[-0.693 \left(\frac{\varepsilon - \varepsilon_p}{\dot{\varepsilon} t_{50\%}} \right)^n \right] \right\}. \quad (6.8)$$

As can be seen from fig. 6.13 the Avrami model simulates only the first DRX cycle and stabilizes at a constant steady state stress value despite the multiple peak stress behavior. In part the simple trajectory of the prediction is because from the beginning the model was not conceived to oscillate. A simple trajectory without oscillations predicts stress values with relatively little error margin. A conceptual mistake of the Avrami implementation is that the recrystallized volume fraction, X , is commonly calculated using the mechanical definition given by eq. 6.7, which is not microstructurally true. Experimental evidence has shown that DRX begins before the peak stress, hence when X is zero according to eq. 6.7 the material already has a certain recrystallized volume. Sandström and Lagneborg later proposed a theoretical definition for X as will be explained by eq. 6.9. Multiple peak DRX has remained an academic curiosity probably because multiple peaks are only observed at temperatures near the

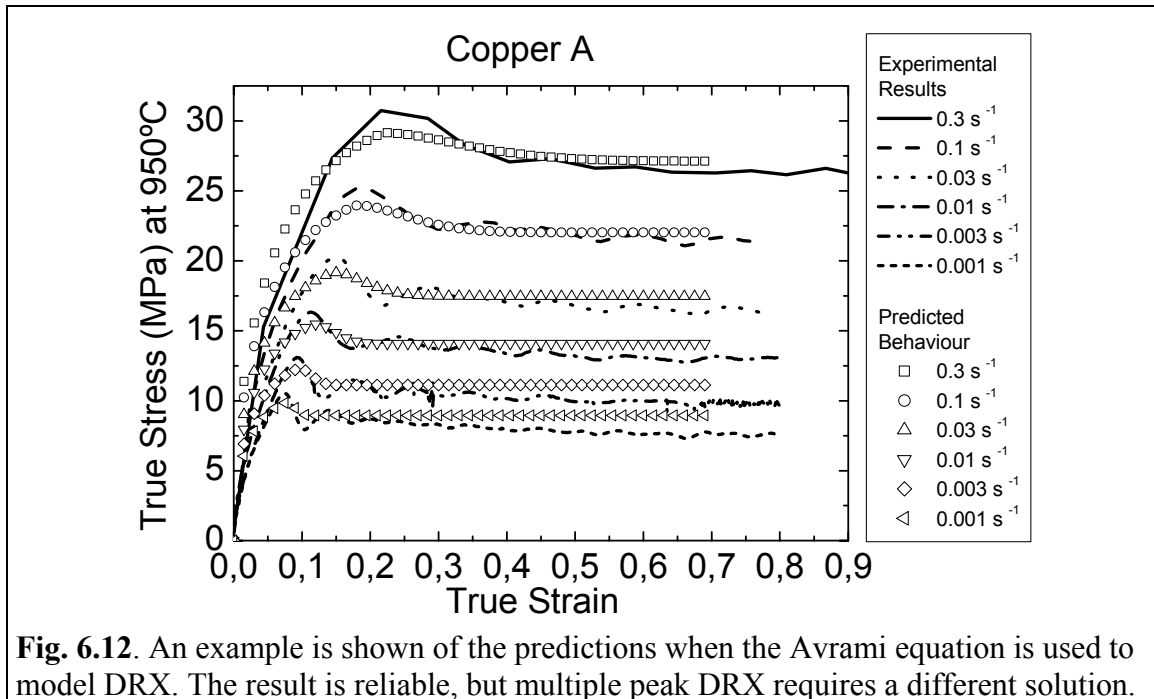


Fig. 6.12. An example is shown of the predictions when the Avrami equation is used to model DRX. The result is reliable, but multiple peak DRX requires a different solution.

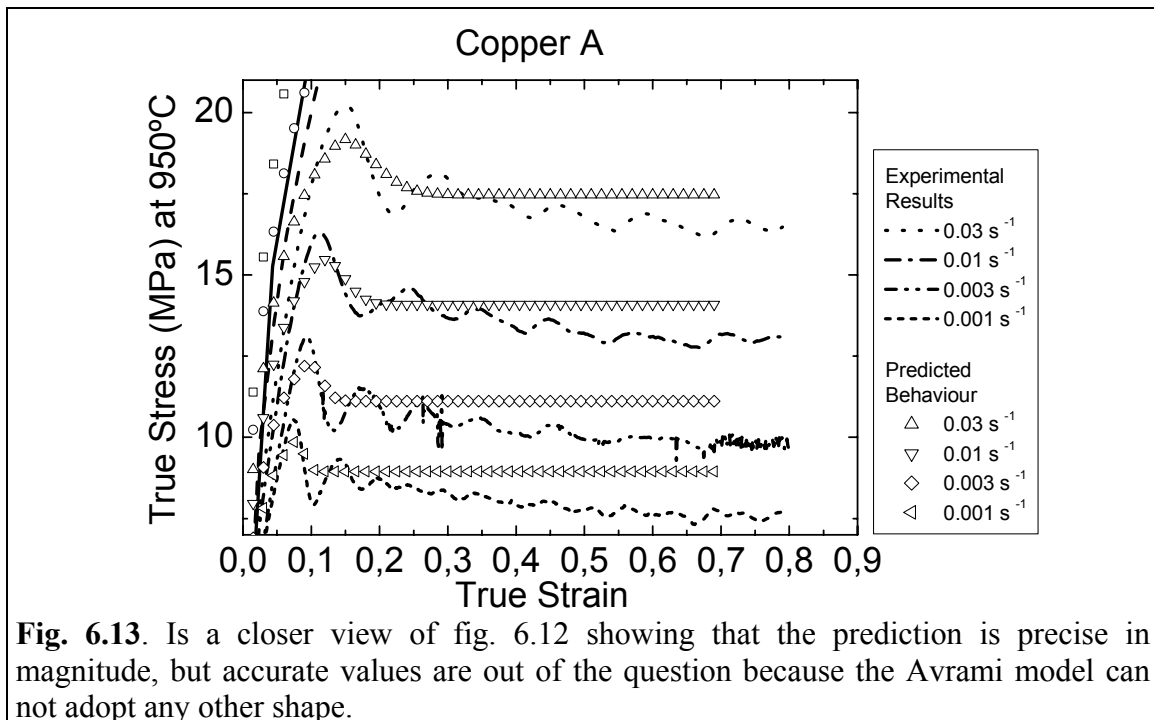


Fig. 6.13. Is a closer view of fig. 6.12 showing that the prediction is precise in magnitude, but accurate values are out of the question because the Avrami model can not adopt any other shape.

melting point and at slow strain rates. However some attempts have been made to model the multiple peak behavior using other means: a dislocation distribution model [21], Monte Carlo simulation methods [43], Cellular Automata algorithms for simulation [44] and complicated mathematical models that tend to be briefly explained, see references [45- 48].

6.5 The Sandström and Lagneborg DRX Model

In 1975 a theoretical model was presented [21] that explained oscillations during DRX and, was also validated using published experimental data on nickel [13], vacuum-melted iron [7] and, zone-refined iron [7]. The Sandström and Lagneborg model divided the hot flow behavior according to the arrangement of dislocation density locally present. As deformation progresses dislocation cell structures within the grain begin to form. Further deformation makes the dislocation cell walls acquire a higher local dislocation density if compared to the cell interior. A homogeneous dislocation density was defined, $g(\rho, t)$, which corresponded to the density within the substructures and, presumably behaved following a well-known relationship ($\tau = \alpha\mu b\sqrt{\rho}$). The other dislocation density was the one that formed sub-grain walls, $G(\rho_d, t)$, which was considered to contribute little to the total stress. At each time interval $\varepsilon/\dot{\varepsilon}$ a particular statistical volume distribution function existed for both dislocation densities defined. The homogeneous dislocation density within sub-grains adopted a normal shaped distribution function. The recrystallized volume fraction X caused $g(\rho, t)$ to widen, but increasing strain-hardening increased the frequency of a particular dislocation density value. The volume distribution function for the dislocation density in the sub-grain walls, $G(\rho_d, t)$, adopted an oscillatory behavior starting at a non-zero frequency for a zero dislocation density value, but as a critical dislocation density was reached the frequency tended to zero, i. e. almost no sub-grain wall sites with a dislocation density higher than the critical value. Both distribution functions were directly interrelated. The volume fraction of material dynamically recrystallized per unit time was defined as

$$\frac{dX}{dt} = \int_{\rho_{CR}}^{\infty} A_{MGB} v(\rho_d) G(\rho_d, t) d\rho_d, \quad (6.9)$$

where A_{MGB} is the moving grain boundary area and $v(\rho_d)$ is the velocity of the recrystallizing grain boundary. Sandström and Lagneborg used

$$\rho_{CR} = \frac{4 A_{Surf}}{A_{EUD} d^*} \quad (6.10)$$

as the critical dislocation density, defined by Bailey and Hirsch [9], where A_{Surf} is the grain boundary energy per unit area, A_{EUD} is the average energy per unit length of a dislocation and d^* is the diameter of the recrystallization nucleus. The advancing dynamically recrystallized volume provided fresh material to be included in $g(\rho, t)$.

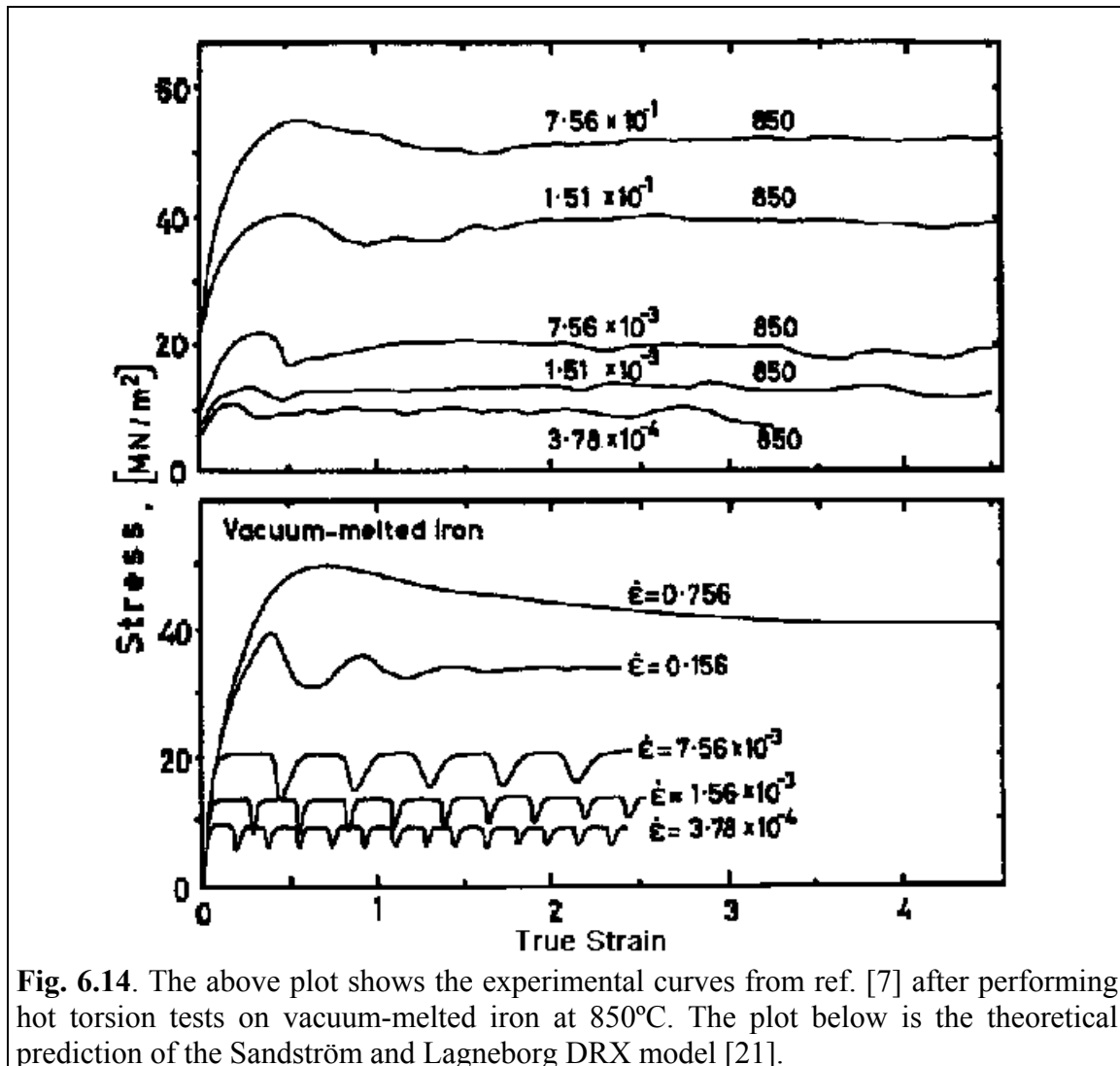


Fig. 6.14. The above plot shows the experimental curves from ref. [7] after performing hot torsion tests on vacuum-melted iron at 850°C. The plot below is the theoretical prediction of the Sandström and Lagneborg DRX model [21].

Stress at a particular time was calculated using the average dislocation density, $\bar{\rho}$, of $g(\rho, t)$ and using $\tau = \alpha \mu b \sqrt{\bar{\rho}}$.

The Sandström and Lagneborg model represents a singular attempt to include DRX into a strain-hardening and dynamic recovery model, however predictions could not follow a detailed match [21] with experimental evidence. The stress-strain predictions made by the Sandström and Lagneborg model are shown on figs. 6.14, 6.15 and, 6.16. Sandström and Lagneborg recognized that to improve the agreement between experimental and theoretical curves the grain boundary mobilities had to be multiplied by a factor. Also the mean free path value a dislocation in $G(\rho_d, t)$ can travel was made to be much larger than possible (10-25 μ m). Apart from the difficult task to reproduce the irregular experimental behavior the model was capable of predicting the periodicity of the oscillations as well as the peak and steady state stress magnitudes. The dependency of the model with temperature was not validated, but temperature enters the model via the change the grain boundary mobilities have with the change in temperature. Sandström and Lagneborg attributed the occurrence of oscillations on the relative magnitudes of the rate of recrystallization, dX/dt , and the rate of dislocation production, $d\rho/dt$. When the rate of recrystallization is sufficiently large compared to

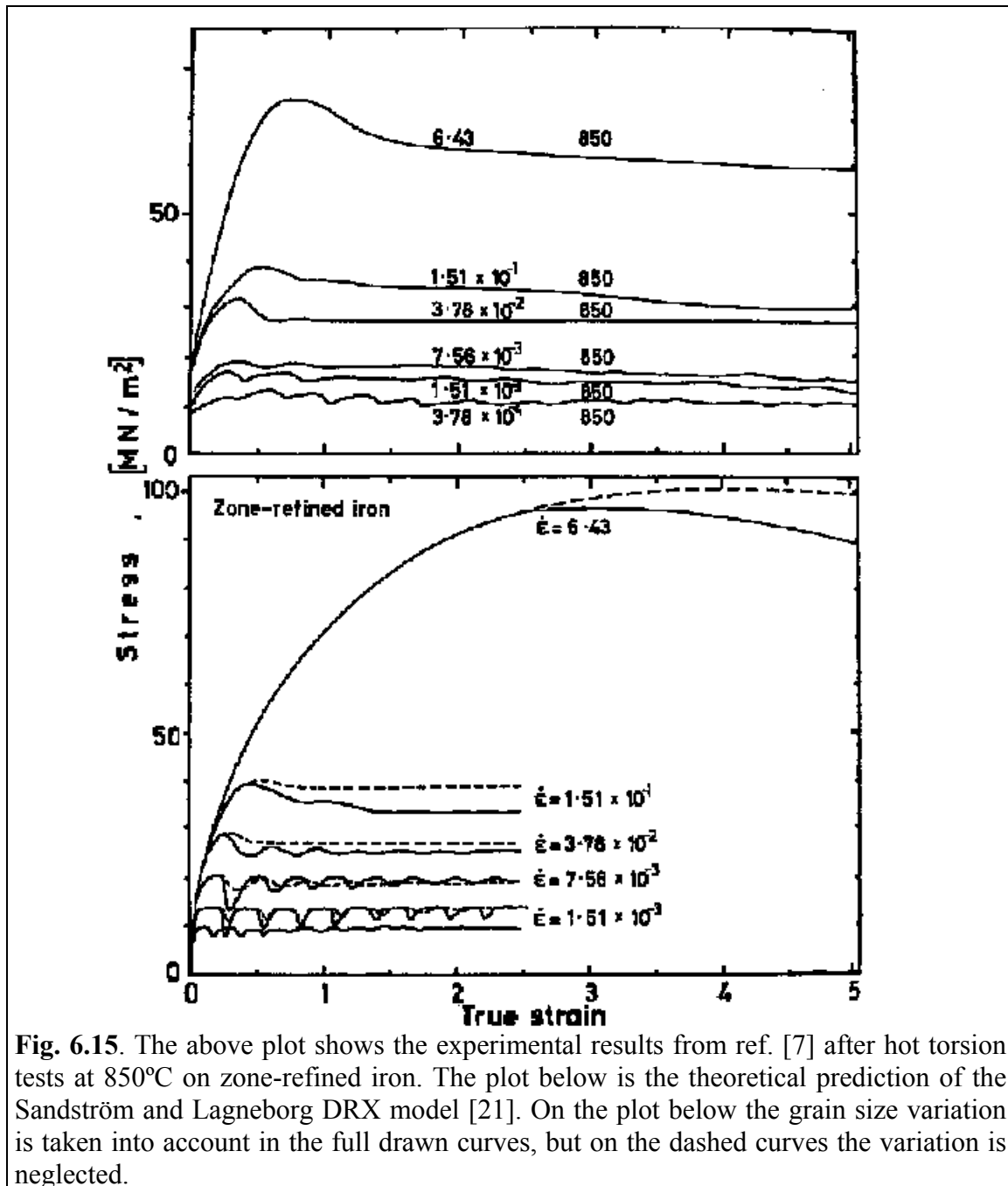


Fig. 6.15. The above plot shows the experimental results from ref. [7] after hot torsion tests at 850°C on zone-refined iron. The plot below is the theoretical prediction of the Sandström and Lagneborg DRX model [21]. On the plot below the grain size variation is taken into account in the full drawn curves, but on the dashed curves the variation is neglected.

the rate of dislocation production (low strain rates) then the recrystallized material is capable of gradually filling with dislocations and another recrystallization cycle will occur. If, on the other hand, the rate of recrystallization is small relative to the rate of dislocation production (high strain rates) then dislocations will be generated at a high rate behind recrystallizing grain boundaries. The critical dislocation density is reached long before the first recrystallization cycle is completed. As a consequence distinguishing between various cycles will not be possible and no stress oscillations will appear. The conceptual ideas put forth by the model seem to be on the right path, however the free use of $\tau = \alpha \mu b \sqrt{\rho}$ to describe strain-hardening and recovery beyond stage II needs revision, nonetheless the Sandström and Lagneborg approach has successfully inspired other experiments, like Cellular Automata [44] simulations.

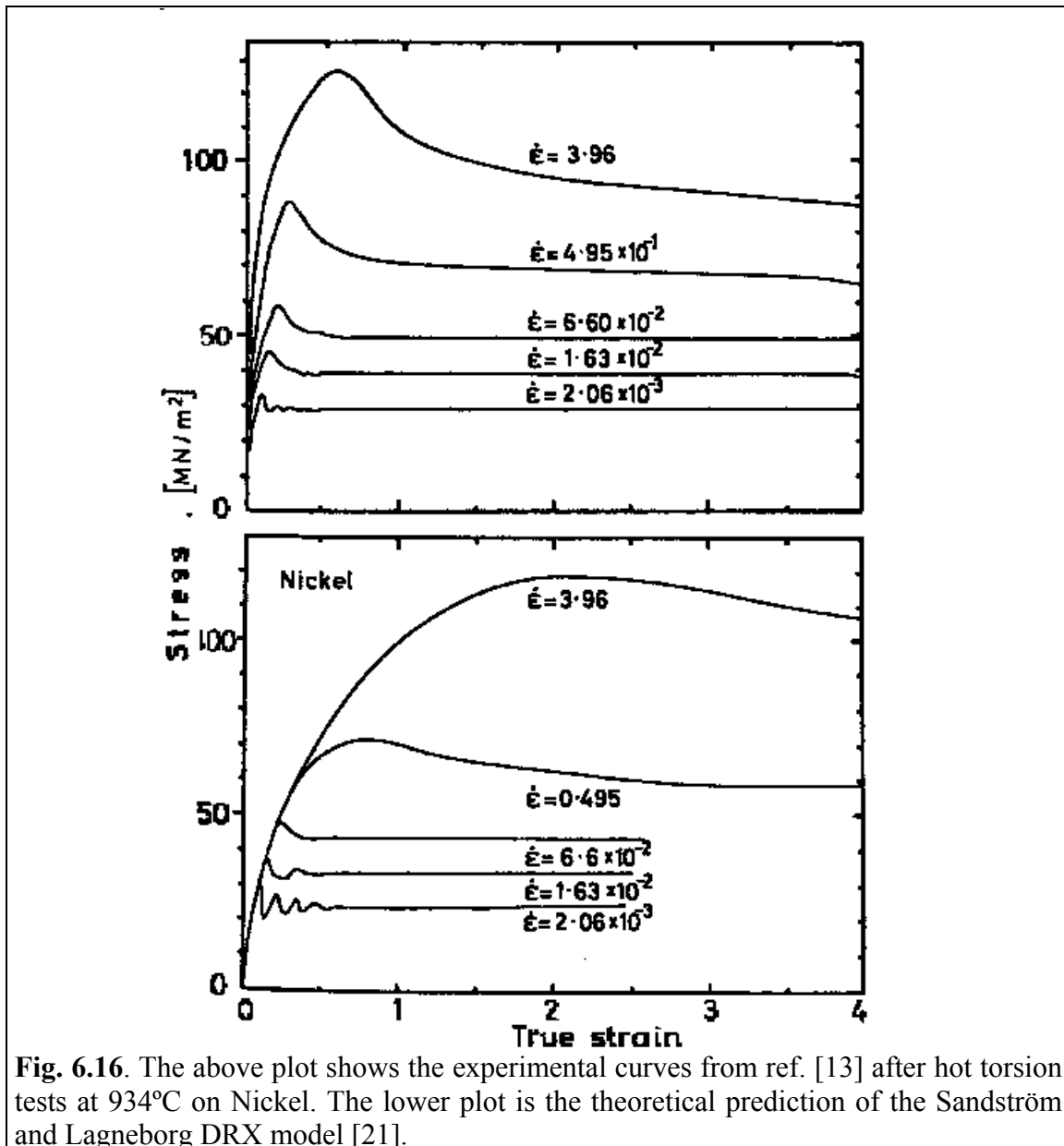


Fig. 6.16. The above plot shows the experimental curves from ref. [13] after hot torsion tests at 934°C on Nickel. The lower plot is the theoretical prediction of the Sandström and Lagneborg DRX model [21].

6.6 Monte Carlo Computerized Models for DRX

Rollett *et al.* [43] employed a computerized Monte Carlo algorithm to simulate the microstructural change during DRX by theoretically creating a two-dimensional triangular lattice where each node or site is assigned a texture, S_i , and a periodically increased stored energy, H , to account for work-hardening. Neighboring sites with different textures marked a grain boundary. Nucleation of recrystallized grains was achieved by adding new grains at randomly chosen positions. Grains would grow or not when the orientation of a site was randomly changed as part of the Monte Carlo method. Then an associated stored energy was added, ΔH , and the total energy, E , was calculated using a particular algorithm. Rollett *et al.* defined the total energy as

$$E = \frac{J}{2} \sum_i^n \sum_j^m (1 - \delta_{s_i s_j}) + \sum_i^n H_{s_i} \quad (6.11)$$

where J scaled the grain boundary energy, the first sum was over all of the sites in the model, the second sum was over the nearest neighbors of site i ($m = 6$), and δ_{ab} was the Kronecker delta function. If the total energy change was less or equal to zero then the randomly chosen site would retain the new orientation (growth), otherwise the old orientation was maintained (no growth). The only nexus to any particular metal came from the proportionality of stored energy, H , to the dislocation density, ρ , which is related to the flow stress, σ , through the known [49] relation

$$\sigma = \overline{M} \alpha \mu b \sqrt{\rho} \quad (6.12)$$

where μ is the shear modulus, b is the Burgers vector, \overline{M} is the Taylor factor [50-52], and α is a geometrical constant of order 0.5. The time was measured in steps or Monte Carlo steps (mcs), which correspond to the number of reorientation attempts of a site. Fig. 6.17 after [43] shows how pseudo stress-strain curves can be plotted by application of $\sigma = \sqrt{H}$ and the assumption that the work hardening rate is directly proportional to strain rate. Unfortunately the multiple peak stress behavior does not approach the stress or strain magnitudes of real hot flow tests. Further analysis seems to be needed to find the appropriate values of \overline{M} and α that could make of the pseudo stress-strain curves a prediction of the hot flow behavior of a metal. If appropriate values of \overline{M} and α were

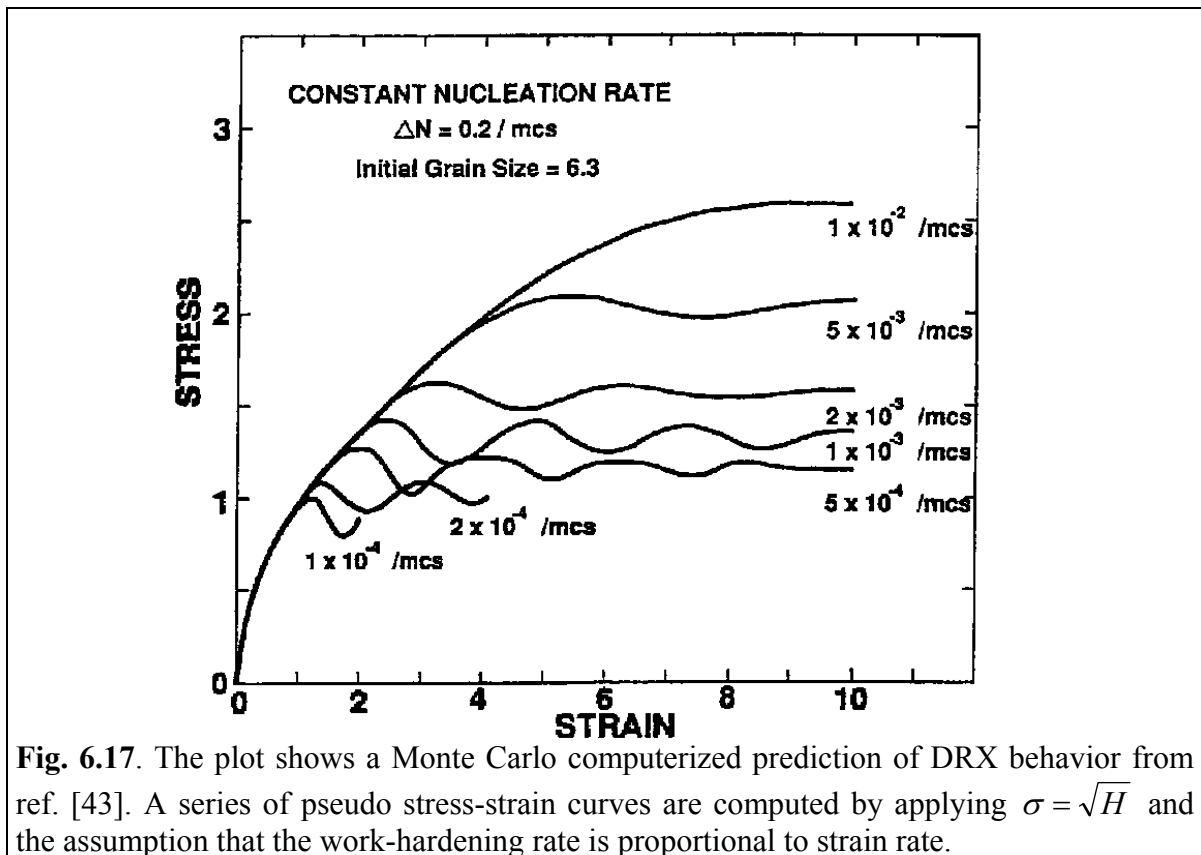


Fig. 6.17. The plot shows a Monte Carlo computerized prediction of DRX behavior from ref. [43]. A series of pseudo stress-strain curves are computed by applying $\sigma = \sqrt{H}$ and the assumption that the work-hardening rate is proportional to strain rate.

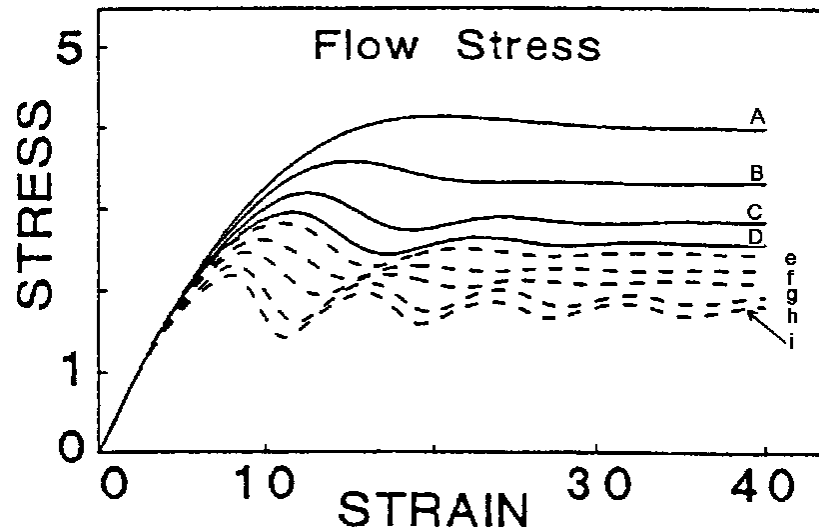


Fig. 6.18. The plot above shows a Monte Carlo computerized prediction from ref. [53]. A comparison between the general shapes of the Monte Carlo generated stress-strain curves above and the experimental curves of fig. 6.8 at least indicates that a detailed match will never be achieved. On the plot below the stress-strain curves for strain rates in the range $0.001 \leq \dot{\epsilon} \leq 0.06 \text{MCS}^{-1}$ and $T = T_{\text{melting}}$ (solid lines) and $\dot{\epsilon} = 0.004 \text{MCS}^{-1}$ and the temperature in the range $0.5 T_{\text{melting}} \leq T \leq T_{\text{melting}}$ (dashed lines). Letters A, B, C, and D, correspond to $\dot{\epsilon} = 0.09, 0.06, 0.04$ and 0.03MCS^{-1} , while e, f, g, h and i correspond to $T / T_{\text{melting}} = 0.7, 0.75, 0.8, 0.9$ and 1.0 respectively. The curves were obtained for a microstructure with $D_0 \cong 12.1$.

to be found then a lack of resemblance with experimental data could be a problem, compare Figs. 6.8 and Fig. 6.18. Another attempt to model multiple peak DRX was done by Peczak [53, 54] shown on fig. 6.18 where the total energy was instead defined by a modified q-state Potts model Hamiltonian [55], again with similar results.

6.7 Cellular Automata models for DRX

Goetz and Seetharaman [44] developed the first Cellular Automaton whose deterministic rules modeled DRX. Like the Monte Carlo method the Cellular Automata technique creates a grid of uniform cells, which are updated every time step with a finite value or state using deterministic rules that consider the neighborhood of cells around. However the phenomenological relationships to simulate grain boundary motion and the use of the Potts energy model in the Monte Carlo method mark a fundamental difference [44]. The Cellular Automaton created by Goetz and Seetharaman is based on the technique developed by Hesselbarth and Göbel [56] for Static Recrystallization. The method relied on keeping track of the dislocation density of each cell, ρ^c , which determined nucleation and growth. A 7-cell neighborhood was used to control growth by impingement after nucleation, when two recrystallized grains came in contact then growth was stopped on both. New grain boundaries were allowed to migrate until the dislocation density of a cell became greater or equal to a critical dislocation density, ρ_{CR} . Critical dislocation densities have been defined elsewhere in literature [9, 57]. The first step of the process [44] required the creation of an initial microstructure. Then

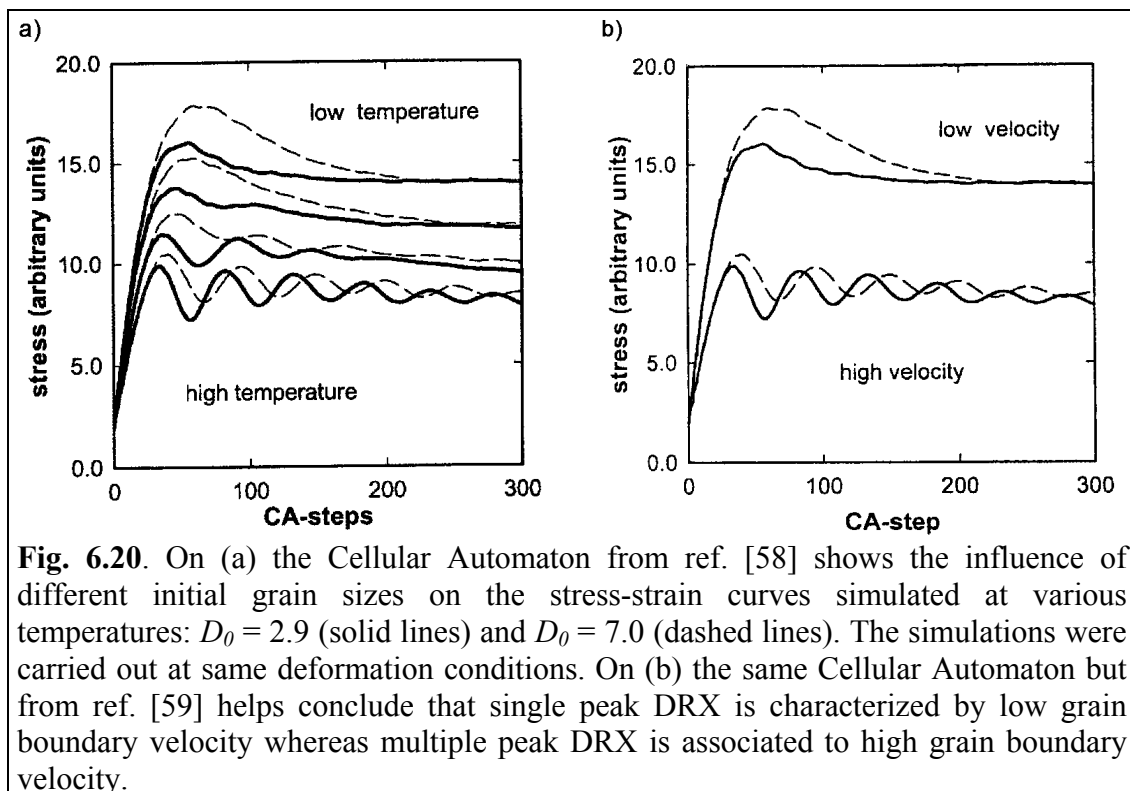
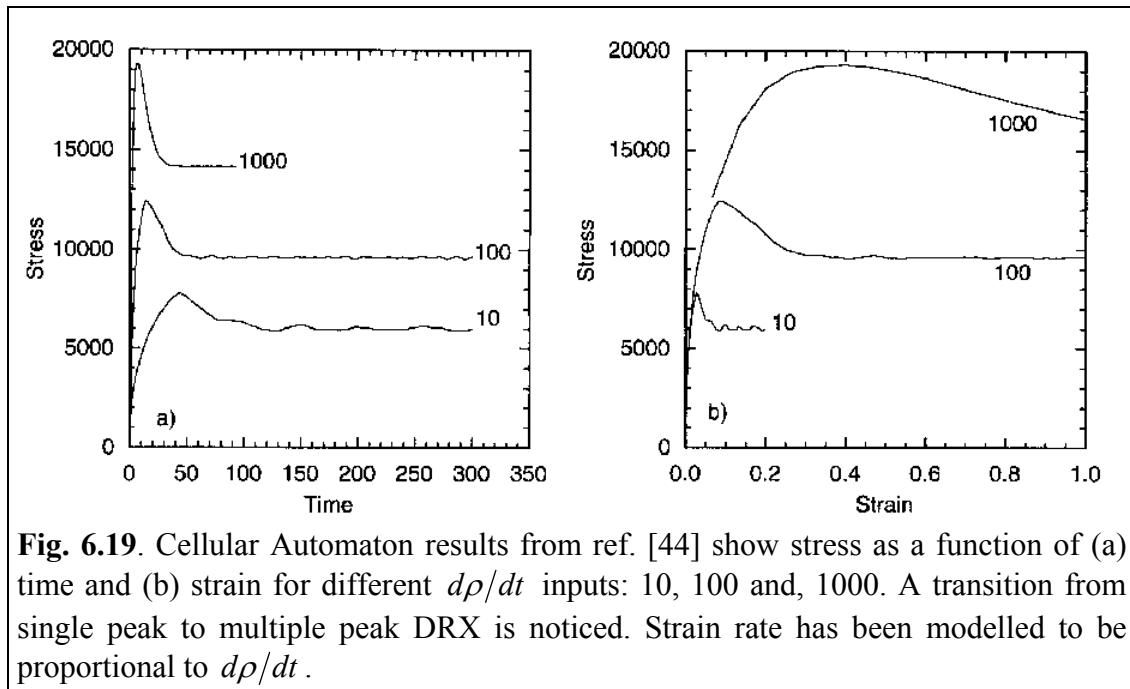
simultaneously four operations were performed at each time step. The dislocation density, ρ , was increased, which simulated strain hardening by assuming that $\varepsilon \propto \rho$ and $\dot{\varepsilon} \propto d\rho/dt$. The dislocation density was halved in a certain number of cells, N , which simulated Dynamic Recovery. Nucleation was achieved by checking the density of an arbitrary fraction ($d\rho/1000dt$) of grain boundary cells. If ρ^C exceeded the average dislocation density during Dynamic Recovery, ρ_{DR} , then the cell became a nucleus and the density was reset to zero. And fourth, boundary cells of new grains were allowed to migrate. The number of cells to be dynamically recovered, N , was made to be a function of the increase of dislocation density per time step, $d\rho/dt$, and thus

$$N = 3170(d\rho/dt)^{0.6}. \quad (6.13)$$

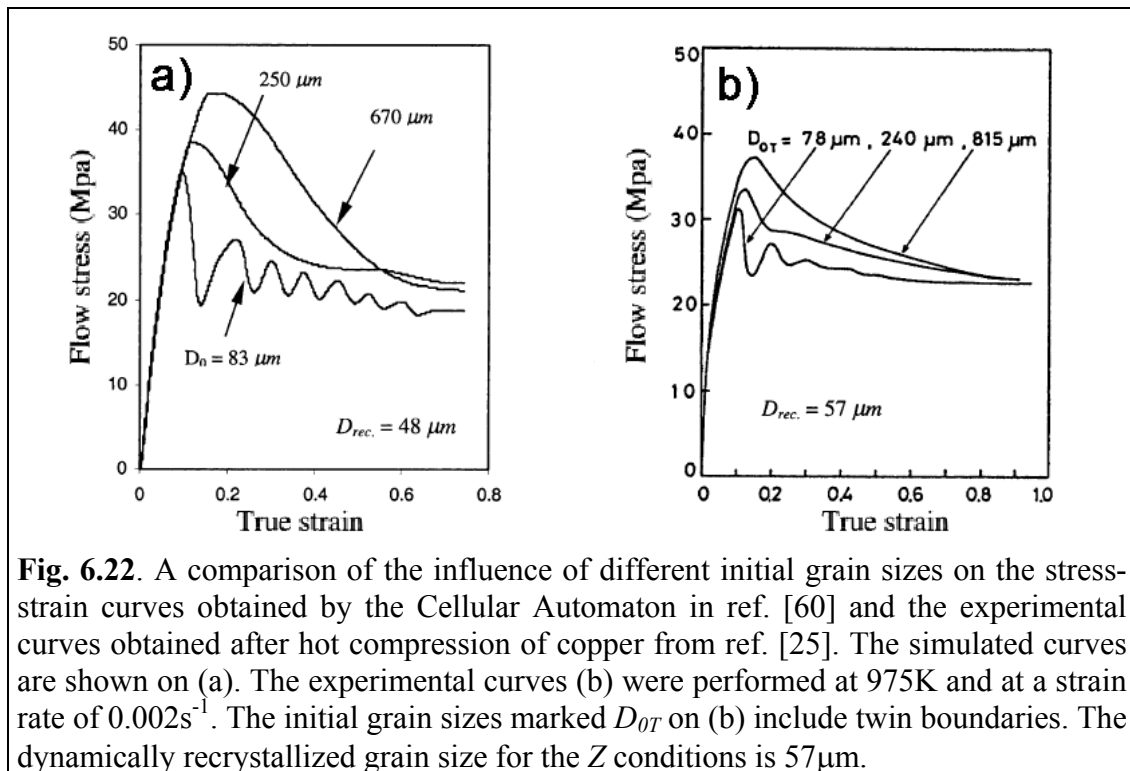
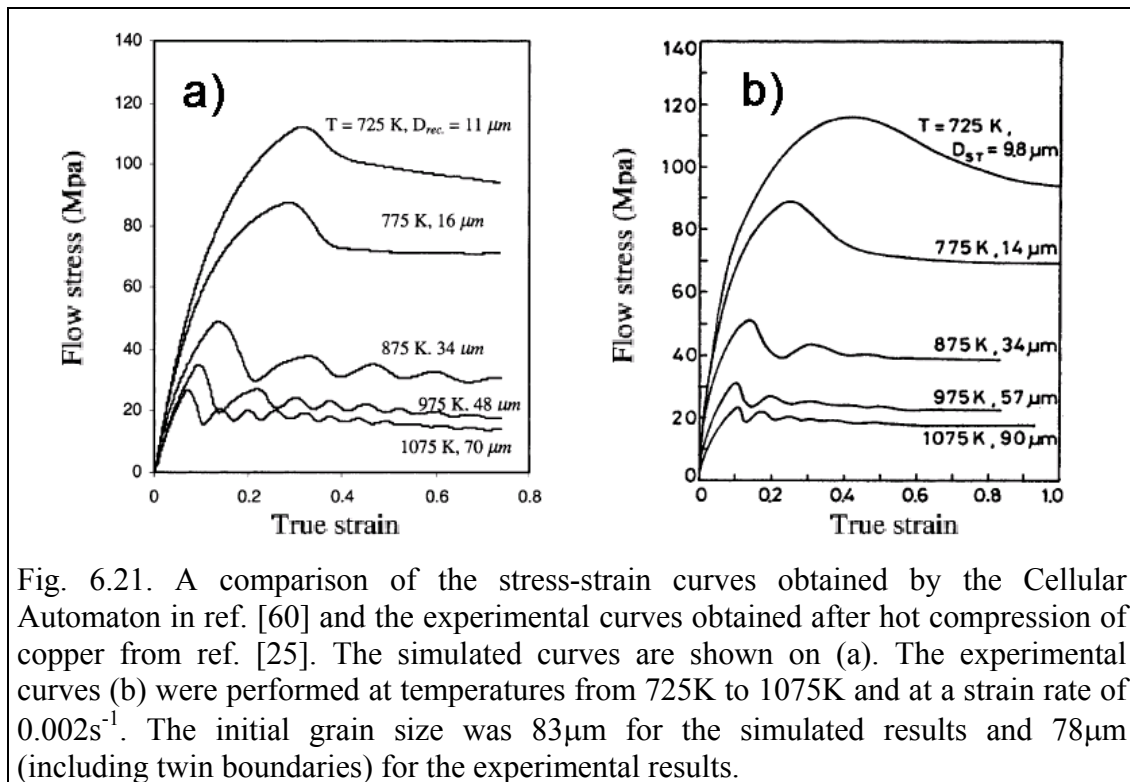
Several questionable assumptions were made to arrive to an expression for N . Like in the Monte Carlo methods instead of directly using eq. 6.12, a physically based equation, the steady state stress during Dynamic Recovery was made equal to $(\rho_T)^{1/2}$. The total number of dislocations, ρ_T , was equal to the total number of cells (Goetz and Seetharaman had 490^2) multiplied by ρ_{DR} . As means of obtaining a value for ρ_{DR} another assumption had to be made, which was based on the concept that during steady state Dynamic Recovery the amount of dislocations generated or increased should be equal to the amount of dislocations annihilated, hence

$$(490^2)(d\rho/dt) = N(\rho_{DR})/2. \quad (6.14)$$

The right-hand side represented the number of cells whose dislocations were halved, however no explanation is given of how annihilating dislocations by half reflected the recovery behavior in a real material. One last unclear value is $K = 6030$, which was used to calculate the coefficient of eq. 6.13, where $3170 = [(490^2)(2^{1/2})/K]^2$. Eq. 6.14 allowed calculating ρ_{DR} , which was needed for comparison after randomly choosing a fraction of grain boundary cells. Goetz and Seetharaman believed that growth of recrystallized grains would also be deformation-controlled by making $\rho_{CR} = 15.88(d\rho/dt)^{0.7}$. However the lack of an associated deformation on all grains when the dislocation density was varied made grains change only their area by growth and not their shape by true strain. On both Monte Carlo methods and the Cellular Automata techniques one visual flaw exists that grains do not flatten despite creating recrystallization collars. Incomplete DRX is experimentally observed on flattened (previously deformed) grains. Nevertheless the Cellular Automata, like the Monte Carlo methods, are also capable of predicting hot flow behavior for different $d\rho/dt$ inputs as fig. 6.19 from Goetz and Seetharaman [44] showed. As happened with the Monte Carlo method no reference was made of how temperature would play a role in the model. Other Cellular Automata models have been created [58, 59] (see fig. 6.20), which reveal the influence of nucleation rate on the hot flow curves, however the results do not seem to improve the attempt of Goetz and Seetharaman. The simulations performed to reproduce the stress-strain behavior did not predict the real behavior at different temperatures for any particular material.



One Cellular Automaton created by Ding and Guo [60] compares simulations to the experimental results obtained by Blaz *et al.* [25] on copper, and seems to have applied eq. 6.12 correctly with remarkable results (see figs. 6.21 and 6.22). Ding and Guo were able to introduce temperature into the simulations, probably by the use of a shear modulus, μ , as a function of temperature [40]. Ding and Guo did not mention what proportionality was used between strain and dislocation density or between strain rate and the increase in dislocation density, but their results show they were also able to



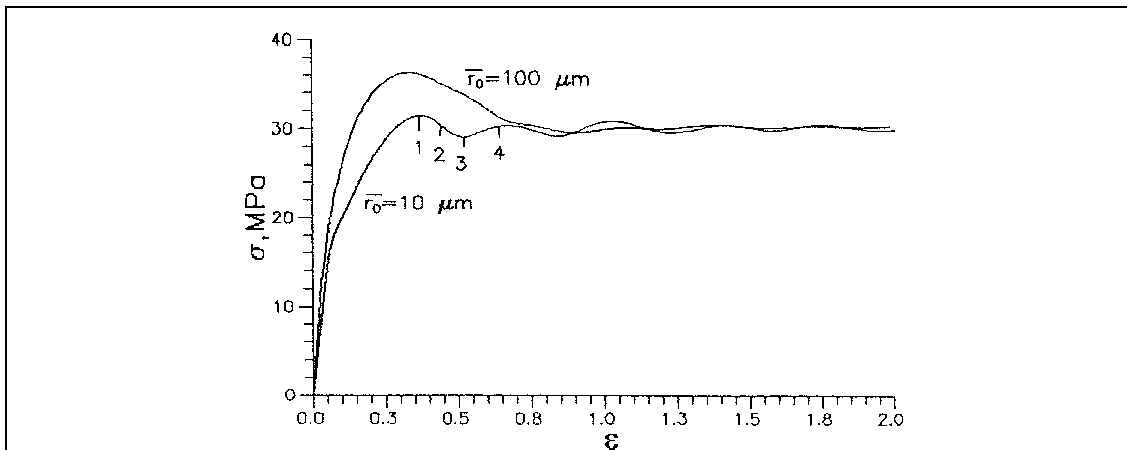


Fig. 6.23. The influence of initial grain size on DRX behavior is shown according to a mathematical model from ref. [45].

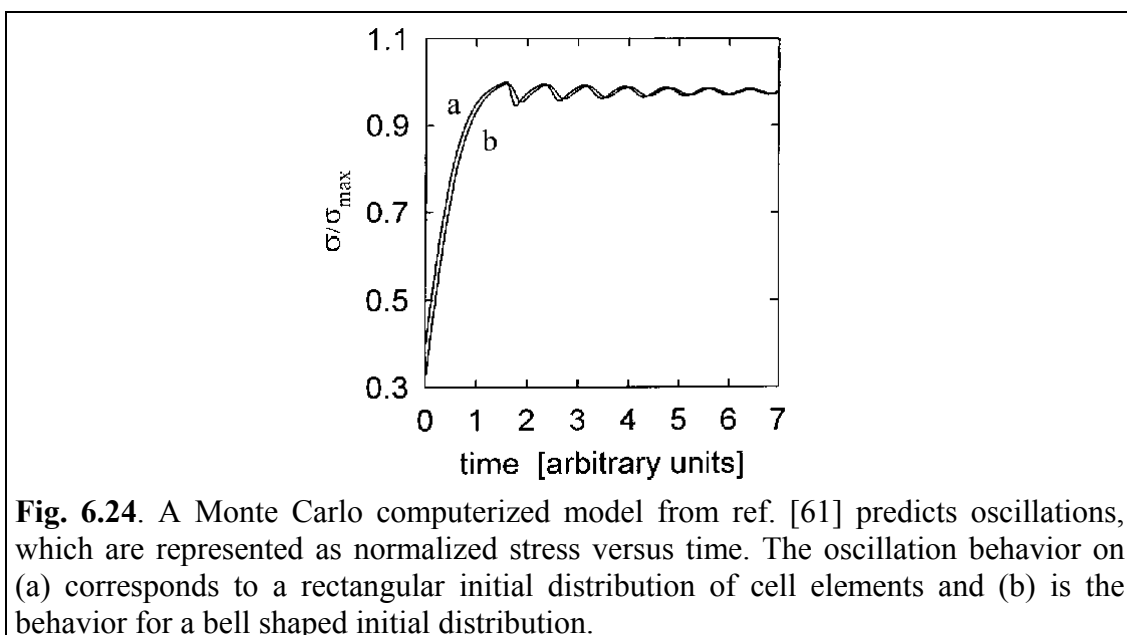


Fig. 6.24. A Monte Carlo computerized model from ref. [61] predicts oscillations, which are represented as normalized stress versus time. The oscillation behavior on (a) corresponds to a rectangular initial distribution of cell elements and (b) is the behavior for a bell shaped initial distribution.

represent true strain correctly instead of using Cellular Automata steps. The work of Ding and Guo still did not address the lack of shape change in the initial grains (initial grains are only consumed by new grains). However without diminishing the remarkable resemblance of the experimental and the simulated curves two differences can be mentioned. The simulated stress-strain curves initially recrystallize at a faster rate than the experimental curves. Secondly the simulated curves oscillate more without attenuating than the experimental curves (see figs. 6.21 and 6.22). The present author believes that the oscillation period and dampening can be described in terms of the Zener-Hollomon parameter as will be shown on a proposed model.

6.8 Other Models for DRX

At least four other DRX models exist, which account for the multiple peak stress behavior. One is a mathematical model presented only at the Recrystallization'92 conferences by Kaptan *et al.* [45]. The Kaptan mathematical model includes concepts

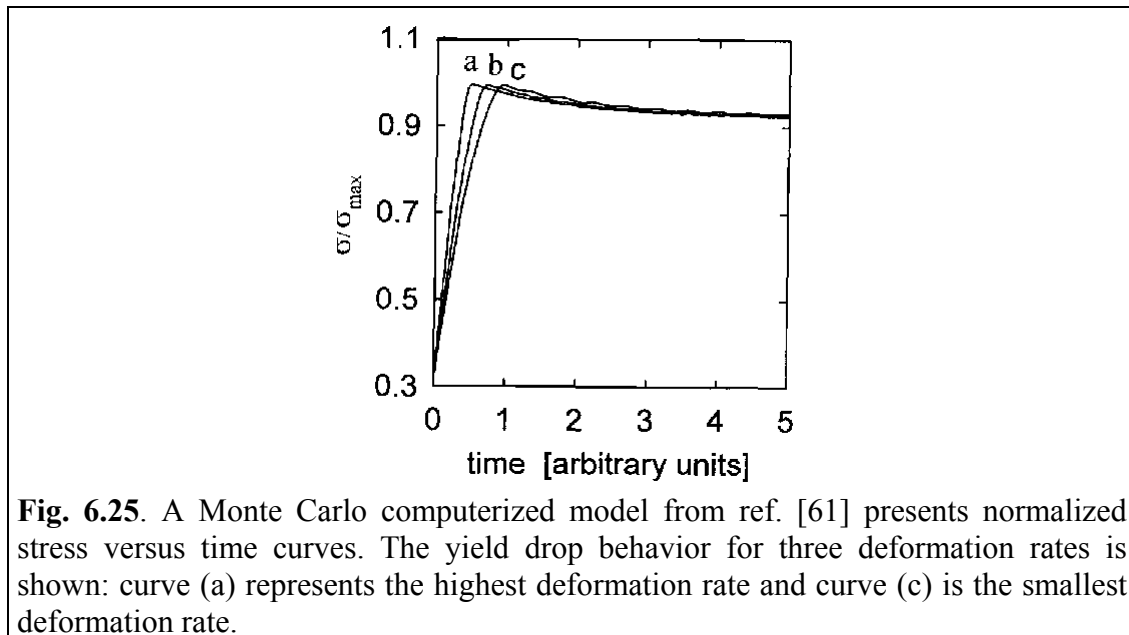


Fig. 6.25. A Monte Carlo computerized model from ref. [61] presents normalized stress versus time curves. The yield drop behavior for three deformation rates is shown: curve (a) represents the highest deformation rate and curve (c) is the smallest deformation rate.

of dislocation density evolution in old and new grains, grain boundary migration and formation of new nuclei. No reference is made to any particular metal, but Kaptan et al. claim to have obtained a stress-strain graph showing the influence of initial grain size on the multiple peak stress behavior (see fig. 6.23). This model is “too complex to be used in practice” [60]. Another DRX model, which also accounts for the multiple peak stress behavior, is the one presented by Kroc et al. [61]. Monte Carlo simulations were used in combination with mathematical, physical and numerical approaches to represent normalized stress versus time curves (see figs. 6.24 and 6.25). These other [45- 48, 61] stress-strain models still need to be compared to real recrystallizing materials. Ponge and Gottstein [62, 63] presented a Percolation model for DRX, but the aim was to model different recrystallizing kinetics on different materials (metals and intermetallics). The question of how to describe the hot flow during multiple peak stress behavior was not addressed. However, a demonstration was presented of how the initial collar of recrystallized grains contributes differently to the total registered stress. The flow behavior of surrounding or percolating new soft grains with low immobile dislocation densities and of initial but hardened grains was expressed as

$$\sigma = (1 - X)\sigma_{def.} + X\sigma_{DRX} \quad (6.15)$$

where $\sigma_{def.}$ is the stress contribution of the initial grain and σ_{DRX} is the stress contribution of new grains, which should have a higher strain hardening exponent. The concept of a registered stress being a contribution of (1) the stress during deformation of initial grains and also of (2) the stress required to deform the new recrystallized grains will be used on this study to model more accurately the transition from single peak to multiple peak DRX.

Table 6.2. The strain increment between the marked lines on fig. 6.26 shows that oscillations may have a relatively constant oscillation period. At higher strain values the marked strain increments seem to decrease slightly.

| ϵ_p | $\epsilon_2 - \epsilon_p$ | $\epsilon_3 - \epsilon_2$ | $\epsilon_4 - \epsilon_3$ | $\epsilon_5 - \epsilon_4$ | $\epsilon_6 - \epsilon_5$ | $\epsilon_7 - \epsilon_6$ | $\epsilon_8 - \epsilon_7$ | $\epsilon_9 - \epsilon_8$ | $\epsilon_{10} - \epsilon_9$ |
|--------------|---------------------------|---------------------------|---------------------------|---------------------------|---------------------------|---------------------------|---------------------------|---------------------------|------------------------------|
| 0.0737 | 0.0307 | 0.0367 | 0.0330 | 0.0225 | 0.0250 | 0.0195 | 0.0284 | 0.0219 | 0.0231 |

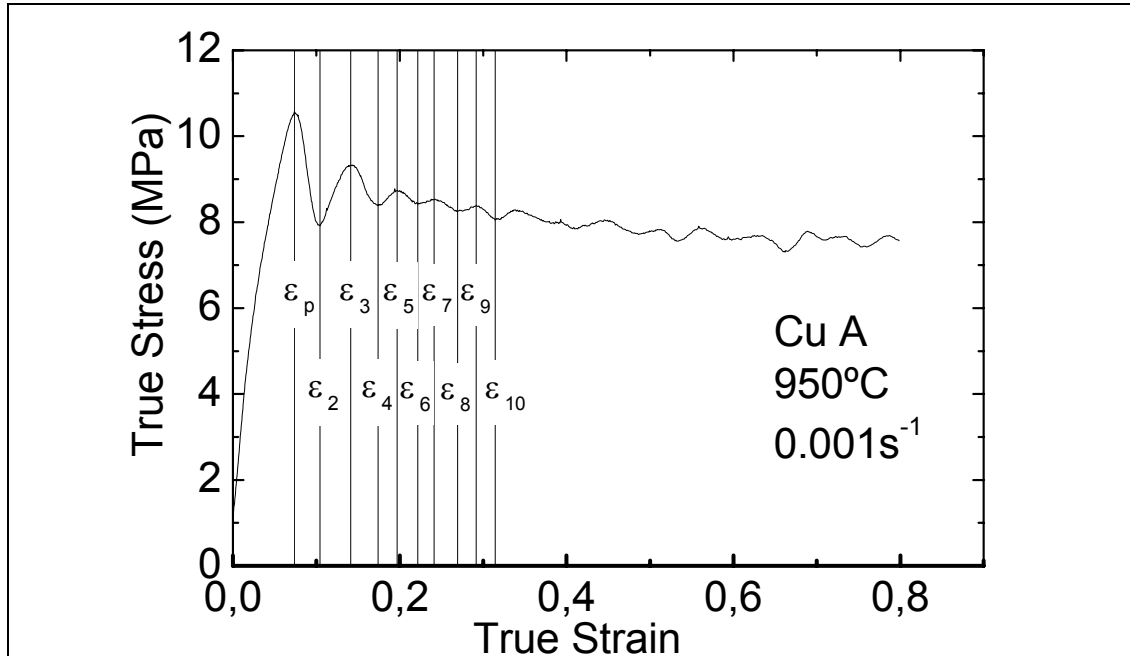


Fig. 6.26. A typical multiple peak hot flow curve shows that oscillation periods are relatively periodic only after the first stress peak, ϵ_p . The stress peaks and troughs are marked with a line and a corresponding strain ϵ_n . The somewhat constant value between peaks and troughs can be seen on Table 6.2.

6.9 A Damped Cosine Avrami Model for DRX

Engineers have modeled dynamic systems of the spring-mass-damper type or the capacitance-inductance-resistance type [64], whose behavior resembles the attenuated oscillations during multiple peak DRX [65]. Another analogy is that of graphed equations used to model transient response characteristics [66] with that of the stress-strain behavior of hot flow curves. The similitude could lead to believe that the fundamental laws that explain DRX have the form of a damped sine mathematical expression. However a comparison would show that damped sine equations have a constant oscillation period whereas in hot flow curves the oscillation period remains somewhat constant only after the first stress peak. Table 6.2 shows the strain registered after each stress peak of fig. 6.26, a typical hot flow curve where multiple peaks are present. The strain necessary for the first stress peak is almost equal to the period during oscillations. One single damped sine equation could never resemble the described behavior during multiple peak DRX.

Some hot flow models, like the Avrami model, have assumed a discontinuity when DRX appears, and separate the hot flow model into two parts: restoration until the peak stress and then by DRX. A comprehensive separation of the two processes would allow use of a damped oscillatory equation to describe the DRX behavior of the hot

flow curves of Cu A. As pointed before for Cu A and other metals the oscillations dampen towards a lower value instead of a central value. The present author in the absence of a reliable model to physically describe the oscillations that may appear during DRX will propose a mathematical equation, which can help describe quantitatively the hot flow behavior patterns. The proposed constitutive equation for DRX after the peak strain can be divided into two stresses: a damped oscillatory stress and a descending stress of the Avrami type, this last stress serves as the mean oscillatory stress value. And represents the stress as the advancing recrystallization collar consumes the initial now hardened grain. An analogy of the hardened grain with a composite material would allow imagining the un-recrystallized volume fraction as the hard particles of the composite. The recrystallized volume would represent a softer continuous path that allows a heterogeneous strain rate under the same stress. The damped oscillatory stress value fluctuates above and below the mean oscillatory stress value. The fluctuations correct the mean oscillatory stress value and thus a better account is made of the percolating recrystallized volume around hardened initial grain.

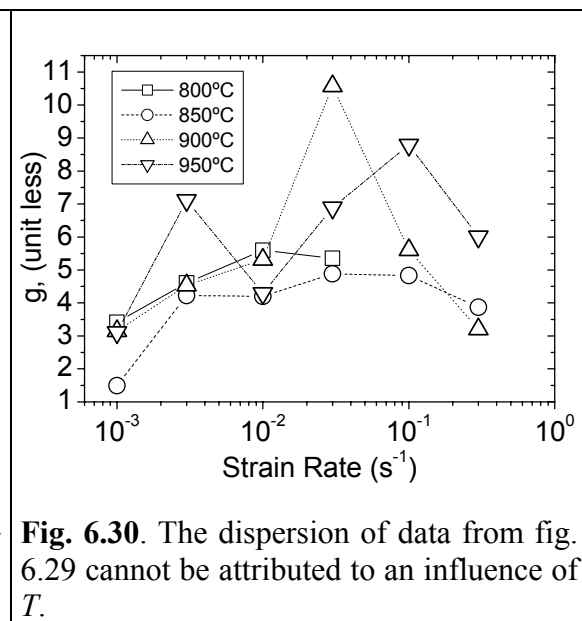
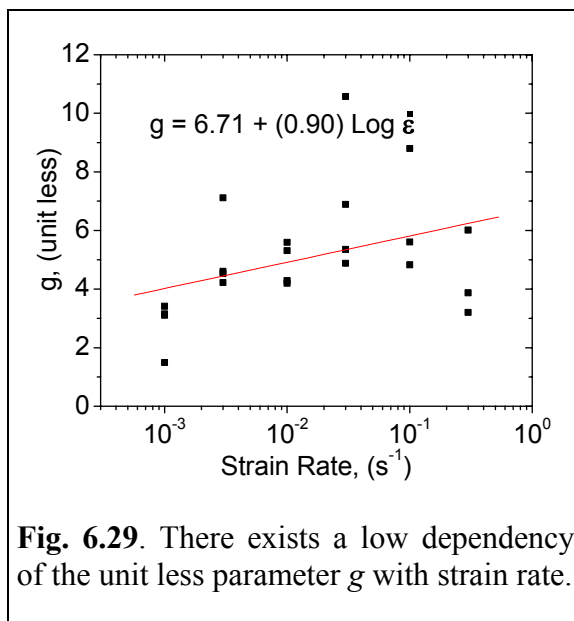
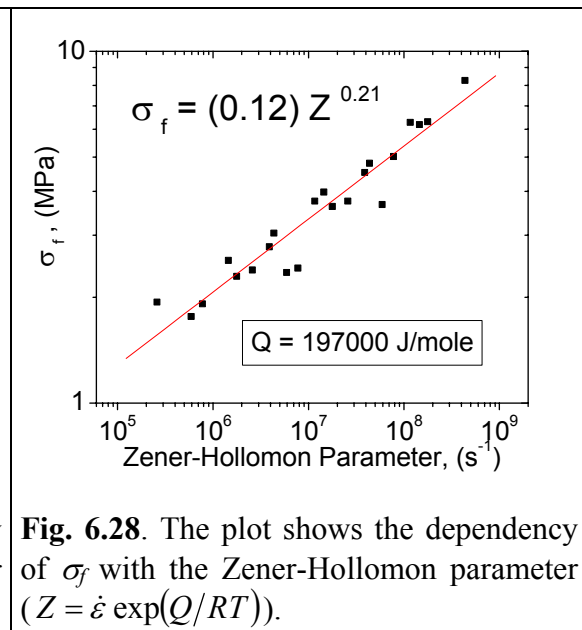
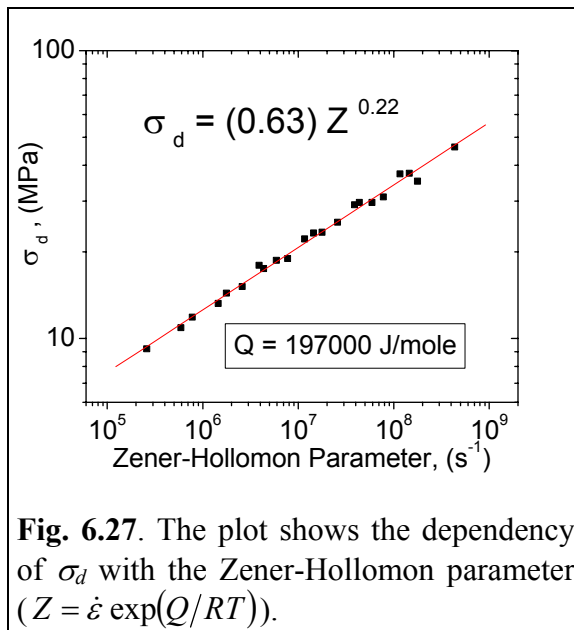
When most of the initial grain volume has been consumed, the first recrystallization collars have grown and if those first collars are strain-hardened until reaching once again a critical dislocation density then an oscillatory stress behavior is noted. In an analogy to the model proposed by Ponge and Gottstein, eq. 6.15, the mean oscillatory stress represents the initial grain size volume contribution, which has not been consumed despite reaching a trough on the stress-strain curve. However the damped oscillatory stress does not represent the percolating collars of new grains, but is a correction due to inhomogeneous strain-hardening rates. New grains grow, harden and recrystallize at a faster rate than the initial grain size volume. The higher grain boundary area on the newer smaller grains increases the nucleation rate locally, but the nucleation rate for the remaining initial grain size is slower, thus two behaviors need to be considered. One behavior is the mean oscillatory stress, σ_{mo} , which has the Avrami form of eq. 6.8 and is written as

$$\sigma_{mo} = \sigma_d - \sigma_f \left\{ 1 - \exp \left[-g(\varepsilon - \varepsilon_p) \right] \right\} \quad (6.16)$$

where σ_d is only equal to the peak stress, σ_p , when DRX is considered monotonic but, as the multiple peak stress behavior appears σ_d represents the maximum value the mean oscillatory stress will have in the absence of stress oscillations. On fig. 6.11 the Avrami exponent n_A had been shown to be approximately equal to one during monotonic stress behavior. The Avrami term on eq. 6.16 proposes that n_A is always equal to one and that other values commonly measured are the result of measuring the oscillatory stress component of DRX. The DRX rate or rate of stress descent is given by g . The steady state stress, σ_{ss} , to which the hot flow tends to, is given by

$$\sigma_{ss} = \sigma_d - \sigma_f \quad (6.17)$$

Figures 6.27, 6.28, 6.29 and 6.30 show the values obtained for σ_d and σ_f , which are a function of Z , however g , which is almost constant, has been correlated to the strain rate. Figures 6.31 and 6.32 show an example of how to calculate these values from an experimental compression test. The values were obtained after performing a number of Levenberg-Marquardt iterations until chi squared could not be reduced. The iterations were performed using commercial data analysis software, Origin 6.0. Only the part of hot flow after the peak stress is analyzed that is why the peak strain is subtracted from



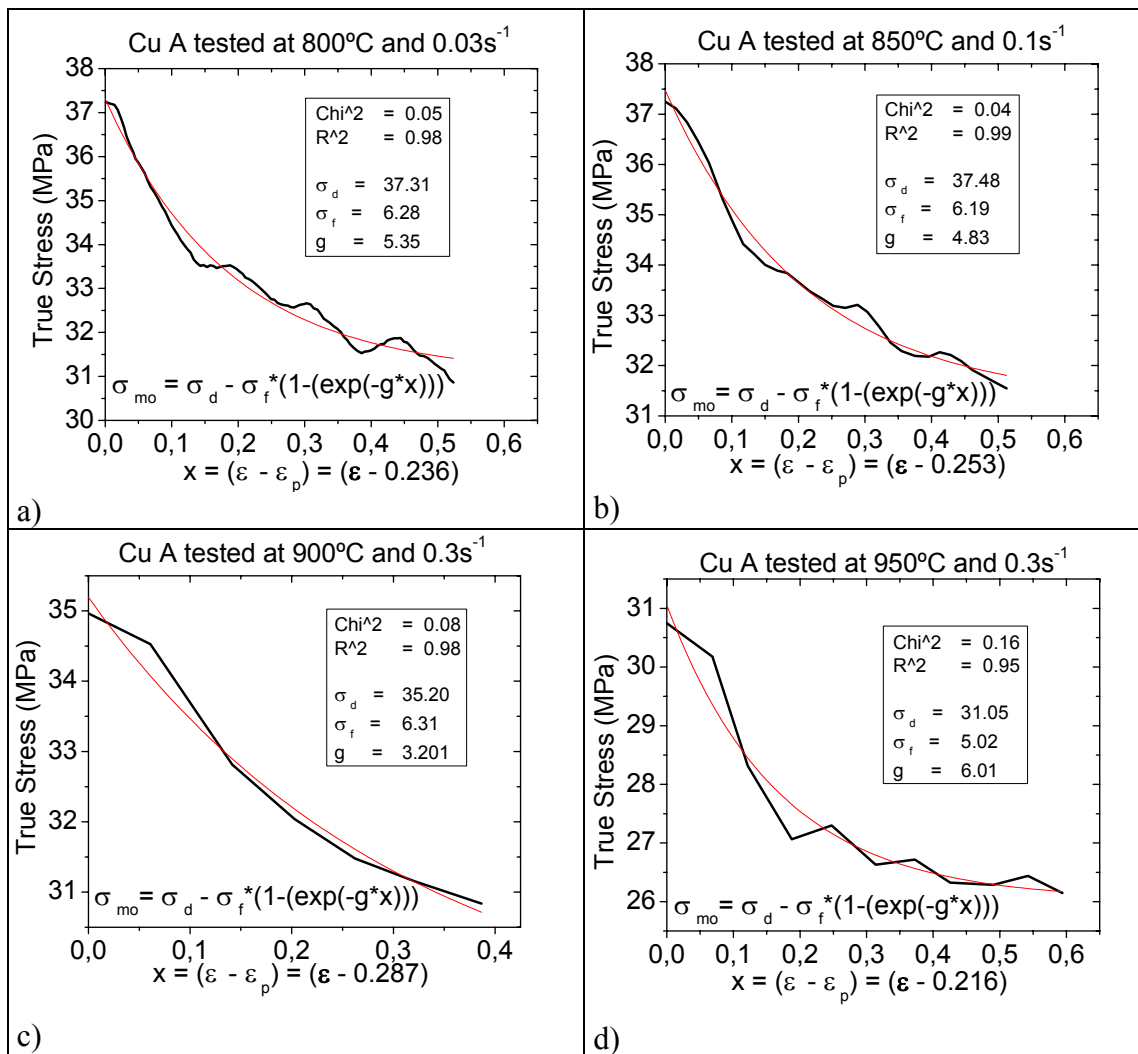


Fig. 6.31. Plots show the calculation method and best fit of the parameters involved on the mean oscillatory stress (σ_{mo}) equation 6.16. The examples belong to higher Z conditions where single peak DRX occurs. The fitted curve evidently does not follow the same DRX kinetic path and will be corrected to account for the steeper slope, which is a consequence of the smaller contribution by dynamically recrystallized grains.

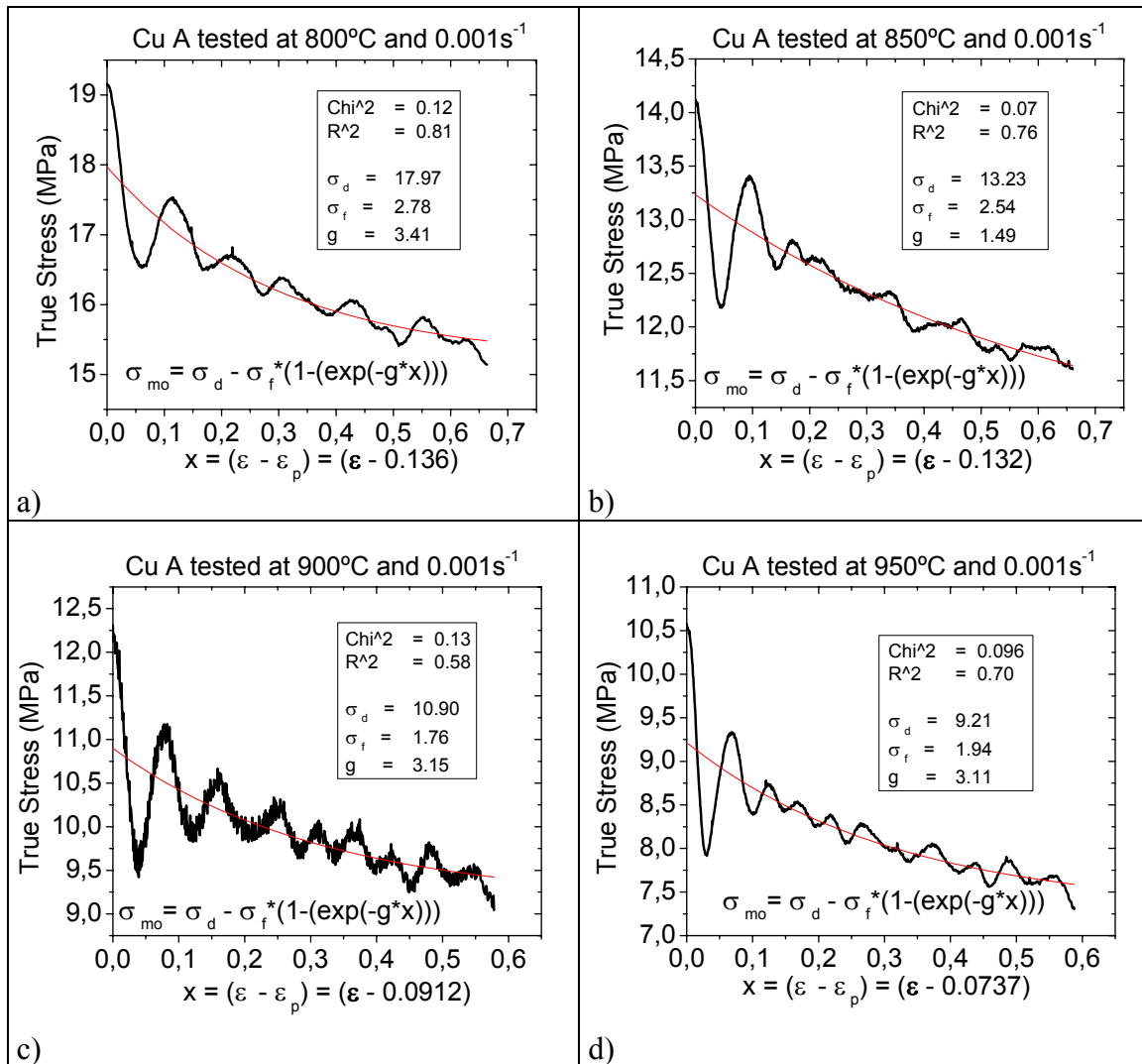


Fig. 6.32. Plots show the calculation method and best fit of the parameters involved on the mean oscillatory stress (σ_{mo}) equation 6.16. The examples shown are of lower Z conditions where multiple peak DRX occurs. The mean oscillatory stress measures the decrease in stress as the initial grain volume is consumed by DRX. The plots show that during the multiple peak behavior parts of the initial volume have yet not recrystallized. The diminishing contribution to total stress of hardened initial volume is evident by the direction of the oscillations. A saturation steady state stress value can easily be foreseen.

the strain axis. Figure 6.31 shows examples of single peak stress behaviors and fig. 6.32 shows examples of tests with multiple peak stress behaviors.

The second behavior is introduced through the damped oscillatory stress, σ_{do} , which is a cosine expression attenuated by an exponential term that tends to zero. When the Z conditions for monotonic DRX are present then the damped oscillatory stress is almost non-existent, but gradually when the temperature and strain rate approach the so-called Z_c conditions the damped oscillatory stress increases. The gradual appearance of multiple peak DRX is contrary to the general description of hot flow curves however an abrupt appearance of oscillations has not been proven yet. The line drawn by the D_0 - Z_c relationship implies that when D_0 is immediately above the line then single peak DRX is expected and that when D_0 is immediately below then multiple peak DRX happens. Instead a gradual change is what has been observed during this study. The damped oscillatory stress, σ_{do} , is written as

$$\sigma_{do} = \sigma_r \exp[-s(\varepsilon - \varepsilon_p)] \cos[v(\varepsilon - \varepsilon_p)] \quad (6.18)$$

where σ_r is a complementary stress to the maximum value of the mean oscillatory stress and is only significant during multiple peak DRX. Thus the peak stress, σ_p , can be defined as

$$\sigma_p = \sigma_r + \sigma_d. \quad (6.19)$$

The coefficients s and v are semi-logarithmically dependent on Zener-Hollomon parameter, Z . Consequently, as Ding and Guo [60] concluded, oscillations depend on the rate of dislocation accumulation in the new recrystallized grains and on the initial grain size, so will the coefficients s and v depend on such conditions, however during this study only one grain size was tested. For copper Blaz *et al.* [25] had already shown that the magnitude of the peak stress depended on the initial grain size (see fig. 6.33 from [25]), hence the parameters that describe hardening until the peak strain (*i. e.* σ_r and σ_d) also depend on the initial grain size. Figures 6.34, 6.35 and 6.36 show the relationship of σ_r , s and v with the Zener-Hollomon parameter. The data seems scattered on fits of σ_r and s , however the value range is small, 1.8 MPa for σ_r and 18 for s . A remarkable measurement this proposed model allows is shown on fig. 6.36, which describes how the period in the oscillations during DRX is completely predictable in terms of temperature and strain rate. Earlier filters [67] had not been able to quantify the variation from experimental data. The period, $2\pi/v$, is the amount of strain between stress peaks, which is smaller at lower Z values (higher temperatures and slower strain rates). If the Luton and Sellars nomenclature is remembered, half a period corresponds to the strain necessary for one DRX cycle, ε_x , and thus can easily be calculated knowing v . At lower Z values the initial amplitude, $2\sigma_r$, of the damped oscillatory stress is maximum. Figures 6.37, 6.38, 6.39 and 6.40 show the values obtained for σ_r , s and v after performing a number of Levenberg-Marquardt iterations until chi squared could not be reduced.

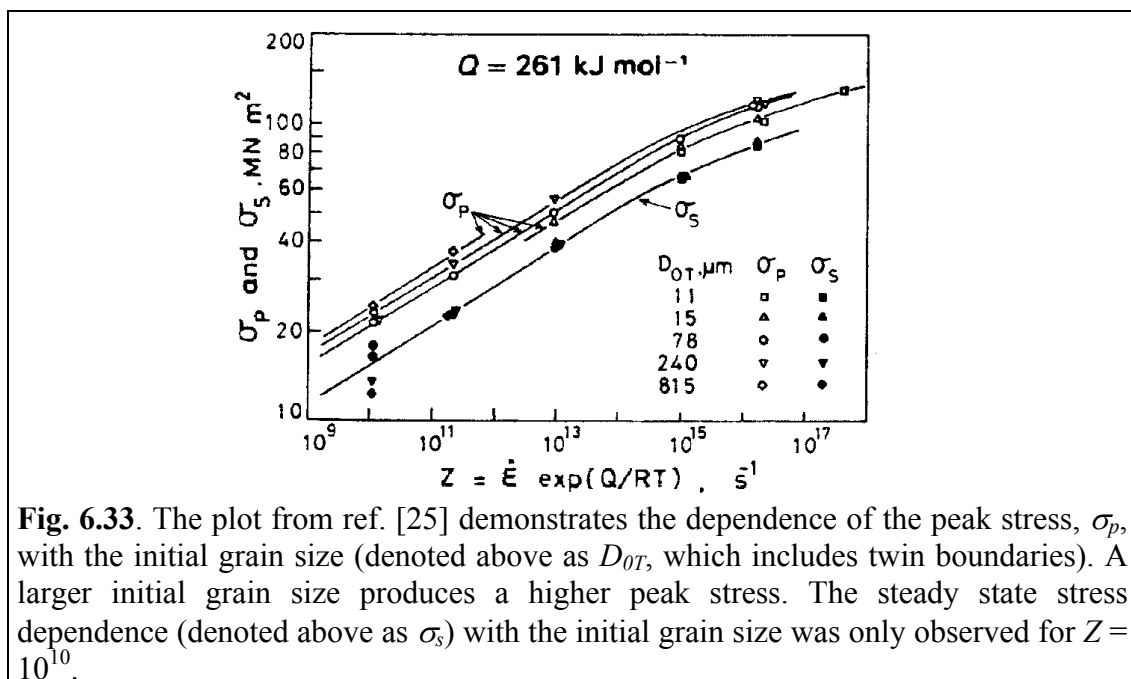


Fig. 6.33. The plot from ref. [25] demonstrates the dependence of the peak stress, σ_p , with the initial grain size (denoted above as D_{0T} , which includes twin boundaries). A larger initial grain size produces a higher peak stress. The steady state stress dependence (denoted above as σ_s) with the initial grain size was only observed for $Z = 10^{10}$.

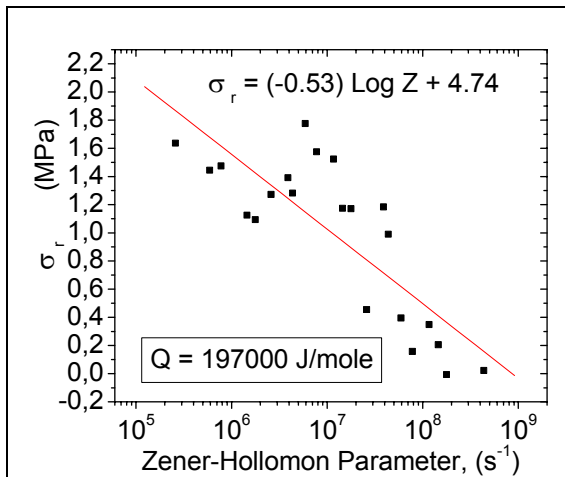


Fig. 6.34. The plot shows the dependency of σ_r with the Zener-Hollomon parameter ($Z = \dot{\epsilon} \exp(Q/RT)$).

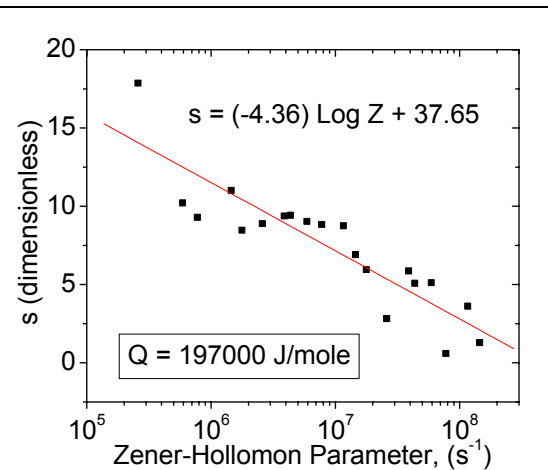


Fig. 6.35. The plot shows the dependency of s with the Zener-Hollomon parameter ($Z = \dot{\epsilon} \exp(Q/RT)$).

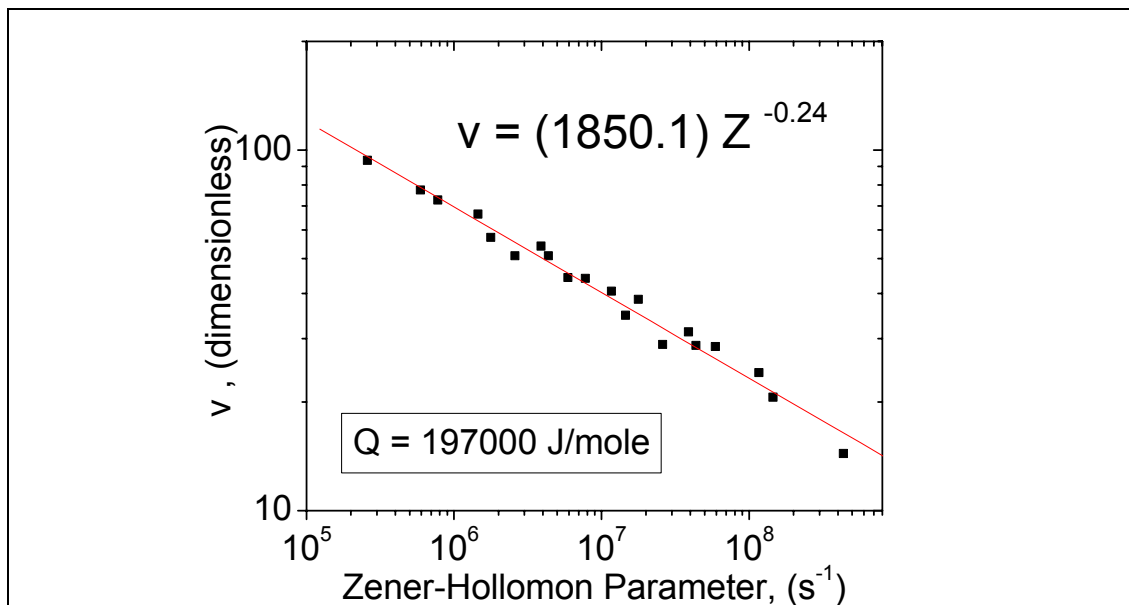


Fig. 6.36. The plot shows the close dependency of v with the Zener-Hollomon parameter ($Z = \dot{\epsilon} \exp(Q/RT)$). The parameter v is related to the period of the oscillations during multiple peak DRX and thus is related to the strain necessary to dynamically recrystallize a major fraction of initial volume (a recrystallization cycle, ϵ_x). The plot demonstrates that the oscillation period is predictable.

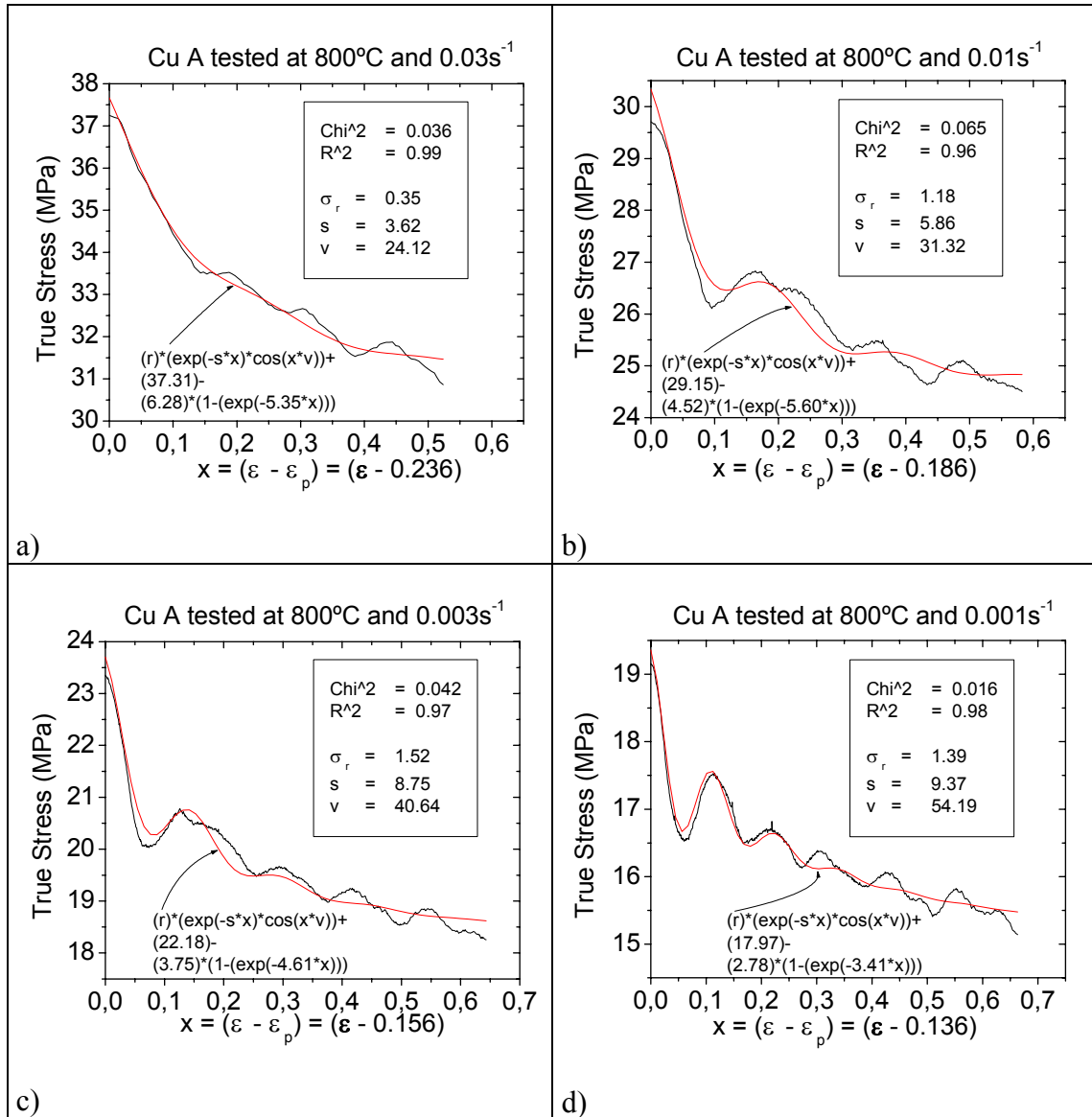


Fig. 6.37. The plots at 800°C show the fitting method for evaluating σ_r , s and v once the parameters involved in the mean oscillatory stress are known. The fitting is achieved by individually adding the mean oscillatory stress (eq. 6.16) to the damped oscillatory stress (eq. 6.18) whose values are unknown. The damped oscillatory stress corrects the mean oscillatory stress for the influence dynamically recrystallized grains have on the total stress. The match created between the fit and the experimental data is unprecedented in literature.

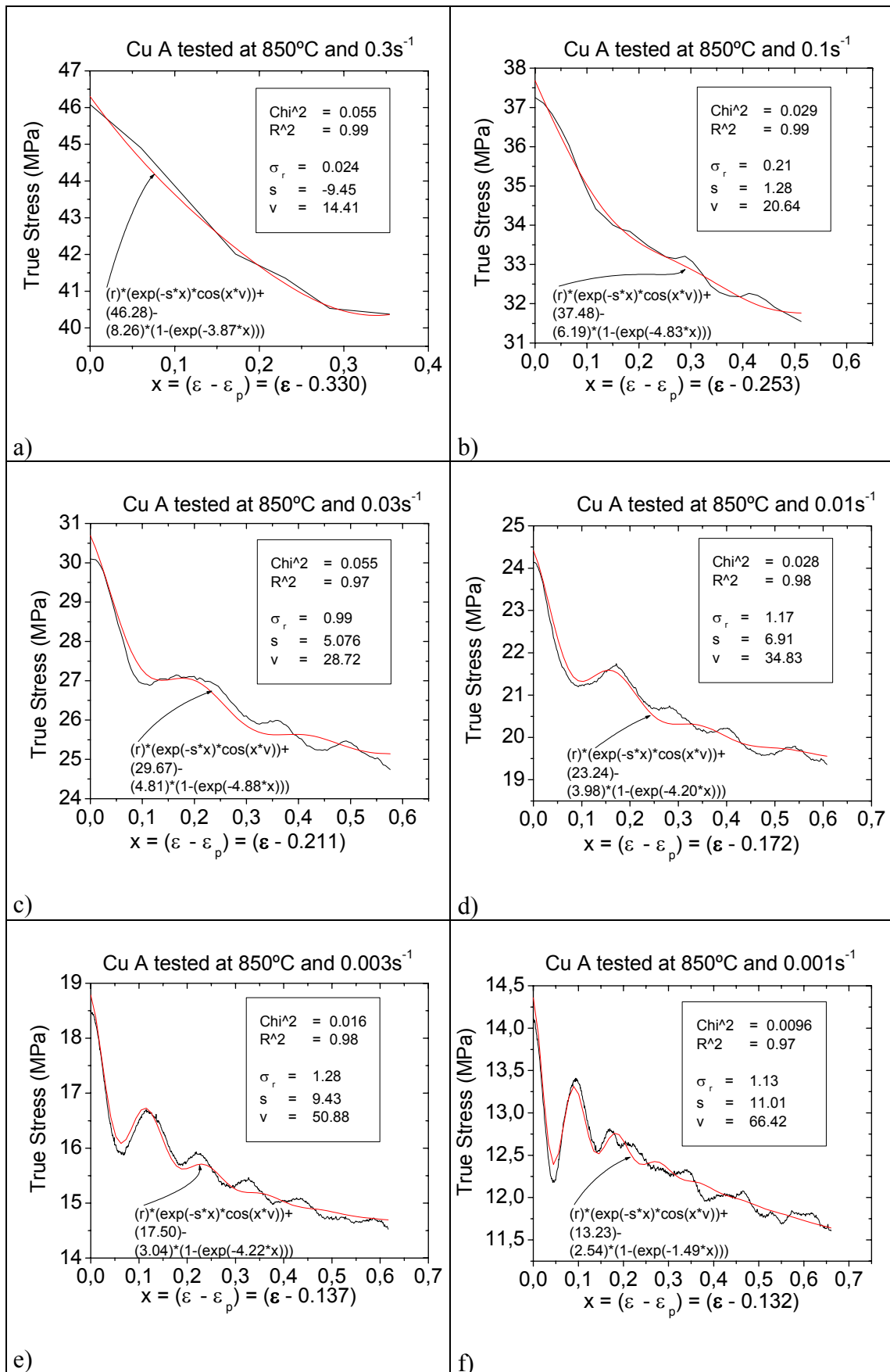


Fig. 6.38. The plots at 850°C show a reliable match between fit and experimental data.

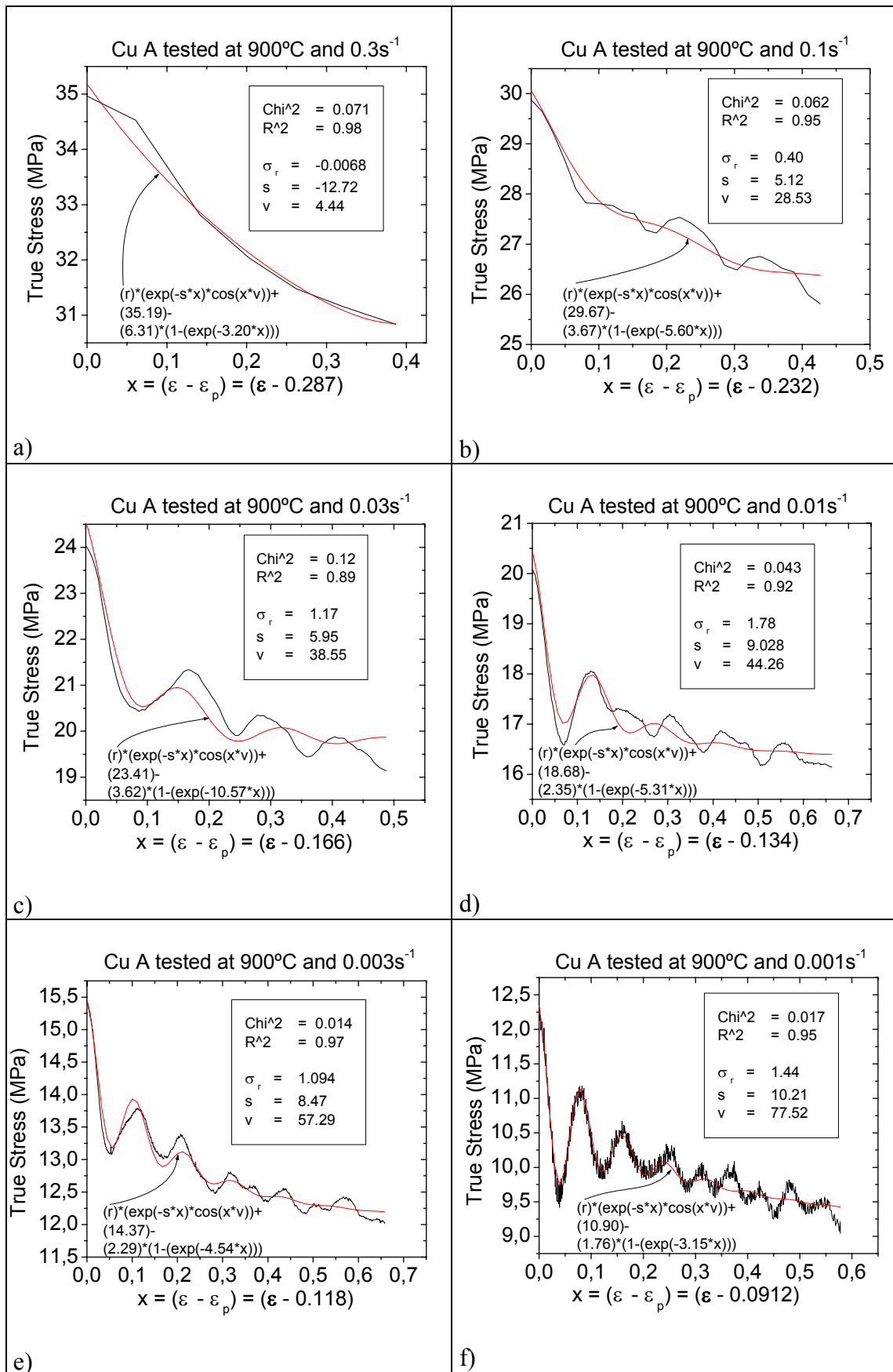


Fig. 6.39. The plots at 900°C show a reliable match between fit and experimental data.

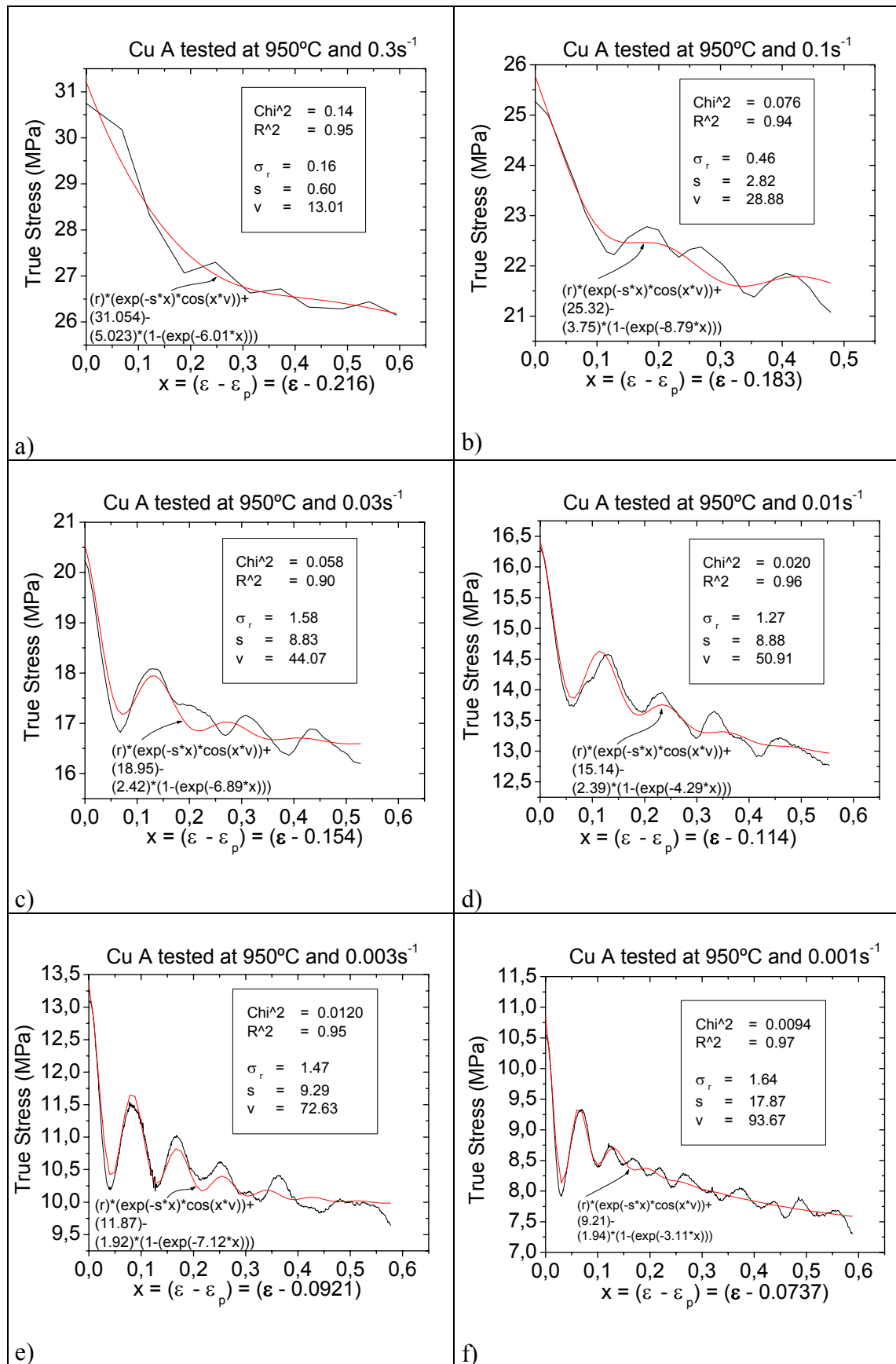


Fig. 6.40. The plots at 950°C show a reliable match between fit and experimental data.

The proposed model was able to discern from experimental noise and DRX cycles. The assumption that not all the initial volume or not all places of the test sample recrystallize after the first cycle is needed to describe stress during multiple peak DRX. The stress registered during hot flow, σ , is then expressed as

$$\sigma = \sigma_{mo} + \sigma_{do} \quad (6.20)$$

where the mean oscillatory stress, σ_{mo} , is the contribution of the initial grain volume or places in the test sample that are about to undergo DRX even during the multiple peak behavior. And the damped oscillatory stress, σ_{do} , is the correction due to the first dynamically recrystallized grains that are able to harden and recrystallize more than once. In a sense, the concept suggested by Ponge and Gottstein [62, 63] still prevails, the registered stress during hot flow is a contribution of a hardened grain volume and of a new grain volume that percolates around harder grains. However the new grain volume can recrystallize again if strain rate and temperature conditions allow.

At slower strain rates less critical strain is necessary to recrystallize a major fraction of the initial volume, but the driving force for growth is higher, because enough time ($\varepsilon/\dot{\varepsilon}$) produces a slow increase the dislocation density of the new grains, thus new nuclei will also have time to grow considerably before hardening once again and the onset DRX occurs. The result is nuclei that grow beyond their initial DRX grain size; consequently multiple peaks are created on the stress-strain curve. At higher strain rates more critical strain is necessary to recrystallize a smaller fraction of the initial grain volume. The new nuclei are not only smaller but have less driving force for growth, because fast strain accumulation increases the dislocation density within new grains faster than the growth rate. The driving force for growth (i.e. a difference of dislocation density on both sides of an advancing grain boundary) rapidly disappears. It has been said [1, 13] that recrystallization collars are not synchronized during single peak stress behavior, because before the initial volume is consumed several collars have reached a critical strain to recrystallize once again. The small stress contribution of the first DRX collars as they soften again by another DRX cycle during the single peak behavior is only noticeable enlarging the graph (see the single peak DRX curves on figs. 6.37, 6.38, 6.39 and 6.40). Even when enlarged one may believe that the small oscillations belong to noise on the load cell of the testing apparatus, however eq. 6.20 (at high Z values) of the proposed model only recognizes the larger strain periods and smaller oscillating amplitudes due to DRX of a major fraction of initial volume. When multiple peak behavior occurs the DRX collars have consumed most of the initial grain volume and thus most of the volume will recrystallize again at the same time in a synchronous manner. The damped oscillatory stress component of eq. 6.20 acquires more relevance during a more synchronized DRX.

The Damped Cosine Avrami Model only explains the hot flow behavior during DRX of types I, II, III and VI (explained earlier on fig. 6.6), which were the grain refinement cases found during this study. The multiple peak DRX of type V where grain coarsening is the result still needs to be explored using the proposed model. However a change in sign on eq. 6.16 can be expected as a result of having a higher growth rate than a dislocation accumulation rate before approaching steady state conditions where the sum of dislocations accumulated and restored should be almost zero. The developed model fits well into existing hot flow theories. No mention has been made yet of important stress-strain curve characteristics, because other researchers have dealt with these characteristics and presented adequate prediction models. Some of the important

stress-strain characteristics to successfully model a hot flow curve are: the peak stress, the onset of DRX, the strain-hardening rate and dynamic recovery. Briefly some prediction theories will be reviewed as means of demonstrating that the proposed Damped Cosine Avrami Model can adequately be used to better predict the hot flow behavior during DRX. One other self-criticism is the fact that during the development of the proposed model the strain, ε , was used as a state variable of the hot flow process when in reality the local and average dislocation densities are the variables that promote deformation. Strain as used on the proposed model is dependent on the history of strain accumulated. However an approximate dislocation density, ρ , can be calculated using eq. 6.12, because eq. 6.16 and eq. 6.18 provide values for the stress contribution of the advancing DRX and the necessary correction due to dynamically recrystallized grains. The density values would be approximate because beyond a certain value of stress α in eq. 6.12 loses validity. In light that the proposed model has been shown to reliably predict the stress-strain values, thus the dislocations densities calculated with eq. 6.12 should allow better estimates of a new stress-strain curve when temperature and/or strain rate conditions are varied. Hence with aid of eq. 6.12 the proposed model acquires an independence from strain history requirements. However the first aim of the proposed Damped Cosine Avrami Model is to help predict the stress-strain behavior during a compression strain path of a particular 99.9% pure copper as critical Z_c conditions are approached.

6.10 Modeling the Peak Stress

The prediction of the peak stress and steady state stress had been an earlier challenge for scientists. Zener and Hollomon [68] cited the work of Nadai and Manjoine [69] on copper where an Arrhenius graph was able to unify stress-strain rate data at different temperatures using a temperature compensated time parameter, now called the Zener-Hollomon parameter. Time rate relationships associated to the deformation of materials and their dependence on temperature and stress have been developed using Arrhenius type equations where an activation energy, Q , governs the process. Table 6.3 shows some of the stress, temperature and strain rate relationships developed.

Table 6.3. Arrhenius equations developed to express strain rate, $\dot{\varepsilon}$, temperature, T , and stress, σ . Where R is the universal gas constant. E is the elastic modulus. D is the diffusion coefficient (see [40]). $A, A', A'', A''', A''', \alpha, \alpha''$ and α''' are material constants.

| Equation | Equation number |
|--|-----------------|
| $\dot{\varepsilon}_s = A'[\sigma/E]^{n'} \exp(-Q/RT)$ | (6.21) |
| $\dot{\varepsilon}_s = A'' \exp(\alpha''' \sigma) \exp(-Q/RT)$ | (6.22) |
| $\dot{\varepsilon}_s = A'''(\sinh \alpha'' \sigma)^{n''}$ | (6.23) |
| $\dot{\varepsilon} = A''''(\sinh \alpha \sigma)^n \exp[-Q_{app}/RT]$ | (6.24) |
| $[\dot{\varepsilon}/D(T)] = [A(\sinh \alpha[\sigma/E(T)])]^5$ | (6.25) |

The study of creep has rendered the understanding of several deformation mechanisms, which are also explained by Arrhenius type diffusion laws [40]. Power laws have

described creep rates (see eq. 6.21 on table 6.3) when stresses are intermediate to low or by exponential expressions (see eq. 6.22 on table 6.3) when the stresses are high. However the transition point to use eq. 6.21 or eq. 6.22 was never established, instead a more general expression was proposed to solve the power law breakdown. Garofalo [70] proposed eq. 6.23 that seemed to unify high and low stress values. Later Sellars and Tegart [71] proposed eq. 6.24, which unified stress data at high and low Z values. Weertman [36] had demonstrated the near equality of the activation energy of high temperature creep, Q_{creep} , and the activation energy for self-diffusion, Q_{sd} . The ultimate rate controlling process during high temperature creep of pure materials was attributed to self-diffusion. Thus the proper Q value to use in equations 6.21, 6.22 or 6.24 should be the activation energy for self-diffusion, however researchers found that using the activation energy for self-diffusion did not produce acceptable correlations when studying alloyed or precipitate bearing materials. The calculation of an apparent activation energy, Q_{app} , is a common practice [72] to best describe data from a wide range of Z values. The apparent activation energy controls the rate of the process and is not necessarily equal to the activation energy of self-diffusion, because Q_{app} is increased to engulf the additional energy required by other strengthening mechanisms (e.g. precipitation hardening in coppers [31]).

Earlier during the introduction of this work it had been mentioned that for Cu A the apparent activation energy and the activation energy for self-diffusion were relatively the same (213KJ/mole and 197KJ/mole respectively). The reason for the proximity is the low oxygen content in Cu A, only 26 ppm, which forms few precipitates that may raise the hot flow stress. The activation energy for self-diffusion has been used during this work, which allowed the study of partial values involved in the description of flow stress (σ_r , σ_d , and σ_f) and coefficients involved in the description of strain (s , v , g , and ε_p). If another copper or material with different apparent and self-diffusion activation energies had been chosen then both energies would have been necessary when applying the Damped Cosine Avrami Model. The apparent activation energy would best fit values correlated to σ_r , σ_d , and σ_f . And the activation energy for self-diffusion would best fit values correlated to s , v , g , and ε_p . The selection of Cu A conveniently allows a clear explanation of the Damped Cosine Avrami Model.

Ever since Sellars and Tegart [71] presented eq. 6.24 much discussion has been raised over the lack of physical basis or the proper means to calculate A''' , α , n and even Q_{app} . Frost and Ashby [40] wrote: "Lacking any physical model it must be considered fortuitous that any set of n and α can correctly describe the behavior over a wide range of stresses". Tanaka *et al.* [73] reviewed the difficulties in calculating n , α and, Q_{app} where a best fit was not possible because of the data's temperature range. Tanaka *et al.* also showed that 10% variation of parameters n and α did not produce serious effects over the regression. However Q_{app} , which is dependent on temperature, strongly affects the regression. Other algorithms to best fit the stress-strain rate data have followed [74]. The stress-temperature-strain rate relationship of eq. 6.24 has been rearranged to have a more physical meaning by acknowledging the role of diffusion and the elastic modulus have on high temperature deformation processes. As a consequence on eq. 6.25 the diffusion coefficient, $D(T)$, normalizes the strain rate, and the elastic modulus, $E(T)$, normalizes the registered stress (see [40]). The exponent n has been found to be close to 5 for many metals [70, 71] when deformation is controlled by dislocation climb and glide over obstacles. The diffusion coefficient is an Arrhenius type equation, which contains the activation energy to be calculated. The graph on

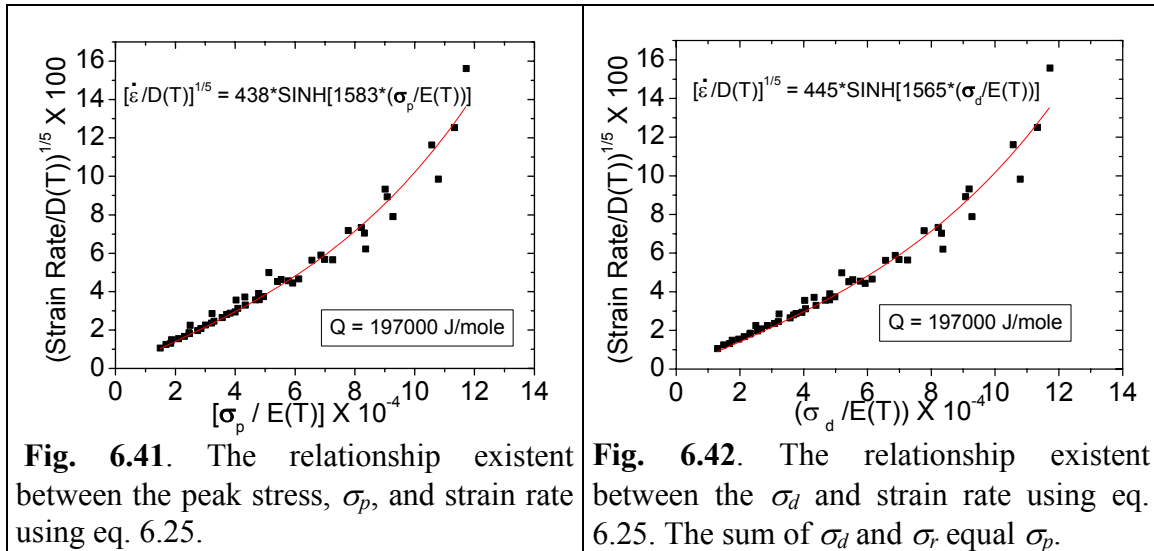


Fig. 6.41. The relationship existent between the peak stress, σ_p , and strain rate using eq. 6.25.

Fig. 6.42. The relationship existent between the σ_d and strain rate using eq. 6.25. The sum of σ_d and σ_r equal σ_p .

fig. 6.41 shows the best fit of the peak stress-strain rate data of Cu A using eq. 6.25. A value of $A_p = 438$ and $\alpha_p = 1583$ had been reported earlier [34] for the relationship between σ_p and $\dot{\epsilon}$. However eq. 6.19 of the proposed model divides the peak stress into two contributing components of which σ_d is always present and is of higher value. Figure 6.42 shows the relationship between σ_d and $\dot{\epsilon}$ where the best fitted values are $A_d = 445$ and $\alpha_d = 1565$. The correlation coefficient r^2 is almost the same for both regressions 0.96929 for σ_p and 0.96947 for σ_d . An objection may be raised to the use of eq. 6.25 to correlate σ_d values when σ_d values are not actual points on the observed stress-strain curve. The value of σ_d represents the maximum value of the mean oscillatory stress. An optimum correlation would and should not be possible, but the correlation coefficient values tell otherwise. Equation 6.25 is equally capable in predicting values of σ_d or σ_p .

The point in exposing the unifying limitations of eq. 6.25 is to justify the use of a power law relationship to better correlate values of σ_d with $\dot{\epsilon}$ and T . Application of the Damped Cosine Avrami model needs that the prediction of σ_d be as close as possible to the actual value. For that matter at low Z values a power law relationship of the form

$$\sigma_d = K_d Z^{n_d} \tag{6.26}$$

is used to make a prediction. Unfortunately using a power law relationship for higher temperatures and low stresses instead of using a hyperbolic sine equation is going back to the time when different relationships needed to be used depending on the data range, but no other choice is available to improve the correlation. Hyperbolic sine equations, like eq. 6.24 and eq. 6.25, unify data at low and high Z values, but do so sacrificing precision at both ends of the data range. Figure 6.27 showed the best fitted values of the power law relationship represented by eq. 6.26 where $K_d = 0.62749$ and $n_d = 0.21697$. The correlation coefficient, r^2 , obtained using eq. 6.26 is 0.9895, which substantially improves the needed prediction of σ_d . The constant K_d is function of the initial grain size so that $K_d = C_d D_0^{m_d}$, however the latter relationship was not set as an objective of this experiment. A transition point where to stop using a power law relationship has

never been established, here and based on observations for Cu A the transition point is set when $Z = 1.5 \times 10^8$. When Z values are above 1.5×10^8 then the hyperbolic sine expression shown on fig. 6.42 will be used. At higher Z values the relative absence of σ_r (because σ_d is much larger) makes less important the precision when predicting the value of σ_d .

The other contributing stress to completely describe the peak stress, σ_p , according to eq. 6.19 is the maximum value of the damped oscillatory stress, σ_r . Figure 6.34 showed the linear semi-log relationship of the form

$$\sigma_r = m_r \text{Log } Z + b_r \quad (6.27)$$

where $m_r = -0.52997$ and $b_r = 4.73648$. The correlation would seem poor ($r = -0.81595$) however σ_r only ranges 0 to 1.8MPa thus deviations from the actual value are even smaller (0.6MPa at the most). An unexpected additional tool the Damped Cosine Avrami Model would allow to quantify is the value of Z_c where the theorized transition from single peak to multiple peak stress lies. When eq. 6.27 produces a value for σ_r lower than 0.4MPa the oscillations due to synchronized DRX waves should cease to be significant. Equation 6.27 becomes zero when $Z = 8.65 \times 10^8$. However the value of $\sigma_r = 0.4\text{MPa}$ was chosen because the experimental points on fig. 6.34 almost reach zero and, coincidentally the corresponding value for Z is 1.5×10^8 , the value chosen to be the transition point where power law breaks down. Hence for Cu A of initial grain size, D_0 , of $637\mu\text{m}$ the corresponding $Z_c = 1.5 \times 10^8$. This latter value is 8.2 times the dynamically recrystallized grain size, D_{rex} . The value of Z_c is 2.87×10^5 if $D_{rex} = D_0/2 = 318.5\mu\text{m}$ according to the relative-grain size model. The relative-grain size model (fig. 6.7) defines Z_c as an offset twice the dynamically recrystallized grain size, however as Sakai and Jonas [16] have recognized the offset is an estimate based on observations of the stress-strain curve. The proposed eq. 6.20 detects oscillating behaviors at a much higher Z value. Figure 6.43 shows the plot for the relative-grain size model applied to the experimental observations of Cu A. The value of K_{rex} is 5385.7; the value of the exponent m_{rex} is - 0.22503 and the recrystallized grain diameter of eq. 6.1 is expressed in μm . In the present study yet another factor may be increasing the value of Z_c , the much larger size of D_0 compared to D_{rex} . The stress oscillations as explained depend on the volume of dynamically recrystallized material that can synchronously begin another cycle before the entire initial grain volume has been consumed. When D_0 is much larger than D_{rex} more strain has to be accumulated before the advancing DRX collars consume all of the initial grain and in these cases enough strain can also be accumulated on new grains for oscillations to be observed. The sum of the maximum value of the mean oscillatory stress, σ_d , and of the maximum value of the damped oscillatory stress, σ_r , completely describe the value of the peak stress, σ_p , however the amount of strain needed to reach σ_p is not considered by the latter equations.

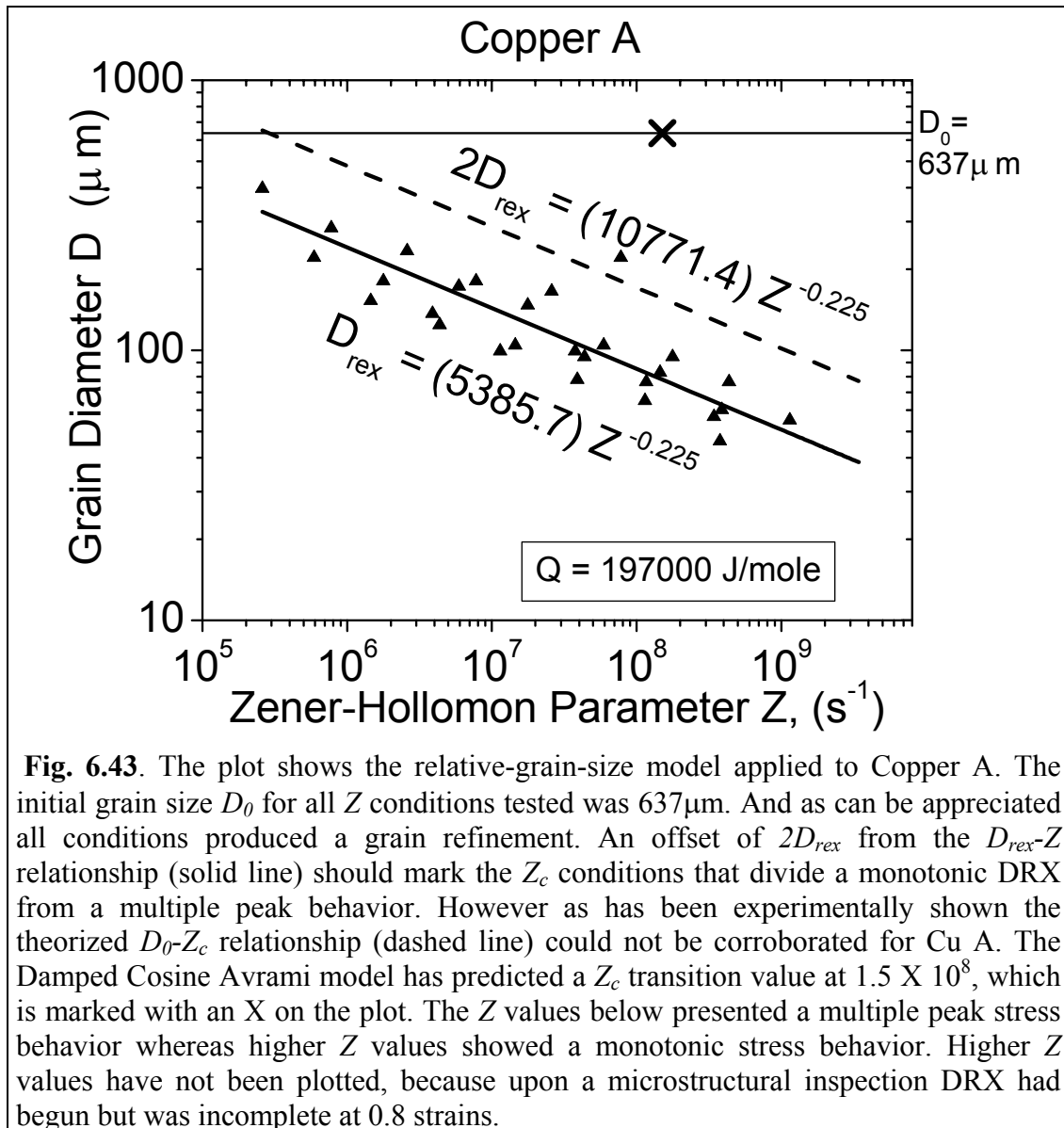


Fig. 6.43. The plot shows the relative-grain-size model applied to Copper A. The initial grain size D_0 for all Z conditions tested was $637\mu\text{m}$. And as can be appreciated all conditions produced a grain refinement. An offset of $2D_{rex}$ from the D_{rex} - Z relationship (solid line) should mark the Z_c conditions that divide a monotonic DRX from a multiple peak behavior. However as has been experimentally shown the theorized D_0 - Z_c relationship (dashed line) could not be corroborated for Cu A. The Damped Cosine Avrami model has predicted a Z_c transition value at 1.5×10^8 , which is marked with an X on the plot. The Z values below presented a multiple peak stress behavior whereas higher Z values showed a monotonic stress behavior. Higher Z values have not been plotted, because upon a microstructural inspection DRX had begun but was incomplete at 0.8 strains.

6.11 The Onset of Dynamic Recrystallization

The peak stress, σ_p , is a characteristic value of many hot-flow curves and is commonly associated to the onset of DRX where the corresponding strain, ε_p , is often described as a power function of the form

$$\varepsilon_p = B D_0^p Z^{n_p}. \quad (6.28)$$

The dependence of the initial grain size with the peak strain ε_p was not taken into account during the experimental design of the present study, so $B D_0^p = K_p$. However Blaz *et al.* [25] using copper with 5ppm of oxygen has shown that the higher the temperature the less sensitive is ε_p to the initial grain size. The sensitivity could increase on tests with initial grain sizes below $40\mu\text{m}$ (see fig. 6.44 from [25]). The graph on fig.

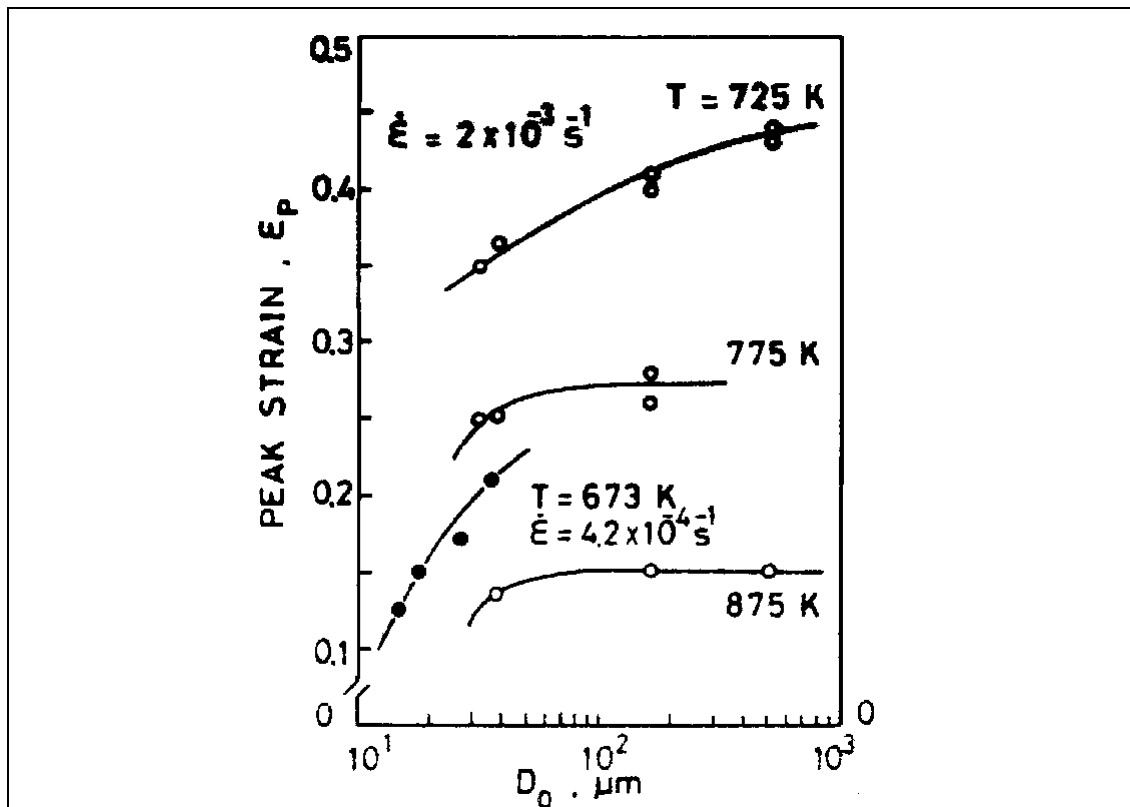


Fig. 6.44. Plot taken from ref. [25] shows the influence of initial grain size, D_0 , on the peak strain in copper. At lower temperatures the peak strain occurs before for smaller initial grain sizes. The full circles from ref. [75] show that the peak strain is more sensible to initial grain sizes lower than $40\mu\text{m}$.

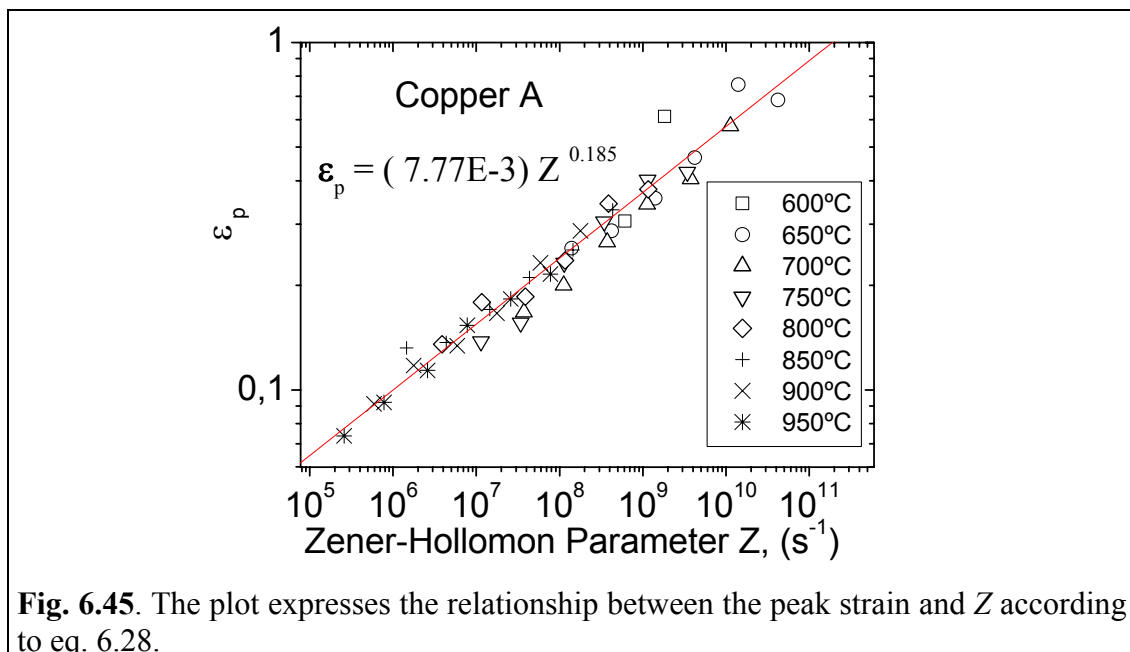


Fig. 6.45. The plot expresses the relationship between the peak strain and Z according to eq. 6.28.

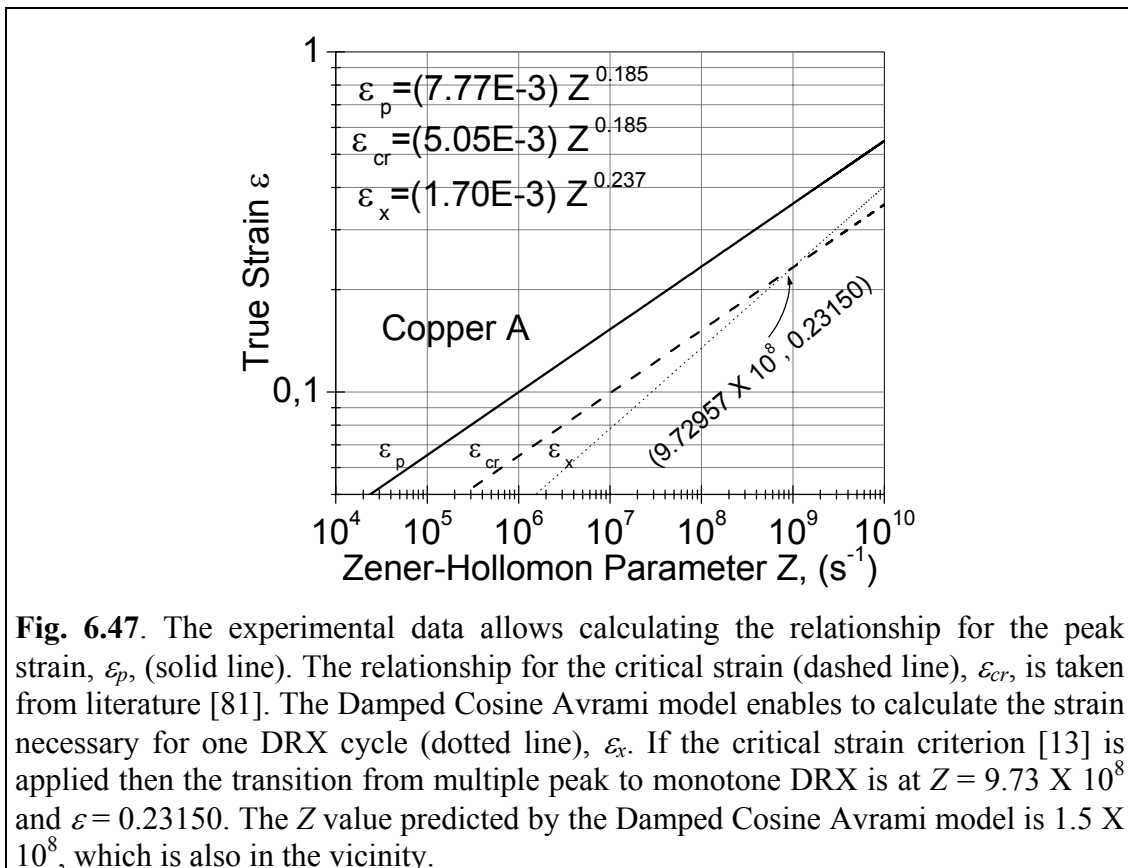
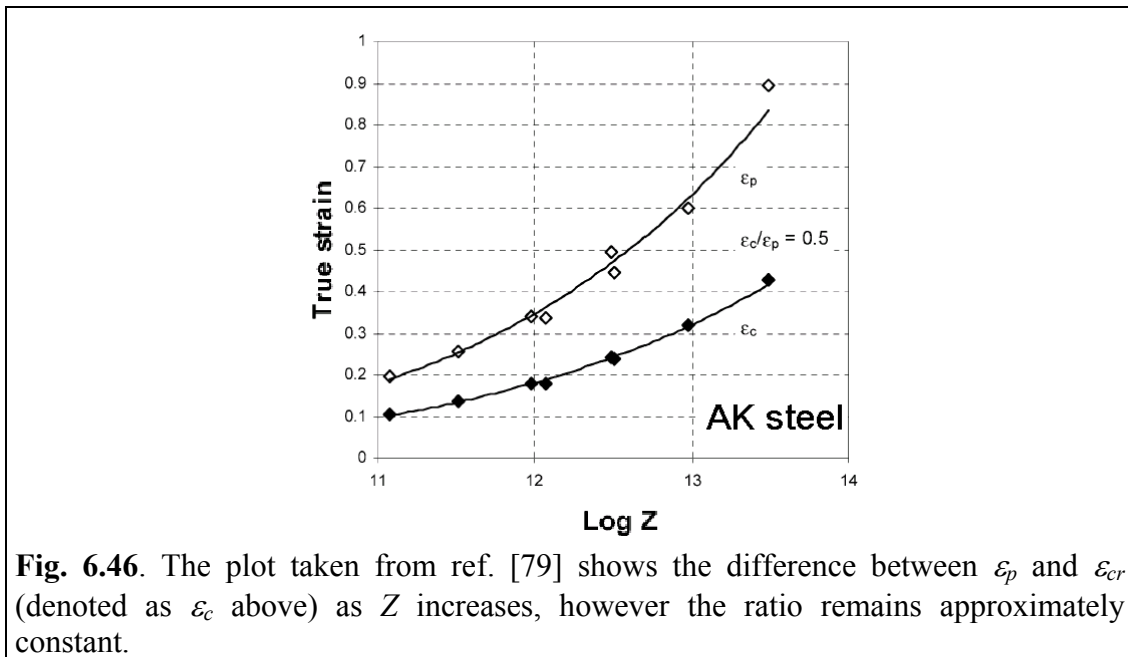
6.45 shows the relationship expressed by eq. 6.28 for Cu A. At lower temperatures and higher strain rates the value of ε_p is higher for Cu A within the range of conditions studied, however there presumably exists a temperature below which the material will fail without presenting any DRX. The value of K_p is 0.0077689 and n_p is 0.18483. If the purpose is to model the stress-strain curve, as is for this study then the description given by eq. 6.28 is enough. However it is well known that before DRX can be noticed on the stress-strain curve DRX has to microstructurally initiate first. Much experimental and laboratory work needs to be done to microstructurally find the critical strain, ε_{cr} , required for the onset of DRX at a particular Z conditions so this path is usually avoided. Although the critical strain is not a characteristic point on the stress-strain curves an analysis of the strain-hardening rate, θ , can reveal a point where the tendency to only harden and recover begins to change.

On constant strain rate tests Ryan and McQueen [76, 77] observed that the presence of a stress peak leads to an inflection in the stress dependence of the strain-hardening rate ($(\partial\sigma/\partial\varepsilon)-\sigma$ plots). The inflections have been shown to be due to the initiation of DRX [78]. More recently Poliak and Jonas [79] have shown that inflections can be seen on $\theta-\sigma$ plots, $\ln \theta-\ln \sigma$ plots and, $\ln \theta-\varepsilon$ plots even when a clear peak stress is not present on the stress-strain curves. The exact inflection point can be determined by plotting the derivative of the strain-hardening rate ($|\partial\theta/\partial\sigma|$) where the minimum points to the critical stress value where DRX begins. The critical strain can also be determined from the minimum of $|\partial \ln \theta/\partial \varepsilon|$ plots. A drawback to the latter analyses is that differentiation causes substantial noise and a double differentiation increases the problem. Poliak and Jonas [79] have suggested using Fourier transform-based procedures to filter the plots. Also the use of logarithmic plots (e.g. $\ln \theta$) further smoothens the noise from the differentiation and is therefore more convenient. One issue that draws attention is that inflections on $\theta-\sigma$ plots also appear for [80] polycrystalline copper tested at temperatures close to the room temperature (and below), however DRX does not occur. Manonukul and Dunne [81] studied the critical strain for DRX in 99.9% pure copper (oxygen content was not reported) and observed that the $\varepsilon_{cr}/\varepsilon_p$ ratio remains between 0.68 and 0.63 for conditions tested at 400°C. Table 6.4 resumes the findings of Manonukul and Dunne [81] for the three Z conditions studied.

Table 6.4. Critical strain to initiation for 99.9% pure copper isothermally deformed at 400°C after ref. [81].

| Strain rate (s^{-1}) | 5×10^{-4} | 5×10^{-3} | 5×10^{-2} |
|------------------------------------|--------------------|--------------------|--------------------|
| Critical Strain ε_{cr} | 0.15 | 0.19 | 0.23 |
| Peak Strain ε_p | 0.22 | 0.30 | 0.36 |
| $\varepsilon_{cr}/\varepsilon_p$ | 0.68 | 0.63 | 0.64 |

Earlier Sample *et al.* [11] based on experimental work had pointed out that the difference between the peak and critical strain ($\varepsilon_p - \varepsilon_{cr}$) increases as Z values increase. The observation made by Sample *et al.* is not contradictory to the accepted principle that the $\varepsilon_{cr}/\varepsilon_p$ ratio remains almost constant. A plot of ε versus $\text{Log } Z$ shows that as Z increases the distance between ε_p and ε_{cr} increases (see fig. 6.46 from [79] as an example) however the ratio remains constant. If the above reasoning is true then the power function of the form of eq. 6.28 that describes ε_{cr} is given by $K_{cr} = 0.65K_p$ and $n_{cr} = n_p$. Where the $\varepsilon_{cr}/\varepsilon_p$ ratio is an average of the work of Manonukul and Dunne [81].



However the temperature used to calculate the ϵ_{cr}/ϵ_p ratio lies outside the temperature ranges of this study and the activation energy used to evaluate Z may not be valid. See fig. 6.47, which shows the calculated critical strain and the peak strain using experimental data. The strain necessary for one DRX cycle, ϵ_x , is also plotted. Figure 6.47 also shows that the $\epsilon_{cr} > \epsilon_x$ criterion for multiple peak DRX presented earlier by Luton and Sellars [13] would almost work for Cu A. We predict a behavior change at Z

$= 1.5 \times 10^8$ using the Damped Cosine Avrami model and the critical-strain model predicts a change at $Z = 9.73 \times 10^8$. Earlier ϵ_p and ϵ_{cr} had been plotted against stress; here the abscissas are the corresponding Z values. Strain-hardening plots have been proven to provide information as to when the onset of DRX occurs, but the reason why nucleation occurs needs to be searched microstructurally and here twinning could be playing an important role.

Microstructural evidence of the steps towards the nucleation of dynamically recrystallized grains is difficult to observe after hot flow tests performed at temperatures closer to the melting point (T_m) when grain growth rates are high. Nucleation of new grains should occur at sites that reach a critical dislocation density, ρ_{CR} , first. As is known the preferential sites for nucleation are grain boundaries [82, 83], deformation bands [25, 84, 85], precipitates [82, 86], hard particles [87] and grain boundary triple junctions [88, 89], because higher stress concentrations and strain accumulations localize first at such sites. Wusatowska-Sarnek *et al.* [90, 91] have studied nucleation of copper at 0.35 to 0.53 T_m and have been able to distinguish two mechanisms, which occur whether deformation is performed at low or high Z conditions. The work of Wusatowska-Sarnek *et al.* [91] further adds evidence to a model proposed by Miura *et al.* [83] and later corroborated by Belyakov *et al.* [92] using 304 stainless steel. The model is best explained by fig. 6.48 from ref. [46]. However an earlier but simpler

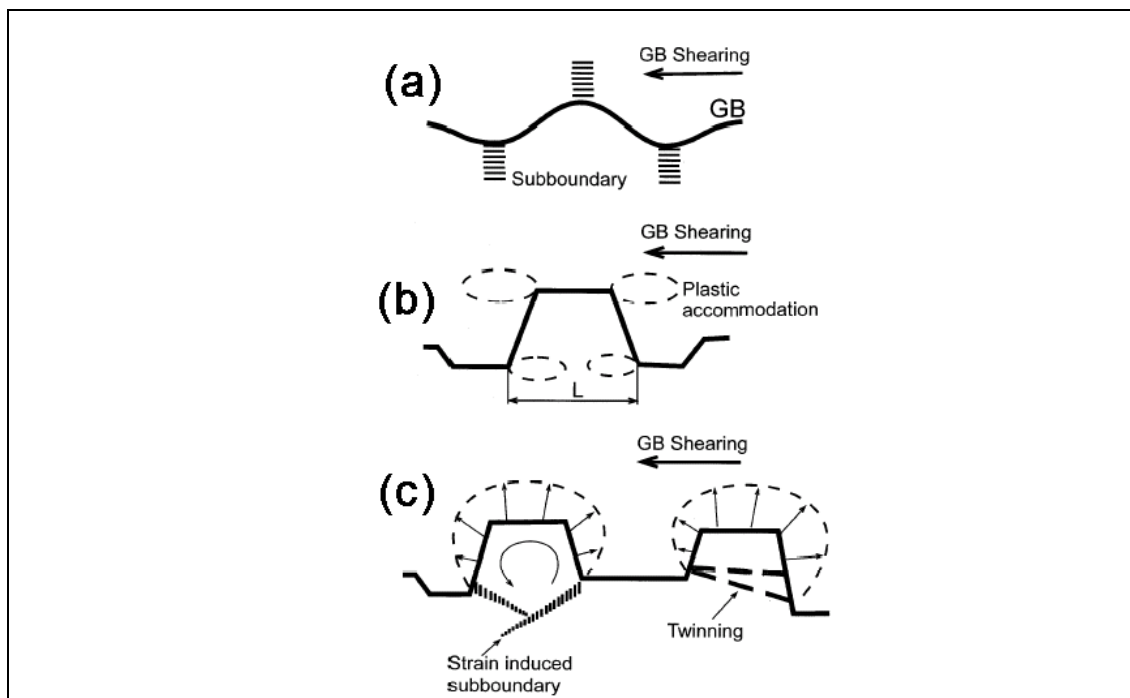
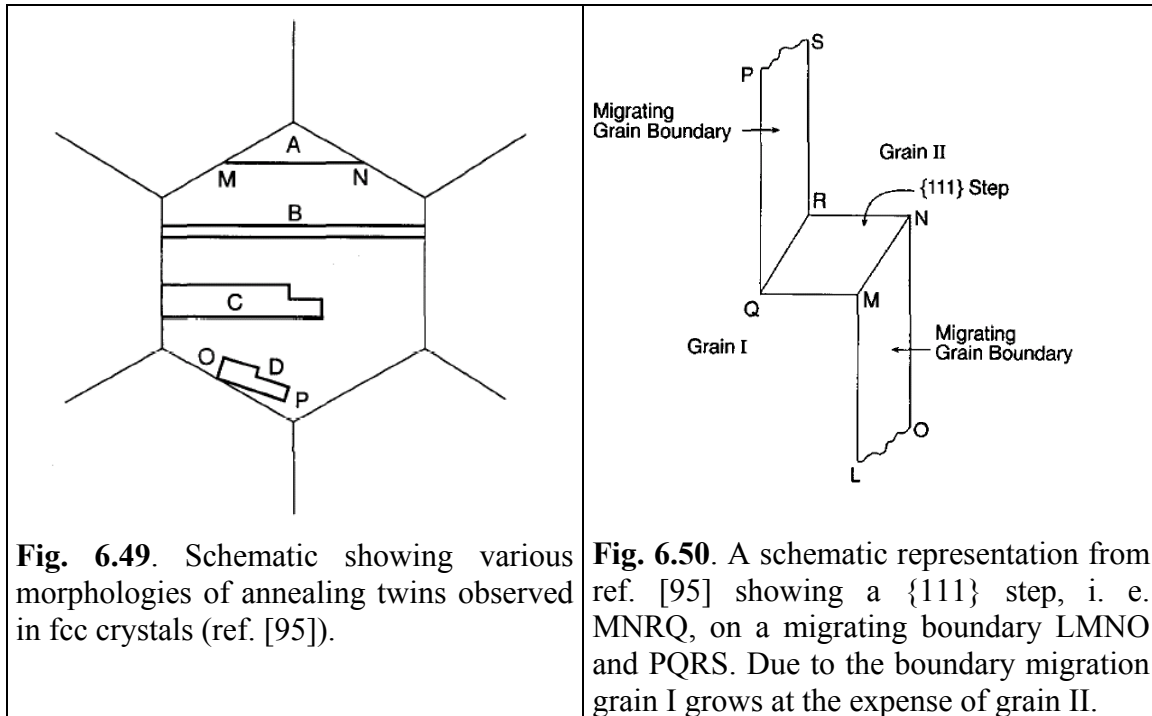


Fig. 6.48. The schematic representation from ref. [46] shows the steps prior to nucleation of a dynamically recrystallized grain. On (a) and (b) boundary corrugation accompanied by the evolution of sub-boundaries. Partial grain boundary sliding occurs which leads to the development of inhomogeneous local strains. On (c) the bulging parts of a serrated grain boundary accompanied by the evolution of dislocation sub-boundaries or twinning cause the formation of a new recrystallized grain.



model for bulging at grain boundaries was first suggested by Hirsch and Bailey [8, 9, 93]. In the more recent model [46] at higher temperatures or lower strain rates the observed serrations or protrusions finally separate from the initial grain by the formation of a twin boundary, which could later with more strain lose coherency and become a grain boundary. Annealing twin boundaries are formed by the dissociation of migrating grain boundaries [94]. At lower temperatures or higher strain rates the observed bulging parts on the serrated grain boundary finally separate as strain induced sub-boundaries close in and allow a crystallographic rotation that creates the new grain boundary. Sample et al. [11] using unique quenching facilities were able to observe a partially recrystallized structure and concluded that DRX proceeds from the formation and growth of dislocation-free annealing twins. The hot flow tests performed during this study, which range $0.64T_m$ to $0.90T_m$, are above the range studied by Wusatowska-Sarnek *et al.* and, as would be expected, because of the increased grain boundary mobility, twinning should be the mechanism mostly responsible for nucleation of new grains.

Several mechanisms have been proposed [94] to explain why the migrating grain boundaries of low stacking fault f.c.c. metals and alloys dissociate to form annealing twin boundaries. Mahajan *et al.* [95] have proposed that migrating grain boundaries contain $\{111\}$ propagating steps, which may find accidents that generate Shockley partial dislocations contiguous to the grain boundary. The partial dislocations with same Burgers vector would repel each other and glide away from the boundary to produce a twin. The glide away of certain partial dislocations causes stacking faults, which may form packets of complicated morphology that nucleate twins [96]. Figure 6.49 from ref. [95] shows various types of annealing twins formed by slightly different dissociations of the migrating grain boundaries. A sequence of shadowed images on amorphous copper where growing grain boundaries leave behind various types of annealing twins can be seen on ref. [97]. Figure 6.50 from ref. [95] shows a schematic drawing of the grain boundary of grain I growing at the expense of grain II and how a propagating

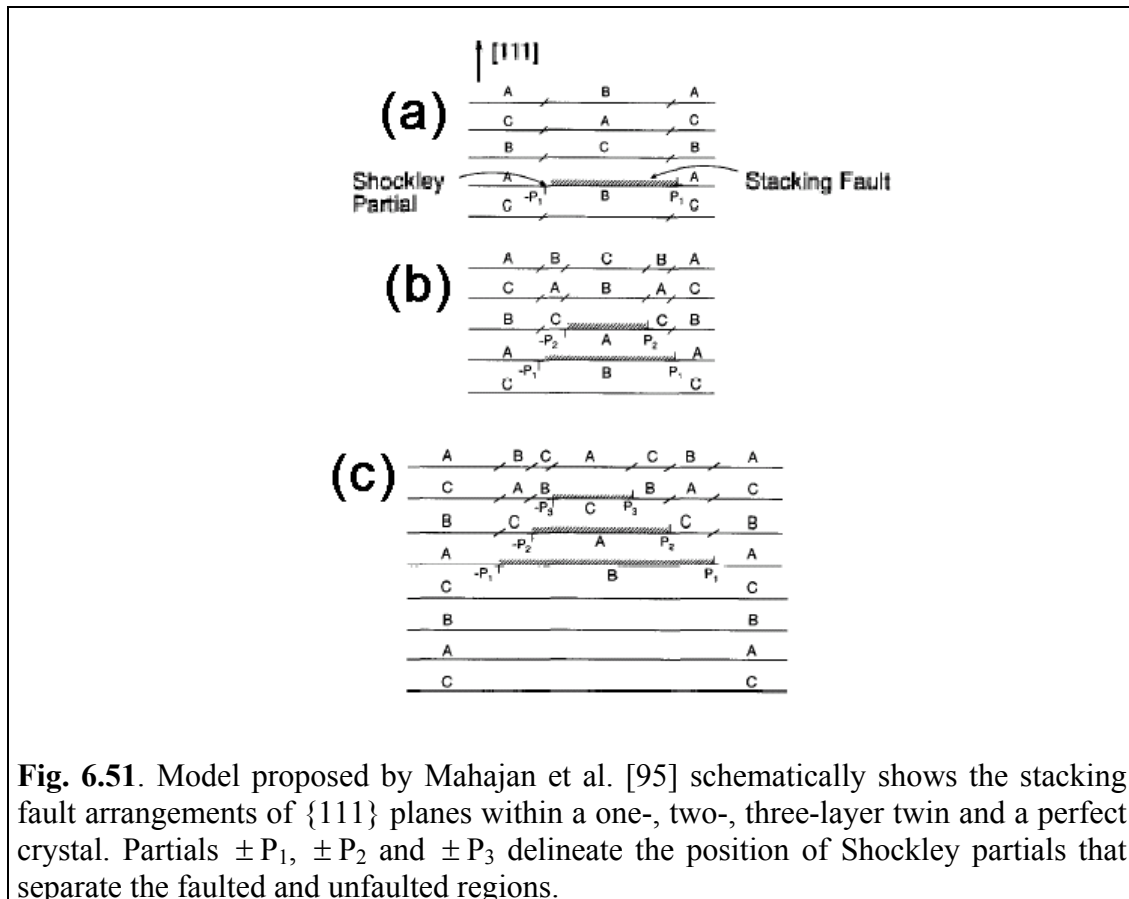


Fig. 6.51. Model proposed by Mahajan *et al.* [95] schematically shows the stacking fault arrangements of $\{111\}$ planes within a one-, two-, three-layer twin and a perfect crystal. Partials $\pm P_1$, $\pm P_2$ and $\pm P_3$ delineate the position of Shockley partials that separate the faulted and unfaulted regions.

$\{111\}$ step moving upward may find an accident that forms partial dislocations, which may repel each other and change the habit plane of the boundary creating a twin as shown schematically on fig. 6.51. Mahajan *et al.* explain that a single $\{111\}$ step can produce annealing twins at different locations and of different thickness. Also the number of twins should increase with increasing grain size, because the probability that the $\{111\}$ may act as a Shockley partial generator increases with the distance the grain boundary moves. If the latter explanations are kept in mind then the concept that at higher temperatures (lower Z values) the bulged grain boundaries finally nucleate because a twin is formed seems reasonable. At lower Z values the driving force for grain growth is promoted making the possibility for the appearance of a twin boundary high, then the twin would lose coherency and the bulging would become a new dynamically recrystallized grain.

Mahajan *et al.* also presented experimental evidence of factors that could decrease or increase the formation of annealing twins during grain growth. An addition of 200ppm of boron in nickel reduced slightly the twin to grain boundary intersections. Also an increase of twins per cm^2 was noticed on surfaces of copper that were closer to a face that was mechanically ground previously before annealing. The possibility that certain elements or certain pre-straining could enhance the formation of twins during DRX at lower Z values remains open for investigation.

6.12 Strain Hardening and Dynamic Recovery

Before DRX can happen a certain amount of strain hardening is needed to reach critical dislocation densities at the preferred nucleation sites. Strain hardening can be defined as the evolution in dislocation structure as a metallic material is deformed. The continued change in dislocation structure requires increasing stress. From another standpoint the movement of dislocations, which causes their rearrangement, is associated to the magnitude of a resolved shear stress. Equation 6.12 explains well the relationship between stress and dislocation density during the initial stages of deformation [10], however after a certain stress value deviations occur as the dislocation structure becomes increasingly affected by strain rate and temperature. Equation 6.12 describes a quasi-athermal component [98] of strain hardening, only slightly affected by the elastic shear modulus, $\mu(T)$. If strain hardening was not affected by strain-rate and temperature a $\Delta\sigma/\sigma - \sigma$ plot would be a straight line, as described by the Cottrell-Stokes law [99] but deviations occur as a thermally dependent component of strain hardening affects the dislocation structure. The thermally dependent component is called the dynamic recovery rate [10], which is a temperature and strain rate dependent evolution of the dislocation density with strain. At particular stress conditions dislocations will move, immobilize, remobilize, multiply and, annihilate, and the rates at which that happens will describe the response during a stress-strain curve.

At a micrometric scale within each annealed grain the initial low dislocation density will first start to move, dislocation tangles and forests appear, which help to delimit areas of high and low dislocation densities. The increase of stress causes dislocations coming from the low dislocation areas to pile-up. These intersections between dislocations stop their movement and form increasingly tighter barriers, which produce dislocation cells. The movement of dislocations from the cell interior to the cell boundary can cause enough crystallographic reorientation to consider the dislocation cell a sub-grain within the grain. The continued strain hardening may cause dislocations to adopt a geometrically necessary arrangement: cell blocks, micro-bands (elongated strands of smaller cell blocks) and dense dislocation walls [100]. Further straining results in the appearance of elongated shear bands. However at higher temperatures the latter dislocation structures are less likely to appear due to the increased recovery rate [101, 102]. Dynamic recovery (DRV) is associated to stress decreasing mechanisms by an increase in cross slip leading to higher dislocation annihilation when screw dislocations of opposite sign cancel each other [103] or when dislocations reach sinks such as grain borders or the surface. Annihilation is a process that happens from early stage II and is indirectly related to dynamic recovery. When a metal presents a high dynamic recovery rate dislocation cell walls are tighter [2, 104], like in the case of high purity aluminum where strains of 0.2 can cause the sub-grains to reorient themselves until forming new grains, which decreases stress as if nucleation through dynamic recrystallization had occurred [105]. The micrometric scale where dislocations can be observed has not been the concern of this study instead dislocations have been treated as deformation carriers whose result is seen through a mechanical response, *i. e.* the stress-strain curve.

Many researchers have studied and proposed models [80, 106-122] to explain the experimental characteristics of strain hardening in metals, but a review belongs to a separate communication. The concern here is to demonstrate that the proposed Damped Cosine Avrami model can adequately couple with a single or several existing strain-hardening and recovery models. One empirical model that has given rise to several phenomenological models is the one proposed by Voce [108, 109], which was later

given a physical interpretation by Kocks [110]. The mechanical characteristics of the Voce model are that stress will tend to saturate at higher strains and that the initial strain-hardening rate is a constant. The model is simple and is compatible with the principle that strain hardening is composed of two components, the quasi-athermal strain-hardening minus a recovery rate. The Voce model was chosen over the Estrin and Mecking [115] model used earlier [34, 35] for Cu A, because the large initial grain size ($D_0 = 637\mu\text{m}$) at high temperatures makes the quasi-athermal strain-hardening less important than the recovery rate. A description of the Kocks interpretation will follow to best understand the latter statements. A comparison between the predicted and experimental hot flow curves will help validate the strain-hardening model selection.

The fact that stress rather than strain is related to the dislocation density ($\sigma = \overline{M}\alpha\mu b\sqrt{\rho}$) during the initial stages of strain-hardening makes stress the parameter that can most adequately describe the micrometric structure responsible for hot flow despite the strain history. However before a saturation level can be reached, stress and strain are inseparable. A parameter that marks the tendency to a specific saturation level is the strain-hardening parameter,

$$\Theta = \left. \frac{\partial\sigma}{\partial\varepsilon} \right|_{\varepsilon, T}, \quad (6.29)$$

where the change of stress as strain increases describes the slope of the hot flow curve. The initial strain-hardening rate, Θ_0 , during a hot flow curve is modeled to represent the quasi-athermal hardening and can be defined as

$$\Theta_0 = \frac{\sigma_{Sat.}}{\varepsilon_C}, \quad (6.30)$$

which can be explained if stress is imagined to tend to the saturation stress, $\sigma_{Sat.}$ (implicitly towards a the dislocation structure also) and, ε_C is the strain value where if a

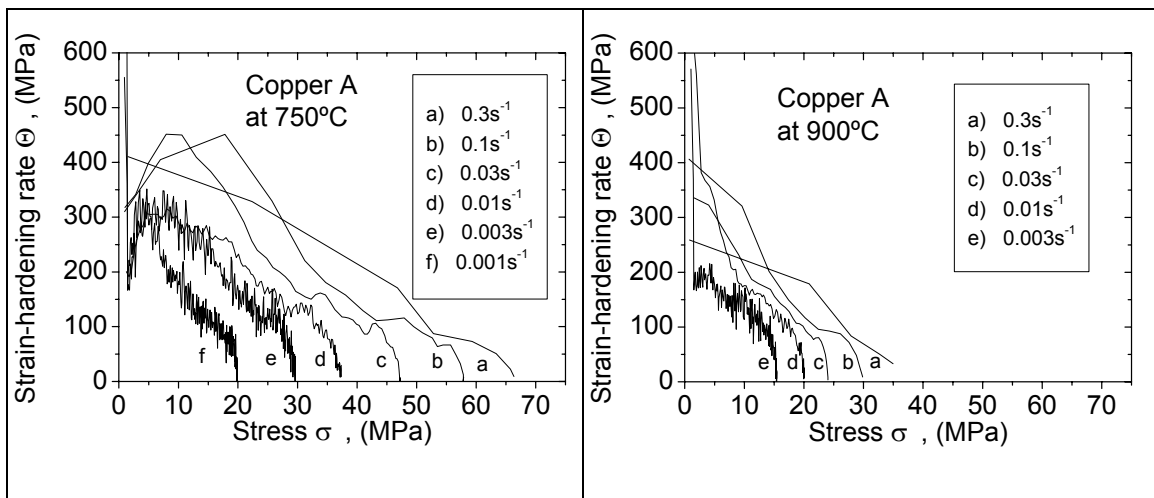


Fig. 6.52. The plots compare the strain-hardening rate calculated from experimental data at 750°C and 900°C. The strain-hardening rate decreases with a steeper slope as the strain rate is lower and as the temperature is higher. The derivative of the stress-strain curve becomes noisier as the strain rate is lower.

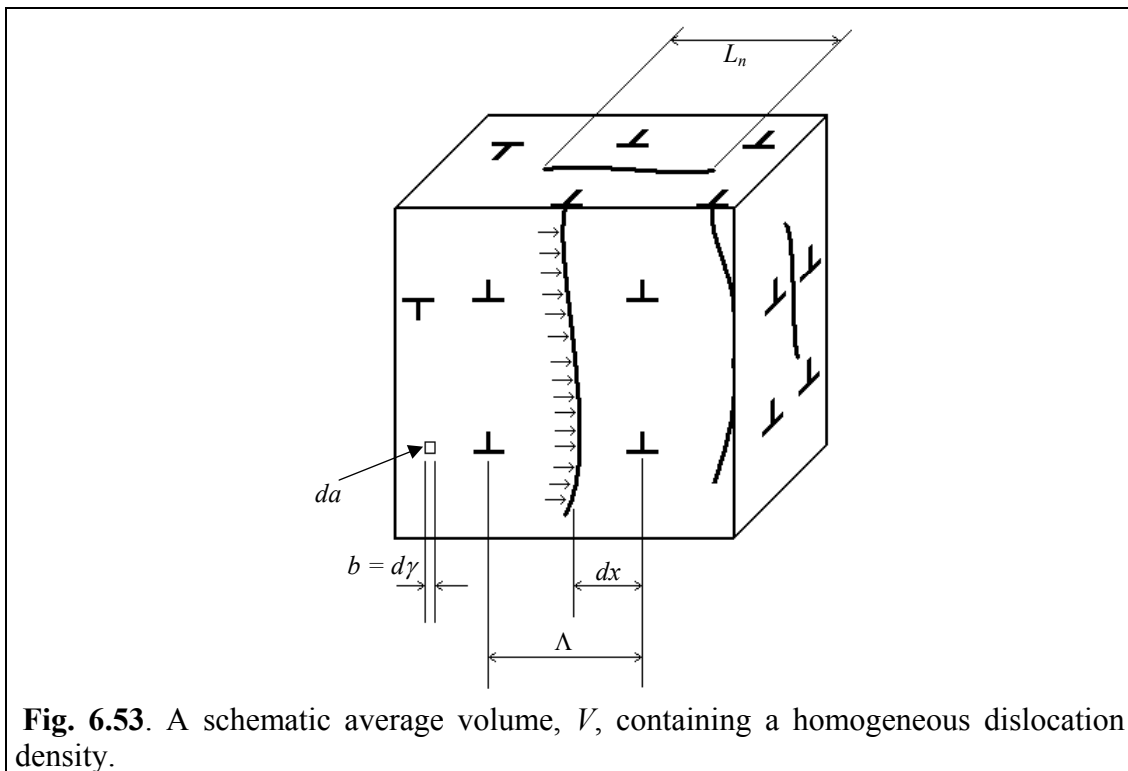


Fig. 6.53. A schematic average volume, V , containing a homogeneous dislocation density.

vertical line was to be drawn the intersection with the initial strain-hardening slope would be the saturation stress. Figure 6.52 shows the experimental $\Theta - \sigma$ plots at 750°C and 900°C for Cu A. The general shape of the curves is similar to others presented for copper single crystals at similar temperatures [123, 124]. The Θ peak at low σ is also observed in the cited reference. Phenomenological models [109-112, 115, 117, 119] exist, which propose several evolution functions to describe the decrease of strain-hardening rate from the initial value (Θ_0) to the highest stress value ($\Theta = 0$). The success of a phenomenological model is in part due to the appropriate selection of an evolution function that describes Θ .

There exists a physical explanation that validates choosing an evolution function of the Voce type when considering an average volume of metallic lattice within a large grain. If the average volume is much smaller than the average grain size then dislocation interactions with the grain border are reduced. If an average volume V having a homogeneous density of dislocations, ρ , is considered like the one shown on fig. 6.53 then the mean free path, Λ , between obstacle dislocations can be statistically defined [125, 49] as inversely proportional to the squared root of dislocation density by a factor of β . The relationship is

$$\Lambda = \beta / \sqrt{\rho}. \quad (6.31)$$

Also in fig. 6.53 the element dx defines the average distance a mobile dislocation travels before immobilizing. When a dislocation moves a distance dx the portion of the slip plane behind has moved a distance equal to one Burgers vector, b . However the

event of displacing a portion of the slip plane happens for every mobile dislocation, ρ_{mob} , on that plane. The change in shear strain on that plane is then

$$d\gamma = \rho_{mob} b dx. \quad (6.32)$$

From fig. 6.53 the total dislocation density can be easily expressed as the sum of all lengths of dislocation segments, $\sum L_n = L_\rho$, divided by the volume, and thus

$$\rho = L_\rho / V. \quad (6.33)$$

Also an area element on a slip plane is defined as da , which in a real metallic lattice can have a minimum displacement equal to the Burgers vector, b , because that is the least distance two parallel planes can move as a dislocation passes. The change in shear strain, $d\gamma$, on a slip plane as da moves is equal to displacing one minimum distance b over the volume in consideration. The relationship deduced is

$$\frac{d\gamma}{da} = \frac{b}{V}. \quad (6.34)$$

The change in dislocation density may be considered to consist of two basic components [110]:

$$d\rho = d\rho_{Stor} - d\rho_{Recov}. \quad (6.35)$$

The term $d\rho_{Stor}$ describes a change in obstacle density due to the fact that a certain fraction of mobile dislocations has been stored in the crystal after moving a distance dx . The term $d\rho_{Recov}$ represents the change of mobile dislocations annihilated by interaction with other dislocations of opposite sign. A potential recovery site on a slip plane is associated to the existence of a dislocation, which is still to be annihilated, thus the number of potential recovery sites is ρda . If a dislocation length at a potential recovery site, L_{Recov} , is annihilated then the dislocation density recovered for the concerned volume changes by L_{Recov}/V . The latter reasoning allows expressing

$$d\rho_{Recov} = \frac{L_{Recov}}{V} \cdot \rho da \quad (6.36)$$

where the change of recovered dislocation density is the product of the minimum dislocation density reduction per volume and the potential recovery sites. The probability that a moving dislocation becomes immobilized will depend on the average distance dx traveled within the available mean free path Λ . If a dislocation is only capable of traveling a small distance dx compared to the available mean free path then the dislocation will probably travel the distance dx without encountering an obstacle thus the probability of being stored is low. On the other hand if a dislocation is capable of traveling a greater distance dx then the probability of encountering an obstacle is high. The change of stored dislocations depends on the existing mobile dislocation density times the probability of finding an obstacle. The relationship is

$$d\rho_{Stor} = \rho_{mob} \cdot \frac{dx}{\Lambda} \quad (6.37)$$

Equations 6.31 through 6.37 allow defining expression 6.38, a description of the change in dislocation density as shear strain on a slip plane changes.

$$\begin{aligned} d\rho &= \rho_{mob} \frac{dx}{\Lambda} - \frac{L_{Recov}}{V} \cdot \rho da \\ d\rho &= \left(\frac{d\gamma}{b dx} \right) \left(\frac{dx}{\Lambda} \right) - \left(\frac{d\gamma}{b da} \right) \cdot L_{Recov} \cdot \rho da \\ d\rho &= \left(\frac{\sqrt{\rho} d\gamma}{\beta b} \right) - \left(\frac{\rho L_{Recov} d\gamma}{b} \right) \\ \frac{d\rho}{d\gamma} &= \left(\frac{\sqrt{\rho}}{\beta b} \right) - \left(\frac{L_{Recov}}{b} \right) \cdot \rho = \frac{(k_1 \sqrt{\rho} - k_2 \rho)}{b} \end{aligned} \quad (6.38)$$

If the known relationship ($\tau = \alpha\mu b\sqrt{\rho}$) is supposed to prevail slightly unchanged during several stages of hardening then eq. 6.39, the change of shear stress as dislocation density changes, can be deduced.

$$\begin{aligned} \tau &= \alpha\mu b\sqrt{\rho}, \quad \frac{\tau}{\alpha\mu b} = \rho^{1/2}, \\ \left(\frac{d\tau}{d\rho} \right) &= \frac{1}{2} \alpha\mu b \rho^{-1/2} = \frac{1}{2} \alpha\mu b \left(\frac{\alpha\mu b}{\tau} \right) = \frac{(\alpha\mu b)^2}{2\tau} \end{aligned} \quad (6.39)$$

If equations 6.38 and 6.39 are combined then expression 6.40 for shear strain-hardening rate is possible.

$$\begin{aligned} \left(\frac{2\tau d\tau}{(\alpha\mu b)^2 d\gamma} \right) &= \frac{\tau}{\alpha\mu b^2 \beta} - \frac{L_{Recov}}{b} \left(\frac{\tau}{\alpha\mu b} \right)^2 \\ \left(\frac{d\tau}{d\gamma} \right) &= \left(\frac{\alpha\mu}{2\beta} \right) - \left(\frac{L_{Recov}}{2b} \right) \cdot \tau \end{aligned} \quad (6.40)$$

The above equation describes hardening on a particular slip plane, however in a polycrystalline material grains are randomly oriented (if no particular texture is present) and an average orientation factor \bar{M} may most appropriately [2] help describe stress and strain as follows:

$$\left(\frac{d\sigma}{d\varepsilon}\right) = \bar{M}^2 \left(\frac{d\tau}{d\gamma}\right). \quad (6.41)$$

For the case of $\{111\}\langle 110\rangle$ slip in FCC metals and $\{110\}\langle 111\rangle$ slip in BCC metals [50, 51] the average orientation factor has been shown to be equal to 3.07. The expression for strain-hardening rate, θ , would then be

$$\left(\frac{d\sigma}{d\varepsilon}\right) = \left(\frac{\alpha\mu\bar{M}^2}{2\beta}\right) - \left(\frac{L_{\text{Recov}}\bar{M}}{2b}\right) \cdot \sigma. \quad (6.42)$$

The theoretically deduced strain-hardening law (eq. 6.42) has a linear behavior composed of a quasi-athermal hardening and a temperature and strain rate dependent hardening. Strain-hardening during deformation will begin at values close to the quasi-athermal hardening ($\sim \mu/20$ according to [119]) and decrease until a hypothetical saturation stress, $\sigma_{\text{Sat.}}$ that in practice is never reached because dynamic recovery reduces further dislocation structure evolution. Equations 6.42, 6.30 and 6.29 may be condensed into the form

$$\Theta = \left(\frac{d\sigma}{d\varepsilon}\right)_{\dot{\varepsilon}, T} = \Theta_0 \left(1 - \frac{\sigma}{\sigma_{\text{Sat.}}}\right), \quad (6.43)$$

which is an evolution function that fulfills the characteristics deduced. A stress-strain law is possible for isothermal and, constant strain-rate loading.

$$\int_{\varepsilon_0}^{\varepsilon} d\varepsilon = \int_{\sigma_0}^{\sigma} \frac{d\sigma}{\Theta}$$

$$\varepsilon - \varepsilon_0 = \int_{\sigma_0}^{\sigma} \frac{d\sigma}{\Theta_0 \left(1 - \frac{\sigma}{\sigma_{\text{Sat.}}}\right)}, \quad r = 1 - \frac{\sigma}{\sigma_{\text{Sat.}}}, \quad dr = -\frac{d\sigma}{\sigma_{\text{Sat.}}}$$

$$\varepsilon - \varepsilon_0 = \int_{\sigma_0}^{\sigma} \frac{-\sigma_{\text{Sat.}} dr}{\Theta_0 r} = \frac{-\sigma_{\text{Sat.}}}{\Theta_0} \ln \left(1 - \frac{\sigma}{\sigma_{\text{Sat.}}}\right) \Big|_{\sigma_0}^{\sigma} = \frac{-\sigma_{\text{Sat.}}}{\Theta_0} \ln \left(\frac{1 - \sigma/\sigma_{\text{Sat.}}}{1 - \sigma_0/\sigma_{\text{Sat.}}}\right)$$

$$\varepsilon - \varepsilon_0 = \frac{-\sigma_{\text{Sat.}}}{\Theta_0} \ln \left(\frac{\sigma_{\text{Sat.}} - \sigma}{\sigma_{\text{Sat.}} - \sigma_0}\right) = -\varepsilon_C \ln \left(\frac{\sigma_{\text{Sat.}} - \sigma}{\sigma_{\text{Sat.}} - \sigma_0}\right)$$

$$-\frac{\varepsilon - \varepsilon_0}{\varepsilon_C} = \ln \left(\frac{\sigma_{\text{Sat.}} - \sigma}{\sigma_{\text{Sat.}} - \sigma_0}\right)$$

$$\sigma = \sigma_{Sat.} + (\sigma_0 - \sigma_{Sat.}) \exp\left(-\frac{\varepsilon - \varepsilon_0}{\varepsilon_C}\right) \quad (6.44)$$

The stress-strain relationship (eq. 6.44) describes the hardening behavior at constant strain rate and temperature conditions. A test performed at a higher temperature would lower the saturation stress and as a consequence the strain-hardening evolution would also decrease at a faster rate. If the strain rate were increased instead the strain-hardening evolution would decrease with a more horizontal slope. Besides the thermally dependent recovery component the hot flow data of this study also includes dynamic recrystallization, which is an additional contribution that decreases the strain-hardening rate, θ . The influence of strain rate and temperature on eq. 6.43 has been dealt with at lower temperature regimes [110, 119] when dynamic recrystallization is not present. The problem at temperatures above 600°C for an almost pure copper is simpler. Beyond 600°C the activation energy for self-diffusion is somewhat constant and as has been established before during the present development; self-diffusion is the ultimate rate controlling process for high temperature deformation. In the forthcoming the activation energy for self-diffusion will be used to correlate parameters on eq. 6.44 within the Zener-Hollomon parameter, Z . First for convenience let $W = 1/\varepsilon_C$, also the values of σ_0 and ε_0 for the annealed large grained copper of this study can be assumed to be equal to zero then eq. 6.44 adopts the form of

$$\sigma = \sigma_{Sat.} [1 - \exp(-W\varepsilon)], \quad (6.45)$$

which is the equation that can be fitted to the available data. Figure 6.54 shows the correlation of W with the Zener-Hollomon parameter. The relationship that describes parameter W of eq. 6.45 is

$$W = K_w Z^{n_w}, \quad (6.46)$$

which is a conventional power law. The values obtained for K_w and n_w are 88.60 and -0.11 respectively.

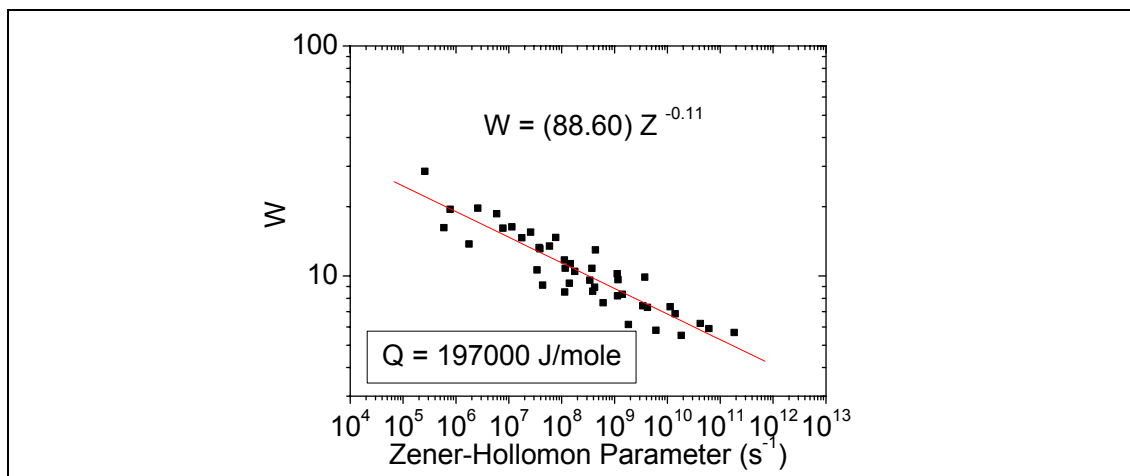


Fig. 6.54. The plot shows the existing relationship between W and Z .

The manner the present author accommodates eq. 6.45 to influences by the shear modulus, dynamic recrystallization, and of course the test conditions, differs to accommodations used at lower temperatures. Kocks [110] had suggested that eq. 6.47 phenomenologically expressed the relationship between $\sigma_{Sat.}$, $\dot{\epsilon}$ and, T of eq. 6.43 through the use of an activation energy, here called A_{76} . The subscript 76 represents the year the article was written, no other reason.

$$\sigma_{Sat.} = \sigma_{Sat.0K} \left(\frac{\dot{\epsilon}}{\dot{\epsilon}_{76}} \right)^{kT/A_{76}} \quad (6.47)$$

On eq. 6.47 the stress $\sigma_{Sat.0K}$ represents the saturation value on a test performed at 0K, the term $\dot{\epsilon}_{76}$ is a constant and k is the Boltzmann constant. Kocks [110, 114, 119] and several researchers [2] agree that θ_0 is roughly equal to $\mu/20$ or in shear resolved stress and strain terms θ_0 is approximately $\mu/200$ regardless of the metal. If instead of using eq. 6.47 to find $\sigma_{Sat.}(\dot{\epsilon}, T)$, the use of eq. 6.46 to find $W(\dot{\epsilon}, T)$ could seem to contradict the observed constant value of θ_0 . However the Voce-Kocks model was not envisaged to include dynamic recrystallization nor is any present strain-hardening and recovery model, thus saturation stress during hot flow is a never achievable dislocation structure state. On the Voce-Kocks model, first the data is corrected for the elastic modulus, then $\sigma_{Sat.}(\dot{\epsilon}, T)$ is defined and because θ_0 is a fixed value the slope of the Voce eq. 6.43, i.e. W , changes. A different procedure will be used to correct for the shear modulus and to adapt the strain-hardening and recovery model to include dynamic recrystallization. Equation 6.46 establishes the general kinetic behavior of the decrease in strain-hardening rate. Studies on dynamic recrystallization have defined the stress value when $\theta = 0$, which allow the use of eq. 6.45 to define $\sigma_{Sat.}(\dot{\epsilon}, T)$. If equations 6.19, 6.25, 6.26, 6.27, 6.28, 6.45 and, 6.46 are combined then eq. 6.48 for saturation stress is possible, which accounts for dynamic recrystallization without changing the general kinetic behavior of W .

$$\sigma_{Sat.} = \frac{\sigma_p}{1 - \exp(-W\epsilon_p)} \quad (6.48)$$

An ambiguous situation seems to have been created, because when fitting for eq. 6.45 not only values for W are generated, but also values for $\sigma_{Sat.}$, which could be correlated with strain rate and temperature by relationships used for hot flow processes (eq. 6.25). If only strain-hardening and dynamic recovery was present then values for $\sigma_{Sat.}$ should be predicted by the relationship established on eq. 6.47. The existence of dynamic recrystallization on the experimental data of Cu A and the required task to correct for the shear modulus justifies the use of eq. 6.48 to adapt the Voce-Kocks model. Figures 6.55 through 6.62 show comparisons between the experimental data, Voce-Kocks model and, the proposed Damped Cosine Avrami Model. Relationships necessary to model hot flow during either monotonic or multiple peak behavior given the temperature and strain rate for the particular case of an initial grain size larger than the dynamically recrystallized grain size have been explained.

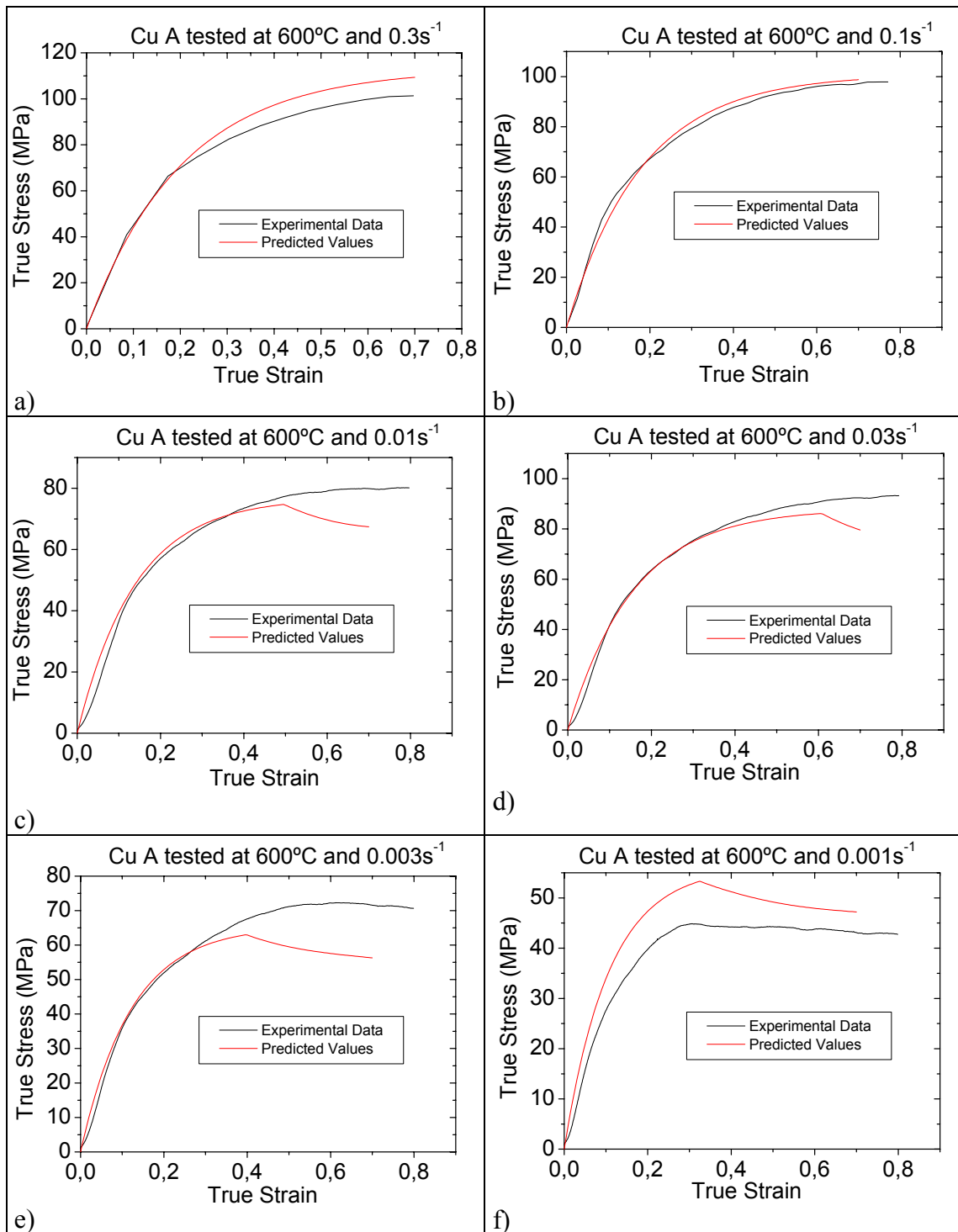


Fig. 6.55. The plots at 600°C compare the adapted Voce-Kocks model and the Damped Cosine Avrami model with the experimental data. At 600°C and below the models developed breakdown, because the normalizing self-diffusion activation energy ceases to be constant.

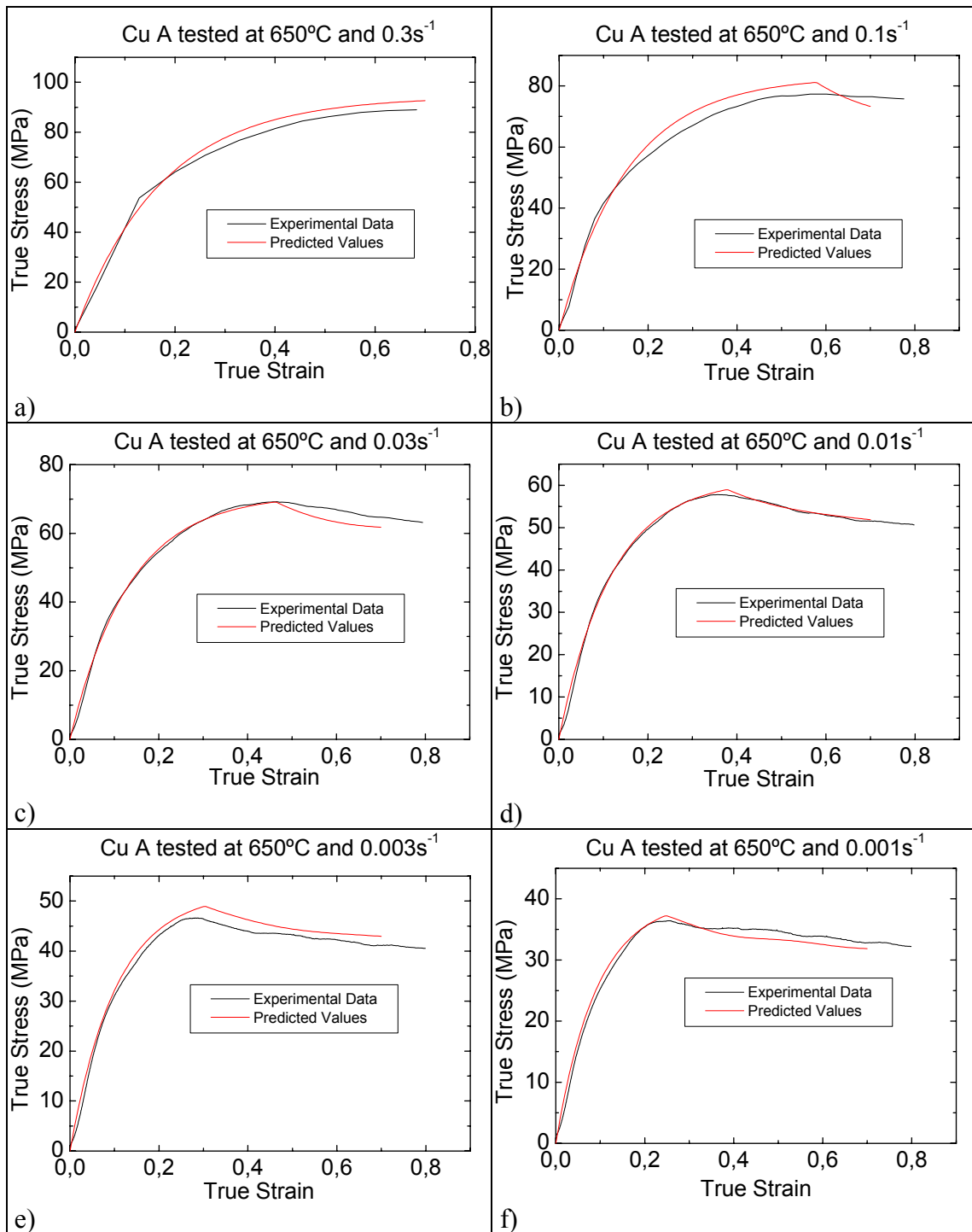


Fig. 6.56. The plots at 650°C compare the adapted Voce-Kocks model and the Damped Cosine Avrami model with the experimental data.

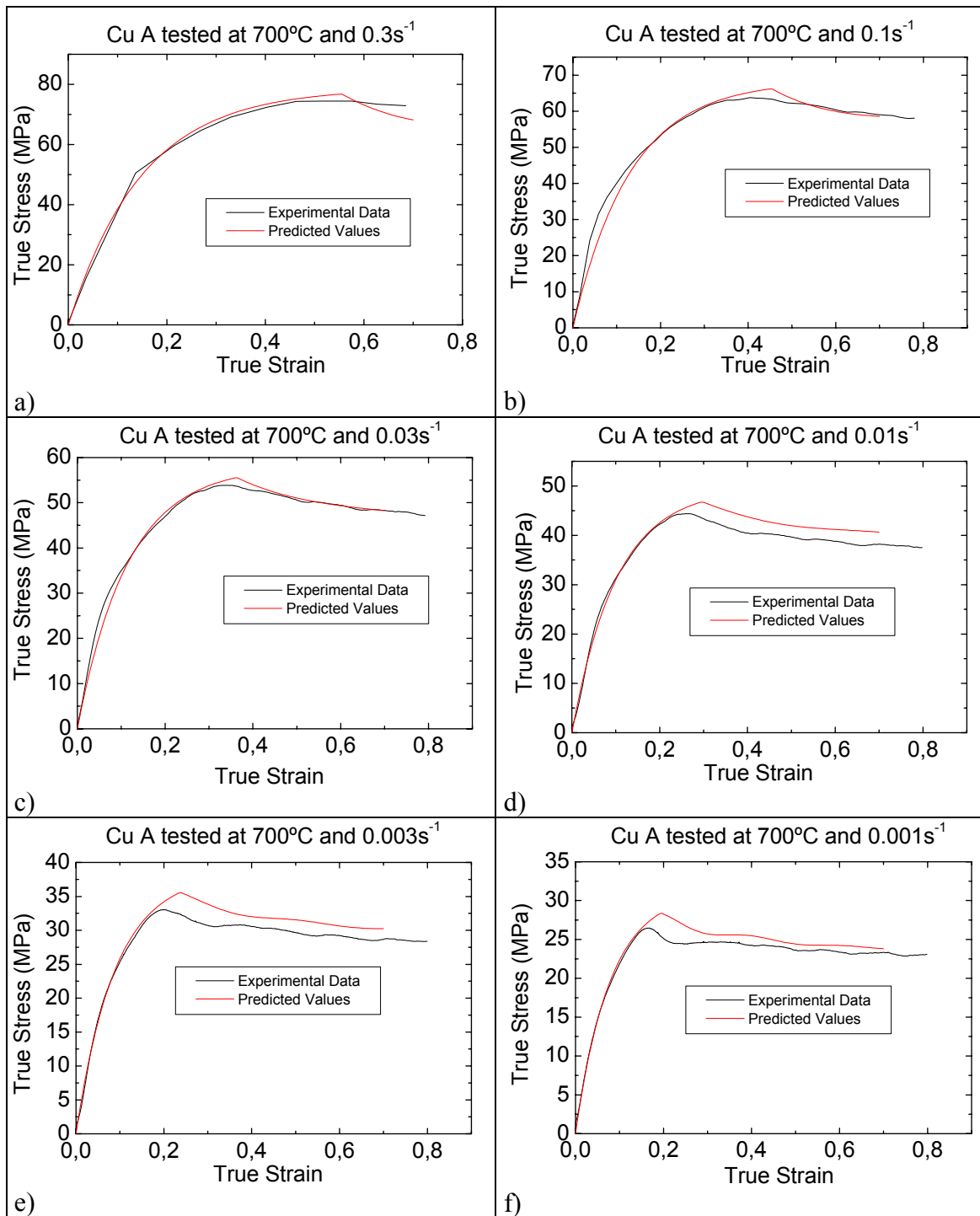


Fig. 6.57. The plots at 700°C compare the adapted Voce-Kocks model and the Damped Cosine Avrami model with the experimental data.

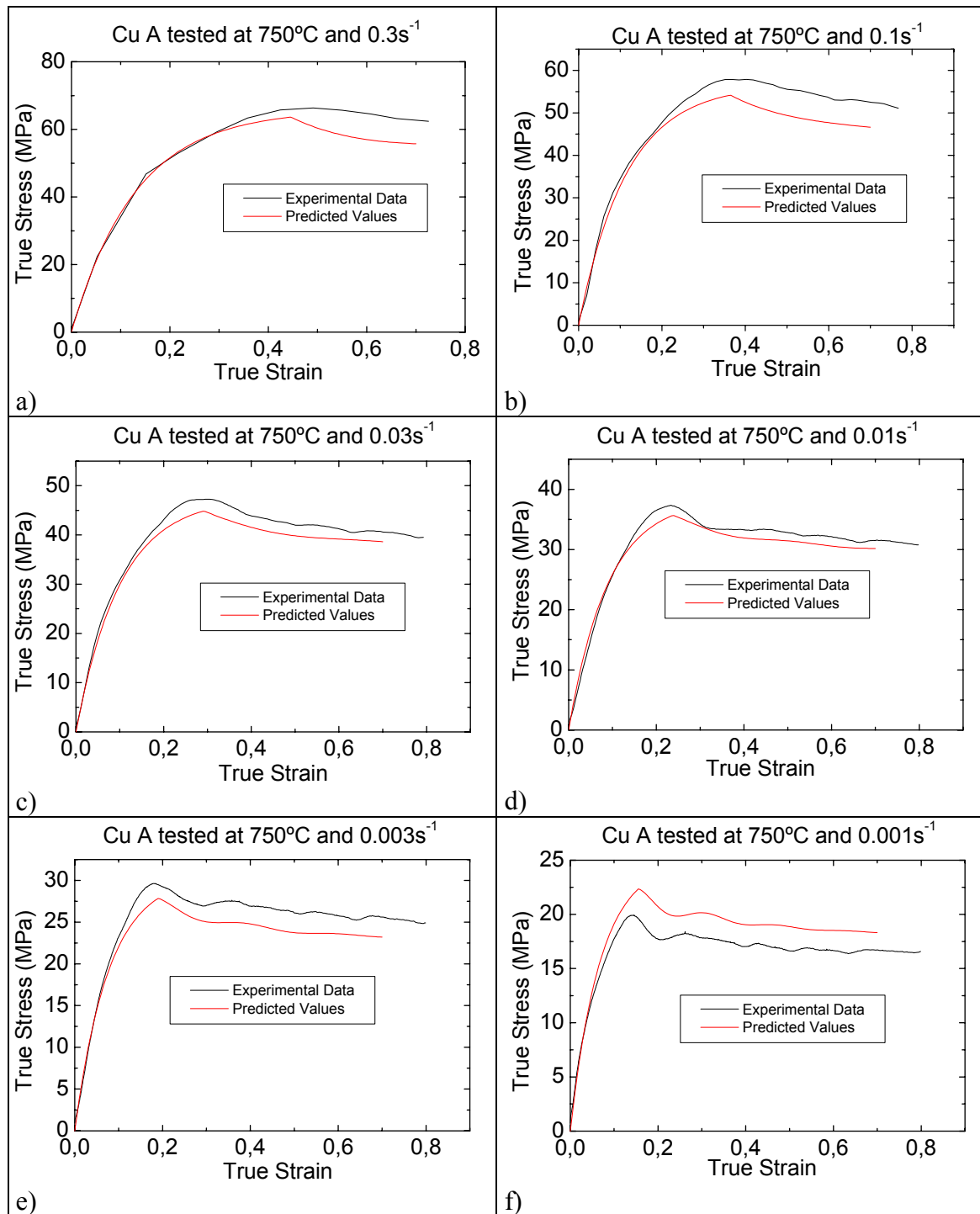


Fig. 6.58. The plots at 750°C compare the adapted Voce-Kocks model and the Damped Cosine Avrami model with the experimental data.

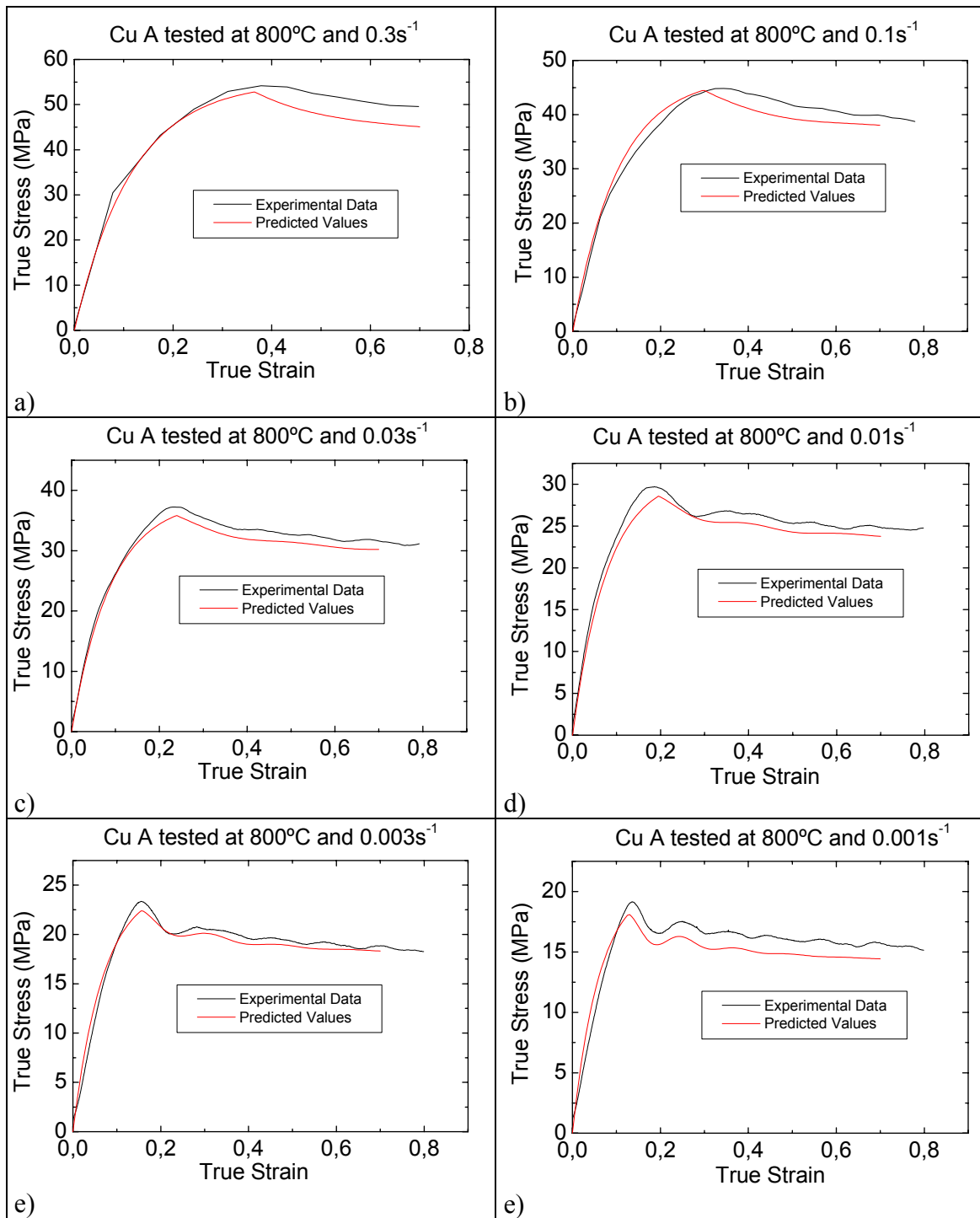


Fig. 6.59. The plots at 800°C compare the adapted Voce-Kocks model and the Damped Cosine Avrami model with the experimental data.

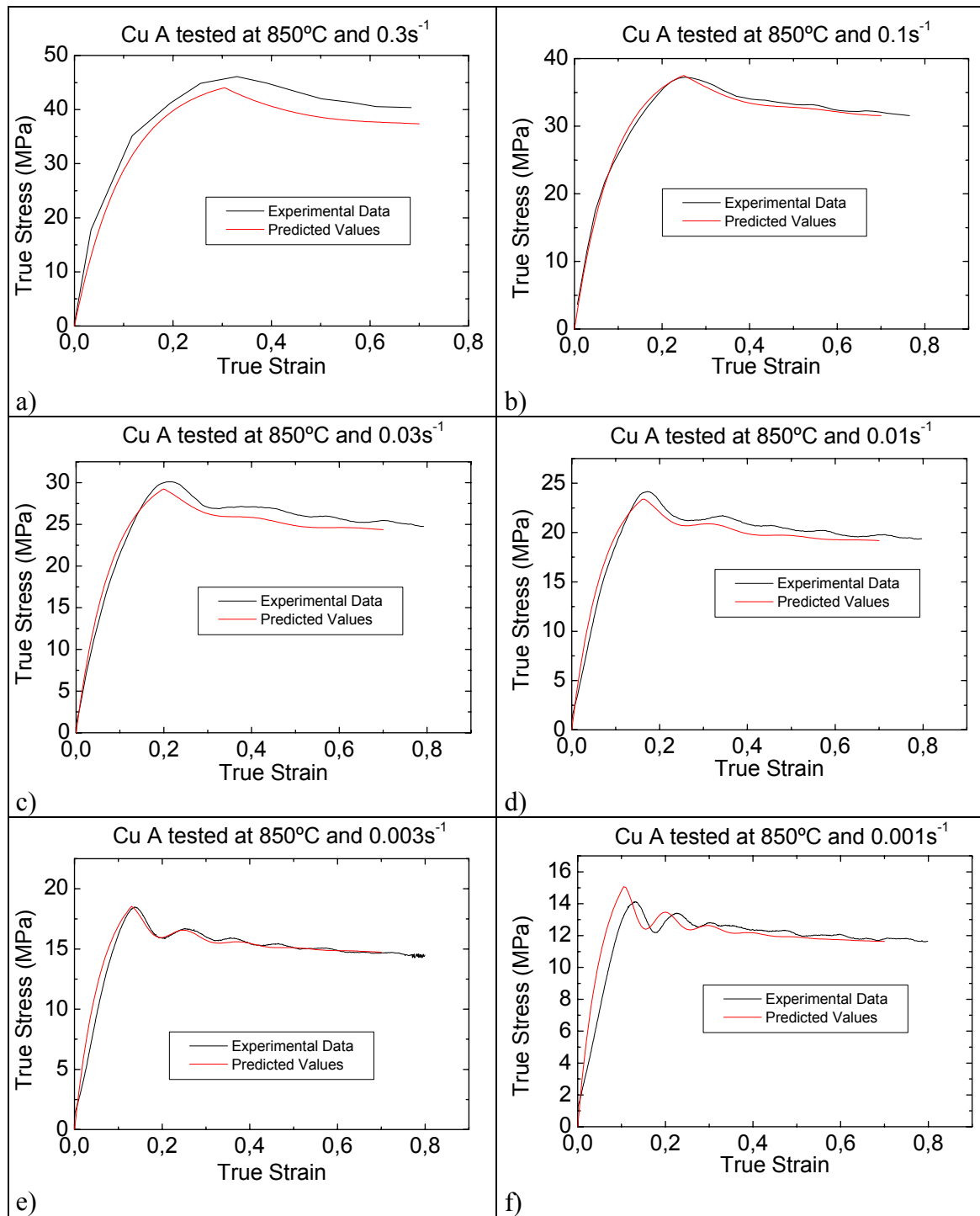


Fig. 6.60. The plots at 850°C compare the adapted Voce-Kocks model and the Damped Cosine Avrami model with the experimental data.

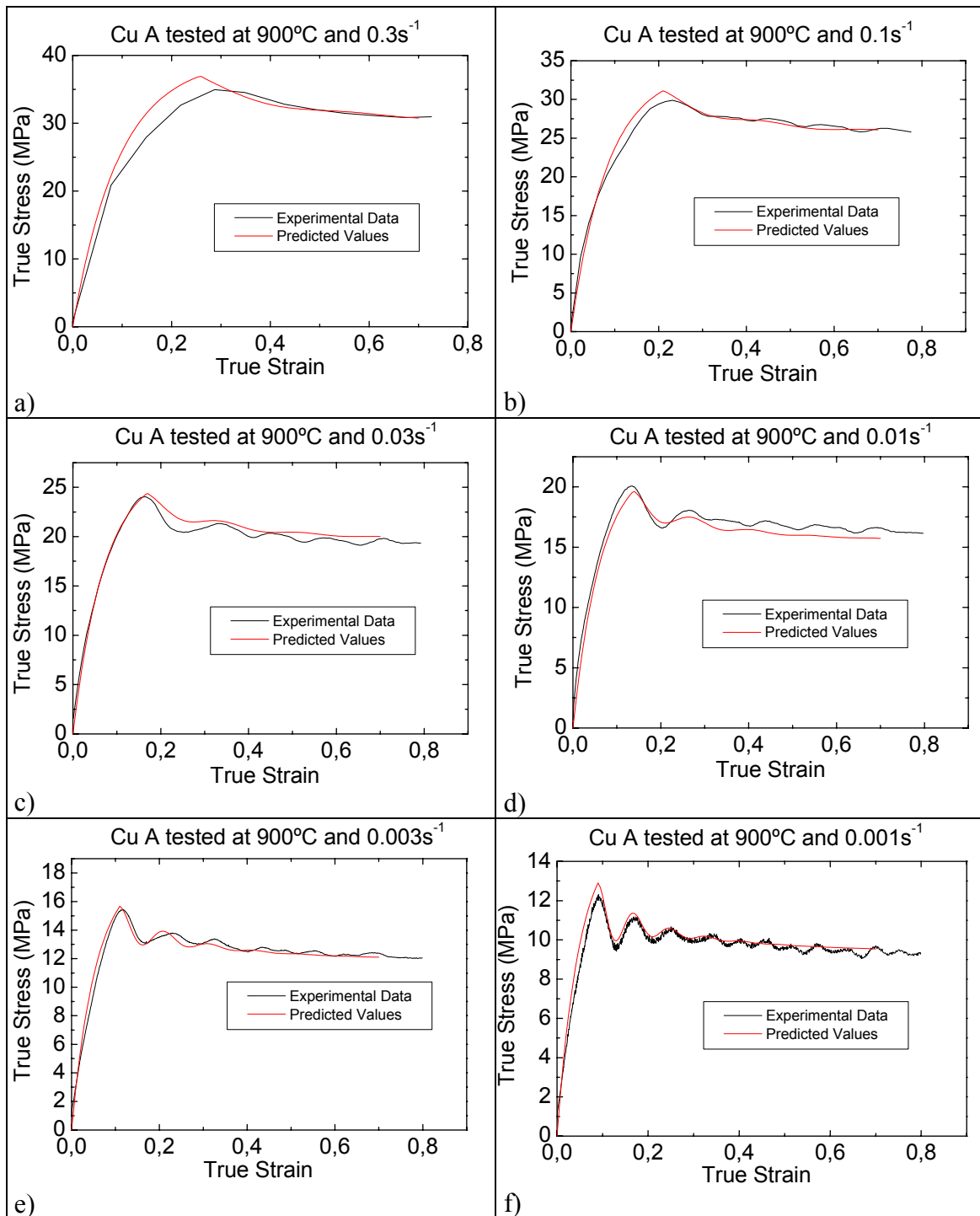


Fig. 6.61. The plots at 900°C compare the adapted Voce-Kocks model and the Damped Cosine Avrami model with the experimental data.

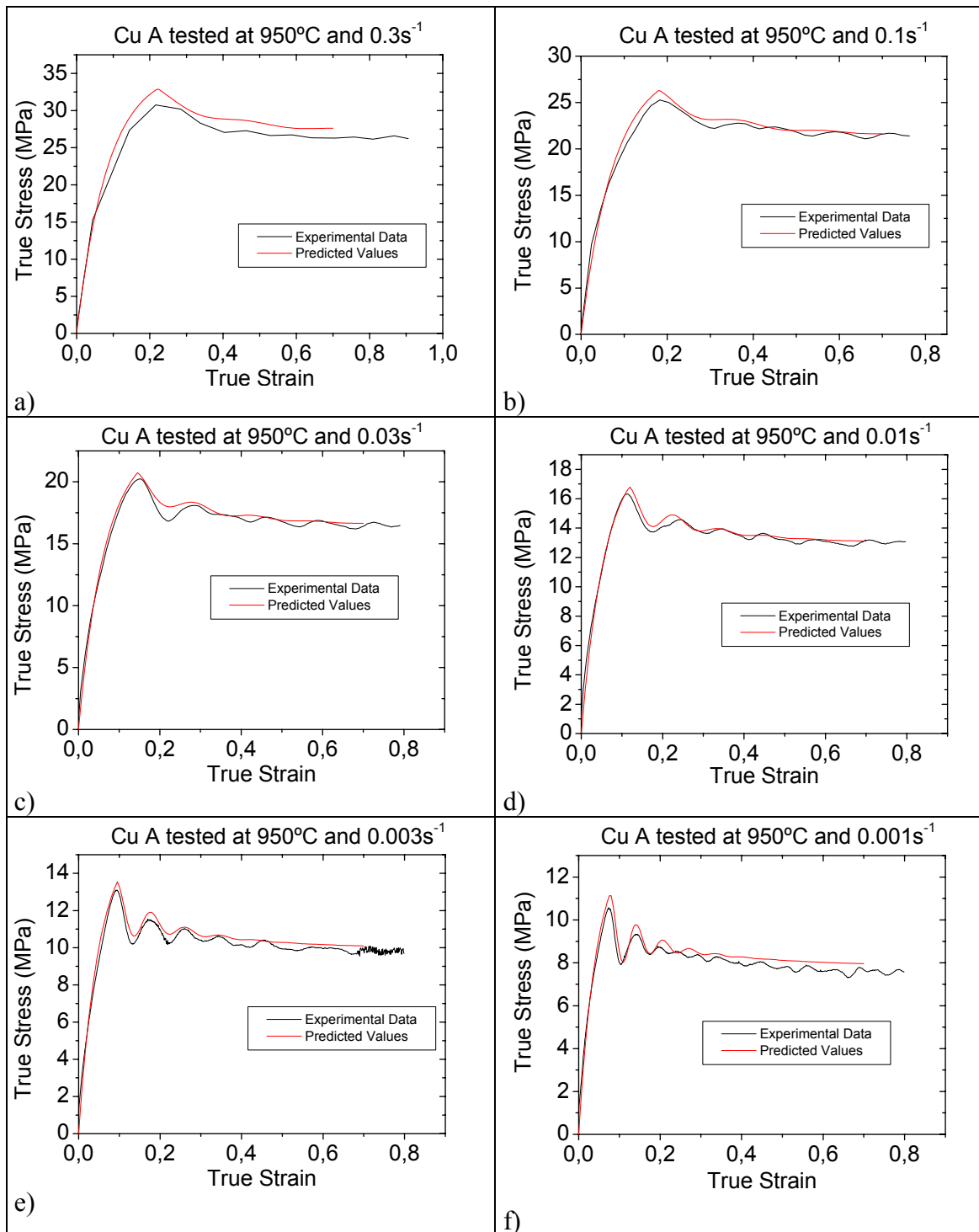


Fig. 6.62. The plots at 950°C compare the adapted Voce-Kocks model and the Damped Cosine Avrami model with the experimental data.

6.13 Implementation Implications

The comparisons between the models and the experimental data shown on figs. 6.55 to 6.62 represent the best correlation between a specific metal and a prediction that the author has found to this date. The joint models break down at temperatures below 600°C as can be seen on fig. 6.55. The reason of the increasing dispersion lays in the activation energy for self-diffusion, Q_{sd} , which normalizes the coefficients throughout the relationships presented and that is no longer the sole normalizing constant below 600°C. For comparisons at 600°C not only the relationship describing ε_p begins to predict a sooner σ_p , but also the hyperbolic relationship that predicts σ_p starts to scatter. The activation energy for self-diffusion plays a key role. Prediction trials outside the experimental range still need corroboration. However the beginning limitation for the models developed is that a pure metal must be the object of study, because otherwise Q_{sd} cannot normalize stress related parameters. For a less pure metal an additional apparent activation energy would need to be used. Also the initial grain size, D_0 , has to be larger than the dynamically recrystallized grain size, eq. 6.1, because when grain growth occurs multiple peaks may begin before reaching a maximum stress. The model has been envisaged to predict oscillations after the maximum stress. In the future different initial grain sizes will need to be tested to further complete the Z_c-D_0 relationship, which seems to be different than theoretically predicted. The slope of the Z_c-D_0 relationship may not be equal to the slope of the $Z-D_{rex}$ relationship, at least for copper. The developed models along with the relative-grain size model are tools that can more accurately predict the final microstructure and the stress-strain behavior during constant strain rate conditions.

6.14 Summary and Conclusions

A review of the contributions to understand monotone or multiple peak DRX has been presented. A review of the relative-grain size model has also helped understand the final microstructure. An analysis of concepts and experimental data of other researchers has lead to propose an empirical solution for hot flow description that uses the physically based self-diffusion activation energy. An elegantly deduced strain-hardening and recovery model by Kocks has been adapted to include DRX by introducing a correction that uses established hot flow relationships. Earlier the relative-grain size model had been calculated for steels and stainless steels [57, 77, 126], however organized data for copper had not been presented until now. The lack of normalization of the $Z-D_{rex}$ data for 70Cu-30Zn brass presented by Roberts [127] is probably due to the difficulty in finding an approximate apparent activation energy. In the future an apparent activation energy besides the self-diffusion activation energy will be shown to help correlate better the $Z-D_{rex}$ data of copper, but for the moment no reasonable explanation can be given for the size of the apparent activation energy value. The stress-strain description begins by predicting the strain hardening and recovery necessary to reach a critical dislocation density (eq. 6.45) then the peak strain is determined (eq. 6.28) and ultimately the Damped Cosine Avrami model is applied (eq. 6.20). A behavioral division is made at a Z of 1.5×10^8 where at lower values a power law relationship more accurately predicts stress (eq. 6.26), but at higher values a hyperbolic sine law is used (eq. 6.25). The proposed models, validated here using

copper, use three initial state variables strain-rate, temperature and initial grain size to predict the stress-strain behavior and final microstructure.

The criticism on the details of other models do not consist a failure at any level, but represent honest attempts to organize concepts, translate ideas into mathematical expressions and actual comparisons whose limitations help further comprehension. An initial objection began with the absence of any particular correlation of Z with the n_A exponent of the Avrami equation (eq. 6.8), which raised questions about the calculation method. Errors in calculation could be introduced if an initial n_A exponent exists for consuming an initial grain and, a change of n_A is due to an increasing contribution of already recrystallized grains, which also may re-recrystallize. The evaluation method for the volume fraction X may also be flawed, as has been explained, the onset of DRX happens before the first stress peak and thus the conventional manner of calculation using eq. 6.7 may be representing delayed values. The Damped Cosine Avrami Model has avoided calculating a volume fraction for that reason. The new model also avoids introducing an arbitrary steady state stress value from hot flow curves that may have not reached a true steady state. Instead a saturation steady stress value is obtained by use of eq. 6.17. In the same manner eq. 6.45 tends to a saturation stress value. The Monte Carlo Simulations and Cellular Automata Models have established that strain-hardening and recovery models already explain the kinetics of hot deformation except that the development of low dislocation nuclei still needs to be introduced as part of more complete strain-hardening model. Dynamically recrystallized grains are responsible for a heterogeneous strain-hardening behavior. Nucleation on computer simulations is carried out by either a random manner or a value imposed occurrence. The Sandström and Lagneborg model did conceptualized the heterogeneous strain-hardening behavior, but the strain-hardening description proved to be too elemental. There exists a widespread use of $\tau = \alpha \mu b \sqrt{\rho}$ to describe hardening stages beyond stage II. The known relationship describes stage II of strain-hardening [114, 98] and, stage III constitutes the breakdown of the mentioned law. Unfortunately no other high temperature strain-hardening and dynamic recovery model includes the extra softening rate caused by recrystallized grains. Also the needed model should describe the $\theta - \sigma$ hot flow behavior specifically regarding the inflection that points to the onset of DRX. Such a model would help filter experimental noise in the same manner the Damped Cosine Avrami model discerns between irrelevant stress vibrations and DRX oscillations. The presented Damped Cosine Avrami model is a solution when accurate industrial predictions are needed however no physical basis is implied here. It should be mentioned that a resemblance exists between the description of the mean oscillatory stress during DRX (eq. 6.16) and the Voce-Kocks model (eq. 6.45), because both equations suppose a saturation value. The Damped Cosine model is an option to quantitatively solve for the hot flow behavior of pure copper especially as low Zener-Hollomon conditions are approached and along with the relative-grain size model can be of help to better control properties and processing not only of copper but of other materials.

Some of the quantitative conclusions allowed by this study have been:

- 1) The Damped Cosine Avrami model points to a behavior change during hot flow. The transition Zener-Hollomon value below which multiple peak DRX occurs on a copper like Cu A is $Z_c = 1.5 \times 10^8 \text{s}^{-1}$. Cu A is an initially large grained 99.9% pure copper, which contains only 26ppm of oxygen and allows correlations with the self-diffusion activation energy, $Q_{sd} = 197 \text{KJ/mole}$.

- 2) The stable dynamically recrystallized grain diameter, D_{rex} , is described by eq. 6.1. For a commercially pure copper, like Cu A, the coefficient K_{rex} is 5385.7 and the exponent m_{rex} is 0.22503. A copper regardless of the initial grain diameter will tend to have the described final microstructure.
- 3) The relative-grain size model predicts a hot flow transition value at $2D_{rex}$ where smaller initial grain diameters, D_0 , produce a multiple peak DRX behavior. However experimental evidence on large grained Cu A has not been able to corroborate the theoretical prediction. The Damped Cosine Avrami model allows a quantitative decision as to when a stress-strain curve can be considered of single or multiple peak DRX. Here we have chosen that when the maximum stress oscillation (given by the σ_r stress) is less than 0.4MPa then the stress-strain curve can be considered to be of the single peak DRX type. The transition value for Cu A is then $8.2D_{rex}$.
- 4) The Damped Cosine Avrami model and published constants [81] have allowed re-plotting a version of the critical strain model ($\varepsilon_{cr} > \varepsilon_x$ criterion), which had been used to predict multiple peak DRX. The ε - Z plot instead of the ε - σ predicts a transition from multiple peak DRX to single peak for Cu A at a Z value of $9.73 \times 10^8 \text{s}^{-1}$, which almost coincides with the observed value using the Damped Cosine Avrami model ($Z_c = 1.5 \times 10^8 \text{s}^{-1}$).
- 5) The comparison between the experimental and predicted hot flow curves shows a reliable agreement except for the temperature of 600°C. As is known for copper the self-diffusion activation energy tends to stabilize to 197KJ/mole for temperatures above 600°C. Thus the constant value used in the Zener-Hollomon parameter to normalize data and allowing high correlation coefficients loses validity. Below 600°C the proposed models breakdown and a different temperature-dependent activation energy would best correlate data.

Other conclusions deduced after reviewing knowledge *opere citato*:

- 1) Investigations have demonstrated that nucleation during DRX at low Z values is finally accomplished by annealing twins, however no existing model includes the influence of twin formation during hot flow or before hot flow. As deformation begins twin boundaries lose coherency and become grain borders (a preferred nucleation site). Relationships involving the initial grain size may be affected. A good strain-hardening and recovery model capable of predicting the formation of sub-grains and their increasing misorientation until the nucleation of a new grain would only describe DRX at high Z values. If the twinning phenomenon is not included the envisaged model is limited from start.
- 2) Monte Carlo computerized models and Cellular Automata algorithms continue [128] to demonstrate that the existing strain-hardening and recovery models are capable of describing the stress-strain behavior even during DRX, because computer simulations allow a localized analysis of the contributions to the total stress. However the lack of a grain shape change associated to an increase of dislocation density and the artificial manner of introducing new recrystallized grains may be preventing a more adequate prediction.
- 3) Before DRX can occur strain-hardening and dynamic recovery must create a certain dislocation structure that serves as a driving force for migrating grain boundaries, which play a role either at high Z DRX (by bulging grain borders) or at low Z DRX (by creating twins as moving grain boundaries

disassociate). Strain-hardening and dynamic recovery models have been adapted successfully to include DRX by anomalously increasing the weight of the recovery component on strain-hardening rate evolution functions. This study chose a strain-hardening model developed for large grained pure metals where the influence of grain boundary sinks is little compared to the mean free path a dislocation can travel. A fine grained Cu A would require a different adaptation of a strain-hardening model that assumes a grain size constrained mean free path.

6.16 Acknowledgements for this Chapter

V.G.G. is grateful to the AECI and the UPC for the financial support provided. Special thanks are due to Prof. J.M. Prado and Dr. J.M. Cabrera for listening, suggesting ideas and welcoming V.G.G. within their facilities. A Co-operation accord between Tertub and UPC gave rise to this study. Dr. E. Jiménez-Piqué is to be thanked for the enlightening conversations on strain-hardening theory.

6.17 References

- [1] Montheillet F., Jonas J.J., Recrystallization, Dynamic, Encyclopedia of Applied Physics, vol. 16, VCH Publishers, Inc., 3-527-28138-X, (1996), pp.205-225.
- [2] Hertzberg Richard W., Deformation and Fracture Mechanics of Engineering Materials, John Wiley & Sons, Inc., New York, (1996) , pp. 166-167, pp. i-786.
- *[3] Steinemann S., Beiträge Geol. Scheiz (Hydrol.), 10, (1958), pp. 1-72.
- *[4] Poirier J.P., Philos. Mag. 26, (1972), pp. 713-725.
- [5] Tsuji N., Matsubara Y., Saito Y., Dyanamic Recrystallization of Ferrite in Interstitial Free Steel, Scripta Mater. Vol. 37, No. 4, (1997) pp. 477-484.
- [6] Glover G., Sellars C.M., Static Recrystallization After Hot Deformation of α -Iron, Metallurgical Transactions, Vol. 3, August (1972), pp. 2271-2280.
- [7] Glover G., Sellars C.M., Recovery and Recrystallization During High Temperature Deformation of α -Iron, Metallurgical Transactions, Vol. 4, March (1973), pp. 765-775.
- [8] Bailey J.E., Hirsch P.B., The Dislocation Distribution, Flow Stress, and Stored Energy in Cold-worked Polycrystalline Silver, Phil. Mag., Vol. 5, (1960), pp. 485-497.
- [9] Bailey J.E., Hirsch P.B., The Recrystallization Process in Some Polycrystalline Metals, Proc. R. Soc. London, A267, (1962), pp.11-30.
- [10] Mecking H., Kocks U.F., Kinetics of Flow and Strain-Hardening, Acta Metallurgica, vol. 29, (1981), pp. 1865-1875.

- [11] Sample, V. M., Fitzsimmons, G. L., DeArdo, A. J., Dynamic Softening of Copper During Deformation at High Temperature and Strain Rates, Acta Metallurgica, vol. 35., No. 2, (1987) pp. 367-379.
- [12] Poliak E.I., Jonas J.J., Initiation of Dynamic Recrystallization in Constant Strain Rate Hot Deformation, ISIJ International, Vol. 43, No. 5, (2003), pp. 684-691.
- [13] Luton M.J., Sellars C.M., Dynamic Recrystallization in Nickel and Nickel-Iron Alloys During High Temperature Deformation, Acta Metallurgica, vol. 17, (August 1969), pp. 1033-1043.
- *[14] Sakui S., Sakai T., Takeishi K., Trans. Iron Steel Inst. Jpn. 17, (1977), pp. 718-725.
- [15] Weiss I., Sakai T., Jonas J.J., Effect of Test Method on Transition from Multiple to Single Peak Dynamic Recrystallization, Metal Science Vol. 18, Feb. (1984), pp. 77-84.
- [16] Sakai T., Jonas J.J., Dynamic Recrystallization: Mechanical and Microstructural Considerations, Acta metall., vol. 32, no. 2, (1984), pp. 189-209.
- *[17] Thomsen E.G., Yang C.T., Kobayashi S., Mechanics of Plastic Deformation in Metal Processing, The MacMillan Company, New York, (1964), p. 113.
- [18] Blaz L. Korbel A., Effect of Hot Deformation on Grain Size in Deformed and Annealed Copper, Hot Working and Forming Processes, ed. C.M. Sellars and G.J. Davies, The Metals Society, London, (1980), pp.57-61.
- [19] Lehnert W., Cuong N.D., Experimental and Mathematical Simulation of Microstructural Evolution During Hot Rolling of Al and Cu Material, Journal of Materials Processing Technology, vol. 60, no. 1-4, (1996), pp. 567-574.
- [20] Cabrera J.M., Al Omar A., Jonas J.J., Prado J.M., Modeling the Flow Behavior of a Medium Carbon Microalloyed Steel Under Hot Working Conditions, Metallurgical and Materials Transactions A, vol. 28A, November (1997), pp. 2233-2244.
- [21] Sandström Rolf, Lagneborg Rune, A Model for Hot Working Occurring by Recrystallization, Acta Metallurgica, Vol. 23, March (1975), pp. 387-398.
- *[22] Sakui S., Sakai T., Takeishi K., Tetsu-to-Hagane 62, (1976), p. 856.
- [23] Rossard C., Blain P., Evolution de la Structure de l'Acier Sous l'Effet de la Déformation Plastique à Chaud, Memoires Scientifiques Rev. Metallur., LVI, No. 3, (1959), pp. 285-300.
- *[24] Petkovic R.A., Luton M.J., Jonas J.J., Can. Metall. Q. 14, 137, (1975).
- [25] Blaz L., Sakai T., and Jonas J.J., Effect of Initial Grain Size on Dynamic

Recrystallization of Copper, Metal Science, vol. 17, December (1983), pp. 609-616.

[26] Blaź Ludwik, Panek Stanislaw, Dynamic Recrystallization of Cu-5.5 Wt% Al Alloy, Archives of Metallurgy, vol. 34, Issue 2, (1989), pp.163-173.

*[27] Ueki M., Hattori M., Horie S., Trans. Iron Steel Inst. Jpn., 26 (1986), p. 907.

*[28] Nazabal J.L., Urcola J.J., Fuentes M., Mater. Sci. Eng., 86, (1987), p. 93.

[29] Tanner, Albert B., Mcdowell, David L., Deformation, Temperature and Strain Rate Sequence Experiments on OFHC Cu, International Journal of Plasticity 15, (1999) pp. 375-399.

[30] Blaź Ludwik, The Structural Effect of Copper Cyclic Dynamic Recrystallization, Archives of Metallurgy, vol. 32, Issue 2, (1987), pp. 213-226.

[31] García V.G., Cabrera J.M. and Prado J.M., Modeling the Hot Flow Stress of Commercial Purity Coppers with Different Oxygen Levels, Thermec'2003, Materials Science Forum, vols. 426-432 (2003), Trans Tech Publications, Switzerland, <http://www.scientific.net>, pp. 3921-3926.

[32] Kuper A., Letaw Jr. H., Slifkin E., Sonder E., Tomizuka C.T., Self-Diffusion in Copper, Physical Review, vol. 96, no. 5, (1954), pp.1224-1225.

[33] Kuper A., Letaw Jr. H., Slifkin E., Sonder E., Tomizuka C.T., Self-Diffusion in Copper (Errata), Physical Review, vol. 98, (1955), pp.1870.

[34] García V.G., Cabrera J.M., Riera L.M., Prado J.M., Hot Deformation of a Commercial Purity Copper, Proceedings of Euromat 2000: Advances in Mechanical Behaviour, Plasticity and Damage, vol. 2, Elsevier Science, Oxford, pp.1357-1362.

[35] García V.G., El Wahabi M., Cabrera J.M., Riera L.M., Prado J.M., Modelización de la Deformación en Caliente de un Cobre Puro Comercial, Rev. Metal. Madrid 37 (2001), pp.177-183.

[36] Weertman Johannes, Dislocations Climb Theory of Steady-State Creep, Transactions of the ASM, Vol. 61, (1968) pp. 681-694.

[37] García V.G., Cabrera J.M., Prado J.M., Dynamically Recrystallized Grain Size of Some Commercial Purity Coppers, Proceedings of the First Joint International Conference on Recrystallization and Grain Growth (Aachen), Eds. Gottstein G. and Molodov D.A., Springer-Verlag, Berlin, vol.1, (2001), pp.515-520.

*[38] Avrami M., Journal of Chemical Physics, Vol. 8, (1940), p. 212.

*[39] Avrami M., Journal of Chemical Physics, Vol. 9, (1941), p. 177.

[40] Frost H.J., Ashby M.F., Deformation-Mechanism Maps, The Plasticity and Creep

- of Metals and Ceramics, Pergamon Press, Oxford, (1982), p. 13.
- [41] Porter D.A., Easterling K.E., Phase Transformations in Metals and Alloys, 2nd Ed., Chapman & Hall, London, (1981), p. 290.
- [42] Cabrera J.M., Prado J.M., Simulación de la Fluencia en Caliente de un Acero Microaleado con un Contenido Medio de Carbono I parte. Aproximación Teórica, Rev. Metal Madrid, 33 (2), 1997, pp. 80-88.
- [43] Rollett A.D., Luton M.J., Srolovitz D.J., Microstructural Simulation of Dynamic Recrystallization, Acta metall. Mater. Vol. 40, no. 1, (1992), pp. 43-55.
- [44] Goetz R.L., Seetharaman V., Modelling Dynamic Recrystallization Using Cellular Automata, Scripta Materialia, Vol. 38, No. 3, (1998), pp. 405-413.
- [45] Kaptsov Y.V., Gornostyrev Yu. N., Urtsev V.N., Levit V.I., Maslennikov V.A., Mathematical Model of Dynamic Recrystallization, Recrystallization'92, Materials Science Forum Vols. 113-115, (1993), pp. 341-348.
- [46] Sakai Taku, Microstructural Development Under Dynamic Recrystallization of Polycrystalline Materials, J.J. Jonas Symposium on Thermomechanical Processing of Steel, S. Yue, E. Essadiqi (eds.), Canadian Inst. Min. Met. and Ptr., Montreal, (2000), pp. 47-62.
- [47] Gao W., Sakai T., Miura H., Modeling the Stress-Strain Curves Under Dynamic Recrystallization, Acta Metallurgica Sinica (English Letters), Vol. 13, No. 1, February (2000), pp. 349-358.
- [48] Montheillet F., Modeling Discontinuous and Continuous Dynamic Recrystallization, J.J. Jonas Symposium on Thermomechanical Processing of Steel, S. Yue, E. Essadiqi (eds.), Canadian Inst. Min. Met. and Ptr., Montreal, (2000), pp. 297-310.
- *[49] Taylor G.I., The Mechanism of Plastic Deformation of Crystals: Part I Theoretical, Part II Comparison with Observations, Proc. Roy. Soc., A145, pp. 362-387 Pt. I, pp. 388-404, Pt. II, (1934), [“The Scientific Papers of Sir Geoffrey Ingram Taylor”, ed. Batchelor G.K., Cambridge University Press, N. Y., 1, Nos. 21 and 22 (1958)].
- [50] Taylor G.I., Plastic Strain in Metals, Journal of the Institute of Metals, May Lecture (1938), pp. 307-324.
- [51] Groves G.W., Kelly A., Independent Slip Systems in Crystals, Philosophical Magazine, Vol. 8, (1963), pp. 877-887.
- [52] Kocks U.F., The Relation Between Polycrystal Deformation and Single-Crystal Deformation, Metallurgical Transactions, Vol. 1, May (1970), pp. 1121-1143.
- [53] Peczak P., A Monte Carlo Study of Influence of Deformation Temperature on Dynamic Recrystallization, Acta metall. mater. Vol. 43, no. 3, (1995), pp. 1279-

1291.

- [54] Luton M.J., Peczak P., Monte Carlo Modelling of Dynamic Recrystallization : Recent Developments, Recrystallization'92, Materials Science Forum, Vols. 113-115, (1993), pp. 67-80.
- *[55] Potts R.B., Proc. Camb. Phil. Soc. Vol. 48, (1952), p.106.
- *[56] Hesselbarth H.W., Göbel I.R., Acta Metall. Mater. 39, (1991), p. 2135.
- [57] Roberts W., Ahblom B., A Nucleation Criterion for Dynamic Recrystallization During Hot Working, Acta Metallurgica, vol. 26, (1978), pg. 801-813.
- [58] Kroc Jiří, Application of Cellular Automata Simulations to Modelling of Dynamic Recrystallization, Sloot et al. (Eds.), Springer-Verlag, Berlin: ICCS 2002, LNCS 2329, (2002), pp.773-782.
- [59] Kroc Jiří, Paidar Václav, Modelling of Recrystallization and Grain Boundary Migration by Cellular Automata, Thermec'2003, Materials Science Forum, vols. 426-432 (2003), Trans Tech Publications, Switzerland, <http://www.scientific.net>, pp. 3873-3878.
- [60] Ding R., Guo Z. X., Coupled Quantitative Simulation of Microstructural Evolution and Plastic Flow During Dynamic Recrystallization, Acta. Mater. 49 (2001) pp. 3163-3175.
- [61] Kroc J., Balík J., LukáčP., Modelling of Work Hardening, Materials Science and Engineering, A234-236, (1997), pp. 936-939.
- [62] Ponge D., Gottstein G., Necklace Formation During Dynamic Recrystallization: Mechanisms and Impact on Flow Behavior, Acta mater. Vol. 46, No. 1, (1998), pp. 69-80.
- [63] Gottstein G., Brüger E., Löchte L., Fischer-Bühner J., Ponge D., Dynamic Recrystallization in Metals and Intermetalics, Proceedings 16th Risø International Symposium on Material Science: Microstructure and Crystallographic Aspects of Recrystallization, Roskilde, Denmark 1995, pp. 37-49.
- [64] Ogata Katsuhiko, Ingeniería de Control Moderna, Prentice-Hall Hispanoamericana S.A., México, (1993), pp. 1-1020.
- [65] Rossard C., Blain P., Procédé de détermination graphique des phénomènes transitoires au cours de la déformation des aciers à chaud, Revue de Metallurgie, LV, No. 6, (1958), pp. 595-598.
- [66] Ogata Katsuhiko, System Dynamics, Prentice-Hall Inc., Englewood Cliffs, New Jersey, (1992), chapter 9, pp. 1-712.
- [67] Chen Shuh Rong, Kocks U.F., On the Strain-Rate Dependence of Dynamic Recrystallization in Copper Polycrystals, Scripta Metallurgica et Materialia, vol.

- 27, pp. 1587-1592, 1992.
- [68] Zener C., Hollomon J.H., Plastic Flow and Rupture of Metals, Trans. Am. Soc. Metals, vol.33, (1944), pp. 163-235.
- *[69] Nadai A., Manjoine M.J., High-Speed Tension Tests at Elevated Temperatures, Parts II and III, Transactions American Society of Mechanical Engineers, Vol. 63, (1941), A-77.
- [70] Garofalo F., An Empirical Relationship Defining the Stress Dependence of Minimum Creep Rate in Metals, Transactions of the Metallurgical Society of AIME, Vol. 227, April (1963), pp. 351-355.
- [71] Sellars C.M., Tegart W.J.McG., La Relation entre la Résistance et la Structure dans la Déformation à Chaud, Memoires Scientific Rev. Métallurg. LXIII, no. 9, (1966), pp.731-746.
- [72] Kocks U.F., Argon A.S., Ashby M.F., Progress in Material Science Vol. 19: Thermodynamics and Kinetics of Slip, Editors: Chalmers B., Christian J.W., Massalski T.B., Pergamon Press Ltd., Headington Hill Hall, Oxford, England, (1975), pp. i-291.
- [73] Tanaka K., Nakamura T., Hoshida Y., Hara S., Determination of the Constants in the Zener-Hollomon Hyperbolic Equation for High Temperature Deformation, Res Mechanica 12 (1984) 41-57.
- [74] Rieiro I., Carsi M., Peñalba F., Propuesta de un Método de Ordenador para Resolver el Ajuste a la Ecuación de Zener-Hollomon (Garofalo), Rev. Metal. Madrid, 32 (5), 1996, pp.321-328.
- *[75] Furushiro N., Okada Y., Hori S., J. Soc. Mater. Sci. Jpn., 29, (1980), 776.
- *[76] Ryan N.D., McQueen H.J., J. Mater. Process. Technol., 8 (1990), 177.
- [77] Ryan N.D., McQueen H.J., Dynamic Softening Mechanisms in 304 Austenitic Stainless Steel, Canadian Metallurgical Quarterly, vol. 29, no. 2, (1990), pp. 147-162.
- *[78] Poliak E.I., Jonas J.J., Acta Metall. Mater. 44, (1996), 127.
- [79] Poliak E.I., Jonas J.J., Initiation of Dynamic Recrystallization in Constant Strain Rate Hot Deformation, ISIJ International, Vol. 43, No. 5, (2003), pp. 684-691.
- [80] Zehetbauer M., Seumer V., Cold Work Hardening in Stages IV and V of F.C.C. Metals-I. Experiments and Interpretation, vol. 41, no. 2, (1993), pp. 577-588.
- [81] Manonukul, A., Dunne, F. P. E., Initiation of Dynamic Recrystallization Under Inhomogeneous Stress States in Pure Copper, Acta mater., vol. 47, no. 17, (1999), pp. 4339-4354.

- [82] Humphreys, F.J., Hatherly, M., Recrystallization and Related Annealing Phenomena, Elsevier Science Ltd, The Boulevard, Lanford Lane, Kidlington Oxford, OX5 1GB, U.K., pp.489, 1995.
- *[83] Miura H., Aoyama H., Sakai T., Effect of Grain-Boundary Misorientation on Dynamic Recrystallization of Cu-Si Bicrystals, J. Japan Inst. Metals, vol. 58, (1994), pp. 267-275.
- [84] Karduck P., Gottstein G., Mecking H., Deformation Structure and Nucleation of Dynamic Recrystallization in Copper Single Crystals, Acta metall., vol. 31, no. 10, (1983), pp. 1525-1536.
- [85] Korbel A., Bochniak W., Blaz L., Embury J.D., Instability of Plastic Flow and Dynamic Recrystallization in Cu Single Crystals, Metal Science, vol. 18, April (1984), pp. 216-222.
- [86] Doherty R. D., Hughes A. D., Humphreys F. J., Jonas J. J., Juul Jensen D., Kassner M.E., King W. E., McNelley T.R., McQueen H. J., Rollett A. D., Current Issues in Recrystallization: a review, Materials Science Engineering 1997; A238: pp.219-74.
- [87] Manonukul, A., Dunne, F. P. E., Dynamic Recrystallisation in a Copper/Stainless Steel Pseudo-two-phase Material, Materials Science and Engineering A293, (2000), pp. 173-184.
- [88] Miura H., Andiarwanto S., Sakai T., Dynamic Recrystallization at Triple Junction in Copper Tricrystal, Proceedings of the First Joint International Conference on Recrystallization and Grain Growth (Aachen), Eds. Gottstein G. And Molodov D.A., Springer-Verlag, Berlin, vol.1, (2001), pp.905-910.
- [89] Miura H., Sakai T., Hamaji H., Jonas J.J., Preferential Nucleation of Dynamic Recrystallization as Triple Junctions, Scripta Materialia 50, (2004), pp. 65-69.
- [90] Wusatowska-Sarnek A.M., Miura H., Sakai T., Blackburn M.J., New Grain Formation under Dynamic Recrystallization of Copper, Proceedings of the First Joint International Conference on Recrystallization and Grain Growth (Aachen), Eds. Gottstein G. And Molodov D.A., Springer-Verlag, Berlin, vol.1, (2001), pp.899-904.
- [91] Wusatowska-Sarnek A.M., Miura H., Sakai T., Nucleation and Microtexture Development Under Dynamic Recrystallization of Copper, Materials Science and Engineering A323 (2002) pp. 177-186.
- [92] Belyakov A., Miura H., Sakai T., Dynamic Recrystallization under Warm Deformation of a 304 Type Austenitic Stainless Steel, Materials Science and Engineering A255 (1998), pp.139-147.
- [93] Bailey J.E., Electron Microscope Observations on the Annealing Processes Occurring in Cold-Worked Silver, Philosophical Magazine, Vol. 5, (1960), pp. 833-842.

- [94] Goodhew P.J., Annealing Twin Formation by Boundary Dissociation, Metal Science, vol. 13, no. 3-4, March-April, (1979), pp. 108-112.
- [95] Mahajan S., Pande C.S., Imam M.A., Rath B.B., Formation of Annealing Twins in f.c.c. Crystals, Acta mater., Vol. 45, No. 6, (1997), pp. 2633-2638.
- *[96] Dash S., Brown N., Acta metall. Vol. 11, (1963), pg. 1067.
- [97] Brongersma S.H., D'Haen J., Vanstreels K., DeCeuninck W., Vervoort I., Maex K., Copper Deposition and Subsequent Grain Structure Evolution in Narrow Lines, Thermec'2003, Materials Science Forum, vols. 426-432 (2003), Trans Tech Publications, Switzerland, <http://www.scientific.net>, pp. 2485-2490.
- [98] Nes Erik, Modelling of Work Hardening and Stress Saturation in FCC Metals, Progress in Materials Science, Vol. 41, pg. 181, (1998), pp. 129-193.
- [99] Cottrell A.H., Stokes R.J., Proc. R. Soc., A 233, (1955), pg. 17.
- [100] Kuhlmann-Wilsdorf D., Theory of Plastic Deformation-properties of Low Energy Dislocation Structures, Materials Science and Engineering, A113 (1989) pp.1-41.
- *[101] Gil Sevillano J., van Houtte P., Aernoudt E., Large strain work hardening and textures, Progress in Materials Science, Vol. 25, Issues 2-4, (1980), pp. 69-134.
- [102] Malin A.S., Hatherly M., Microstructure of Cold-Rolled Copper, Metal Science, Vol. 13, No. 8, August (1979), pp.463-472.
- [103] Sherby, O. D., Factors Affecting the High Temperature Strength of Polycrystalline Solids, Acta Metallurgica, vol. 10, February,(1962), pp. 135-147.
- [104] McQueen H.J., Hot Working and Recrystallization of Face-centred Cubic Metals, Trans. Japan Inst. Metals, Vol. 9, (1968), pp. 170-177.
- [105] Yamagata H., Ohuchida Y., Saito N., Otsuka M., Nucleation of new grains during discontinuous dynamic recrystallization of 99.998 mass % Aluminum at 453 K, Scripta Materialia, vol. 45, (2001), pp. 1055-1061.
- *[106] Ludwik P., Elemente der Technologischen Mechanik, Julius Springer, Berlin, (1909), pg. 32.
- *[107] Hollomon J.H., Trans. AIME, vol. 162, (1945), pg. 268.
- *[108] Voce E., The Relationship Between Stress and Strain for Homogeneous Deformation, Journal of the Institute of Metals, vol. 74, (1948), pp. 537-562.
- *[109] Voce E., A Practical Strain-Hardening Function, Metallurgia, vol. 51, (1955), pp. 219-226.

- [110] Kocks U.F., Laws for Work-Hardening and Low-Temperature Creep, Journal of Engineering Materials and Technology Trans. AIME, Vol. 98, January (1976), pp. 76-85.
- [111] Sah J.P., Richardson G.J., Sellars C.M., Recrystallization During Hot Deformation of Nickel, The Journal of the Australian Institute of Metals, vol. 14, no. 4, November (1969), pp. 292-297.
- [112] Puchi-Cabrera E.S., Modeling Cold-Rolling Processes of Commercial Twin Roll Cast Aluminum Alloys, Trans. ASME, Journal of Engineering Materials and Technology, vol. 123, April (2001), pp. 149-154.
- [113] Bergström Y., A Dislocation Model for the Stress-Strain Behaviour of Polycrystalline α -Fe with Special Emphasis on the Variation of the Densities of Mobile and Immobile Dislocations, Materials Science and Engineering, ASM, vol. 5, (1969/70), pp. 193-200.
- [114] Mecking H., Kocks U.F., Kinetics of Flow and Strain-Hardening, Acta Metallurgica, vol. 29, (1981), pp. 1865-1875.
- [115] Estrin Y., Mecking H., A Unified Phenomenological Description of Work Hardening and Creep Based on One-Parameter Models, Acta Metall. Vol. 32, No. 1, (1984), pp. 57-70.
- [116] Christodoulou N., Jonas J.J., Work Hardening and Rate Sensitivity Material Coefficients for OFHC Cu and 99.99% Al, Acta Metall., vol. 32, no. 10, (1984), pp. 1655-1668.
- [117] Tome C., Canova G.R., Kocks U.F., Christodoulou N., Jonas J.J., The Relation Between Macroscopic and Microscopic Strain Hardening in F.C.C. Polycrystals, Acta metall., vol. 32, no. 10, (1984), pp. 1637-1653.
- [118] Kocks U.F., Argon A.S., Ashby M.F., Progress in Material Science Vol. 19: Thermodynamics and Kinetics of Slip, Editors: Chalmers B., Christian J.W., Massalski T.B., Pergamon Press Ltd., Headington Hill Hall, Oxford, England, (1975), pp. i-291.
- [119] Follansbee P.S., Kocks U.F., A Constitutive Description of the Deformation of Copper Based on the Use of the Mechanical Threshold Stress as an Internal State Variable, Acta Metall. Vol. 36, No. 1, (1988), pp. 81-93.
- [120] Zehetbauer M., Cold Work Hardening in Stages IV and V of F.C.C. Metals-II. Model Fits and Physical Results, Acta metall., vol. 41, no. 2, (1993), pp. 589-599.
- [121] Nes Erik, Modelling of Work Hardening and Stress Saturation in FCC Metals, Progress in Materials Science, vol. 41, (1998), pp. 129-193.
- [122] Nes E., Marthinsen K., Modeling the evolution in microstructure and properties during plastic deformation of f.c.c.-metals and alloys- an approach towards a

unified model, Materials Science and Engineering, A322, (2002), pp. 176-193.

- [123] Karduck P., Gottstein G., Mecking H., Deformation Structure and Nucleation of Dynamic Recrystallization in Copper Single Crystals, Acta metall., vol. 31, no. 10, (1983), pp. 1525-1536.
- [124] Gottstein G., Kocks, U. F., Dynamic Recrystallization and Dynamic Recovery in $\langle 111 \rangle$ Single Crystals of Nickel and Copper, Acta Metallurgica, vol.31, (1983), pp. 175-188.
- *[125] Seeger A., Dislocations and Mechanical Properties of Crystals, John Wiley and Sons, New York, (1967), pg. 243.
- [126] Ryan N.D., McQueen H.J., Comparison of Dynamic Softening in 301, 304, 316 and 317 Stainless Steels, High Temperature Technology, vol. 8, no. 3, August (1990), pp.185-200.
- [127] Krauss George (editor), Deformation, Processing and Structure, 1982 ASM Materials Science Seminar, American Society for Metals, Metals Park, Ohio 44073, (1984), pp.i-524.
- [128] Qian M., Guo Z.X., Cellular Automata Simulation of Microstructural Evolution During Dynamic Recrystallization of an HY-100 Steel, Materials Science and Engineering, A365 (2004), pp. 180-185.